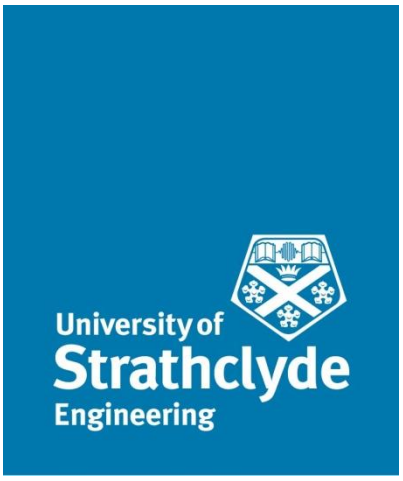

Department of Mechanical and Aerospace Engineering

The Study of Corrosion and the Investigation of Peat Contamination in Steel

Author: Graeme Leitch (201289583)

Supervisor: Professor Margaret Stack

A thesis submitted in partial fulfilment for the requirement of the degree

Master of Science

Sustainable Engineering: Renewable Energy Systems and the Environment

2015

Copyright Declaration

This thesis is the result of the author's original research. It has been composed by the author and has not been previously submitted for examination which has led to the award of a degree.

Signed: Graeme Leitch Date:30/08/2015

Abstract

As the development of renewable energy systems continues to be promoted through the use of energy policy it is becoming increasingly important to consider corrosion and its effects on the long term sustainability of the energy systems infrastructure.

A literature study on corrosion, particularly galvanic corrosion and the factors contributing to its development has been undertaken. The literature review has led to a collection of guidelines on how to minimise galvanic corrosion being produced including data on the severity of different material couplings in a tabular form.

The deterioration of steel as a result of its interaction with its surroundings has been investigated in this project through the use of electrochemical experimentation methods. The solution that the metal was immersed in was changed during each test for varying peat / pH concentrations, which in turn has allowed the effects of peat contamination on steel to be studied.

The results of the electrochemical tests performed were used to generate corrosion rate maps with the changing pH and chromium contents addressed. The conclusions drawn from the heat maps show that at lower chromium contents the resistance of the material to corrosion is significantly reduced. It was also evident that the pH of the solution is have a direct effect on the corrosion rates, at higher pH values (closer to pH value of 7) the severity of corrosion witnessed is low. Interestingly a severe rate of corrosion is seen between 19 - 20% composition of chromium and at a pH value of 4.7 to 5, whereas at this same point for a reduced 17-18% chromium content only a medium corrosion rate is observed. This is assumed to be due to molybdenum being present in the overall composition of the smaller chromium percentage samples which is improving the corrosion resistance far more than that of the higher chromium content only.

Acknowledgements

I would like to extend my thanks to the University of Strathclyde and Dr Paul Strachan for allowing me the opportunity to study the MSc Sustainable Engineering: Renewable Energy Systems & the Environment.

I would like to thank my project supervisor, Professor Margaret Stack for agreeing to support my project and her continued guidance throughout.

Thanks must also go to Shayan Sharifi and Ghulam Rasool, both of whom were of great assistance during the course of the project, particularly during the testing phase. Without them I would no doubt still be trying to complete this project!

A special message of thanks has to go to Martin Deeks for his help in coming up with the topic idea and the advice offered throughout.

Contents

List of Graphs

List of Figures

1 Introduction

1.1 Background to Project Selection

To promote the development of energy from renewable sources within the European Union, the European Parliament and Council have established the Renewable Energy Directive. The directive states that it requires the EU to fulfil at least 20% of its total energy needs with renewables by 2020 – to be achieved through the attainment of individual nation targets. All member states must also ensure that at least 10% of their transport fuels come from renewable sources by 2020, to be introduced in a cost-effective way (European Directive, 2009). Renewable energy is now at the core of every informed discussion concerning energy security, sustainability and affordability. As the development of new and existing renewable energy systems continues it is becoming increasingly important to consider corrosion and its effects on the long term sustainability of the energy systems infrastructure.

Corrosion is the deterioration of a material as a result of its interaction with its surroundings. Furthermore, corrosion processes not only influence the chemical properties of a metal or metal alloys, but they also generate changes in their physical properties and mechanical behaviours (Speight, 1st Edition). The direct cost of corrosion is difficult to ascertain however (Zarras and Stenger-Smith, 2014) reveal that the annual costs of corrosion worldwide exceeds $US 1.8 trillion. A more in depth study of corrosion and its effect will be made during the literature review section.

The initial driver for why the author wanted to investigate corrosion was to try and achieve an understanding of the reasons why at some hydro power stations (within Scotland) there are varying severities of corrosion taking place. It is hoped that by researching the subject in detail an appreciation of the corrosion types and possible consequences will be gleaned subsequently allowing the author to provide guidance on the subject matter. An early observation that has been made is that the main components making up a hydro power station are of carbon steel material, however due to problems of peat contamination on sections pipework they are being replaced for stainless steel counterparts which in turn is creating new problems associated with

galvanic corrosion. A balance is required to be found, as although stainless steel increases component life and is not readily affected by peat contamination it is about one order of magnitude higher in material cost than carbon steel (Abreu and others, 2002).

1.2 Aims and Objectives

The overall aim of the project is to achieve an understanding on material combinations that can be used within a hydro power station to limit the effects of galvanic corrosion. The main objectives that this thesis will attempt to tackle over the upcoming months are:

1. Undertake a literature study to establish how and why corrosion arises and to identify any limiting factors
2. Provide guidelines on how galvanic corrosion may be reduced
3. Through laboratory testing and on site investigation examine the severity of corrosion in a variety of circumstances

2 Literature Review

2.1 Corrosion

Corrosion is a naturally occurring development, typically defined as degradation of the material properties as a result of its interaction with the environment over a period of time (Zarras and Stenger-Smith, 2014). This definition is true for any type of material including plastics, however it is often reserved for metallic alloys. In the region 80 of the known chemical elements are metals (Figure 1). Of these metals roughly half can be alloyed with other metals, the subsequent composition of the alloy will determine the physical, chemical and mechanical properties (Speight, 1st Edition). The literature illustrates that the corrosion resistance of alloys such as stainless steels can be significantly enhanced by appropriate alloying (Olsson and Landolt, 2003).

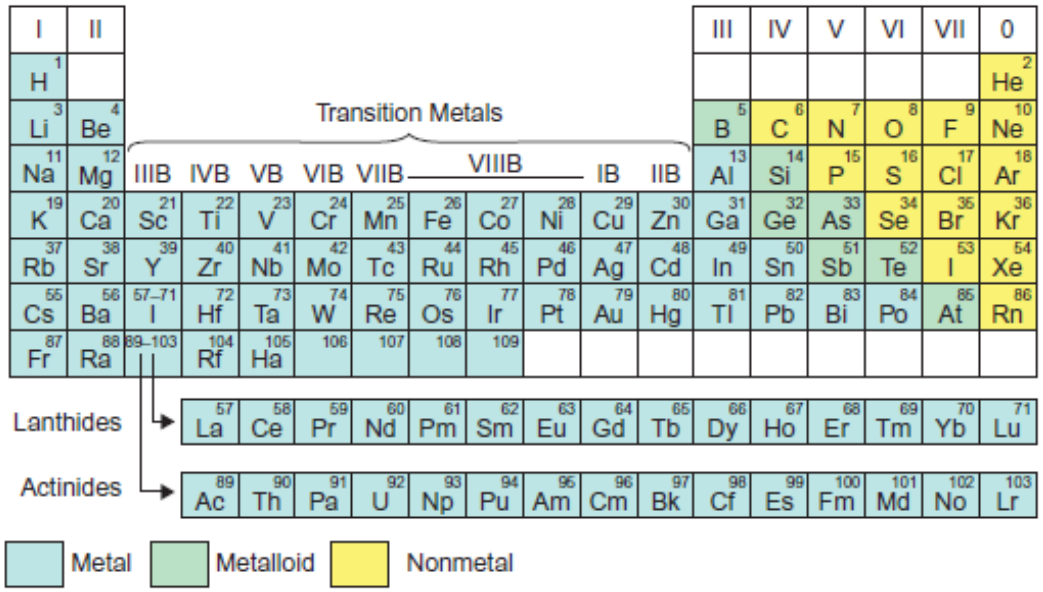

Figure 1 Periodic Table of the Elements (Speight, 1st Edition)

The surface of all metals with the exception of gold contain an oxide film when in air. This protective oxide film has a tendency to dissolve when submerged in an oxidising environment, exposing the bare metal surface resulting in a susceptibility to corrosion (Hinds). However a passive film is formed during the bare metal surface exposure

which will reduce the reaction rate of the corrosion by several orders of magnitude (Olsson and Landolt, 2003).

2.1.1 Electrochemistry of Corrosion

The discussion of the electrochemistry of corrosion below has been summarised from the literature found in (Hinds).

In the case where an oxide film has dissolved entirely with the metal surface exposed to the oxidising solution, the positively charged metal ions will transfer from the metal into the solution, leaving electrons behind on the metal i.e.

$$\underset{\text{atom in metal surface}}{M} \rightarrow \underset{\text{ion in solution}}{M^{n+}} + \underset{\text{electron(s) in metal}}{ne^-} \qquad (1)$$

The left over electrons in the metal lead to an increase in negative charge resulting in an electrode potential between the metal and solution, which in turn becomes further negative. As the electrode potential changes the reaction that was taking place above is slowed down until it is reversed with the deposition of dissolved metals ions from the solution on the metal surface now being encouraged i.e.

$$M^{n+} + ne^- \leftrightarrows M \qquad (2)$$

A stable potential also known as the reversible potential (E_r) is achieved when the rate of dissolution of metal ions becomes equal to the rate of deposition i.e.

$$E_{r,M^{n+}/M} = E^{\circ}{}_{M^{n+}/M} + \frac{RT}{nF} \ln a_{M^{n+}} \qquad (3)$$

Where, E^o is the standard reversible potential, $a_M{}^{n+}$ the unit activity of dissolved metal ions, R the gas constant, T the absolute temperature, F the Faraday and n the number of electrons transferred per ion. No further metal dissolution is witnessed once the potential reaches the reversible potential. Typically only a very small quantity of metal is dissolved during this process.

However the reverse potential is not often reached and the potential stays more positive due to other reactions which are removing the electrons from the metal. For example, in acid solutions hydrogen gas is produced as the electrons react with hydrogen ions that have been absorbed on the metal surface from the solution

$$\underset{\text{adsorbed on metal surface}}{2H^+} + \underset{\text{in metal}}{2e^-} \rightarrow \underset{\text{gas}}{H_2} \qquad (4)$$

The presence of the above reaction (4) allows the metal ions to continue to leave the metal and transfer into the solution, which subsequently leads to the metal corroding. This reaction is also reversible and has a reversible potential set by:

$$E_{r,H^+/H_2} = E^{\circ}{}_{H^+/H_2} - \frac{RT}{F} \ln \frac{p_{H_2}^{\frac{1}{2}}}{a_{H^+}} \qquad (5)$$

with P_{H2} representing the partial pressure of the hydrogen gas. The reverse potential of reaction (4) can be achieved if this partial pressure continues to build up without any interference. However normally the corrosion continues as hydrogen escapes from the system leading to the potential remaining more negative.

Where the solution is neutral, the reaction (4) is unlikely to occur at a noticeable rate due the concentration of hydrogen ions been very minimal. However it is possible that the metal electrons could react with the oxygen molecules which have been adsorbed onto the surface of the metal from the air dissolved in the solution, producing hydroxyl ions, i.e.

$$\underset{\text{adsorbed on metal surface}}{O_2 + 2H_2O} + \underset{\text{in metal}}{4e^-} \rightarrow \underset{\text{in solution}}{4OH^-} \qquad (6)$$

Similar to the reactions above the potential of the metal will remain more negative than the reversible potential seen in reaction (6). The reverse potential is found from:

$$E_{r,O_2/OH^-} = E^{\circ}{}_{O_2/OH^-} - \frac{RT}{4F} \ln \frac{a_{OH^-}{}^4}{p_{O_2}} \qquad (7)$$

Hence combining the reactions (1) and (6) will allow corrosion to continue.

2.1.2 Cost of Corrosion

As described by (Popov, 2015) corrosion compromises structure safety and is a leading factor in catastrophic failure in bridges, nuclear facilities, airplane components and construction industries. Due to the time required to evaluate the extent of corrosion, it is often underestimated in industrial equipment and structure design. An interesting comparison is made by (Zarras and Stenger-Smith, 2014), they

highlight that over the past 22 years the United States has experienced in excess of over 52 major weather related disasters. The resultant cost has been over US $17 billion annually. When this is compared against the current costs of metallic corrosion on the US economy and estimates of over $276 billion annually representing 3.1% of the US gross domestic product (GDP). The large costs relating to corrosion issues is not refined solely to the US as studies done in China, Japan, UK, Europe and South America showed corrosion costs similar to the US. (Koch, 2001) further backs up the excessive costs of corrosion within industry when he states that the cost of management of corrosion in gas transmission pipelines has been evaluated to be approximately $5 billion annually. (Singh, First Edition) provides six key reason when highlighting the cost of corrosion in realistic terms to show why it is important to acquire proper knowledge of corrosion, these are:

- Cost of environmental damages; No monetary value can justify the loss to the environment due to the failure of a structure. The environmental damages cost does not include regulatory fines nor the costs involved in the clean up.

- Production loss and down time due to corrosion damage; This leads to reduction in production output and reduced revenues as the repairs are undertaken.

- Accidents; the loss of lives and injuries caused due to severe accidents resulting from corrosion damage. Costs resultant from accidents also cause adverse public image and loss of market share.

- Product Contaminations; for many industries, product contamination with corrosion can affect the quality of the good and lead to poorer business reputation.

- Loss of efficiency; a lack of full understanding of the corrosion and its impact on the system can lead to over designing of plant and the system, which can often lead to an inefficient system. Costs to the final product are also increased as the inefficient system uses excessive energy to run the plant.

- Increased Capital Cost; over designing a system also increases the capital cost of a project

2.2 Types of Corrosion

There are various forms of corrosion some of which are well known and can be seen in day-to-day life, typically in the appearance of brown rust deposited on steel and iron surfaces, while others are less so and require very specific combinations of materials and environments. Below a selection of the most common types will be reviewed.

2.2.1 Galvanic Corrosion

Of the many different types of corrosion problems experienced in the energy industry, corrosion arising from the interaction between different metals and alloys is one of the most troublesome and complex, this type of issue is commonly referred to as Galvanic Corrosion (also known as Bimetallic Corrosion). Galvanic corrosion occurs when a metallic material is in electrical contact with another metallic material or conducting non metal in the same electrolyte causing a galvanic current to flow between them. M.Finsgar (2013). The potential difference that exists between the two metal encourages the corrosion, where the more noble material acting as a cathode (negatively charged electrode) will remain unchanged whereas the more active metal acting as the anode (positively charged electrode) will corrode. (Oldfield 1988). A large number of factors in addition to the potential difference between the dissimilar metals play a role in the galvanic corrosion process. Depending on the situation some or all of the factors illustrated below in Figure 2 may be involved.

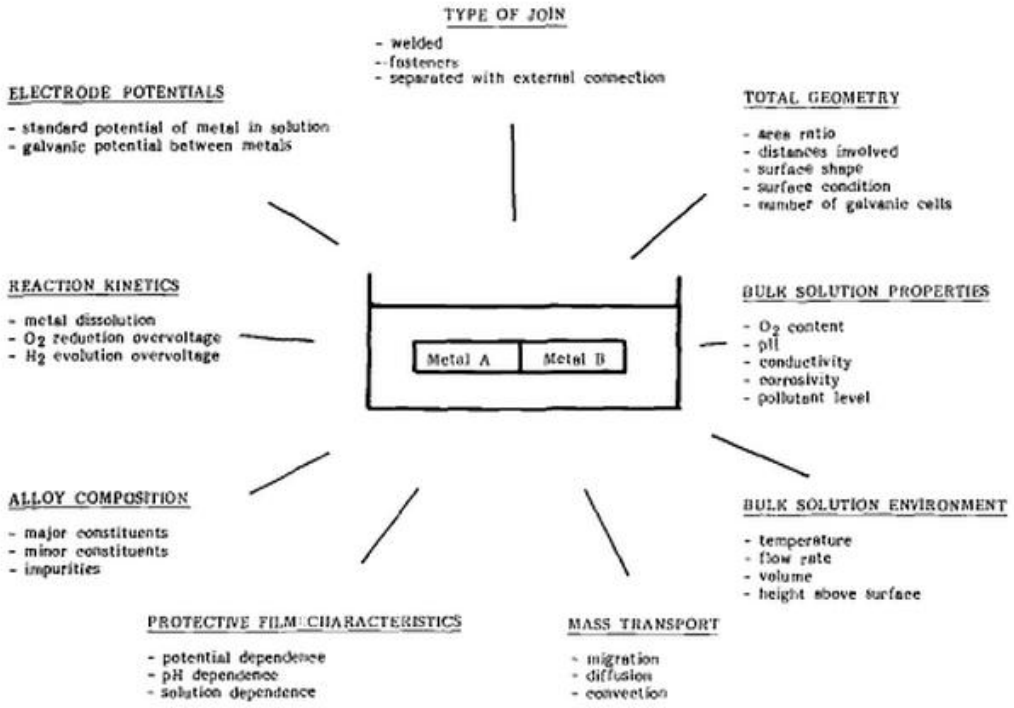

Figure 2 Factors involved in galvanic corrosion (Oldfield 1988)

A short summary of the factors shown above are discussed below:

- *Electrode Potential;*

The feature of electrode potential in galvanic corrosion is that the standard potential of a metal in a solution of its ions highlights where the approximately the metal is in the galvanic series - discussed further later on. However the electrode potential is often very different between the core metal and the surface oxide film as such in practice it is the oxide that locates the material in the galvanic series (Oldfield 1988) and (Zhang, 2011).

- *Reaction Kinetics;*

The reaction kinetics are significant factors in determining how quickly the rate of corrosion can occur. The corrosion potential of the metal is typically between the equilibrium potential of the anodic metal dissolution and the cathodic oxidant reduction. The rate of the anodic reaction is given from the metal dissolution kinetics, whereas the rate cathodic reaction provided from the oxygen reduction on the metal/alloys concerned (Oldfield 1988).

- *Alloy Composition;*

The importance and the effects of alloy composition can't be underestimated and as such it is examined later on in more detail. However in the interim it is worth noting that the alloy composition can directly affect the corrosion resistance of material.

- *Protective Film Characteristics:*

The severity and type of corrosion that will occur are determined by the metal/alloy protective surface film characteristics. How the protective film protects the bare metal under differing potential dependence, pH levels and its resistance to a selection of solution constituents needs to be considered (Oldfield 1988).

- *Mass Transport:*

The form of mass transport - migration, diffusion and convection - occupy an important role in galvanic corrosion. The type of mass transport being considered is dependent on the situation occurring (Oldfield 1988).

- *Bulk Solution Environment;*

The environment the solution is in can determine the severity (if any) of galvanic corrosion that will arise. Examples of those factors that can have an impact are, the temperature of the solution, its volume, the height above couple, and the rate of flow across the surface of the material (Oldfield 1988).

- *Bulk Solution Properties;*

The properties of the bulk solutions i.e. oxygen level and pH, play a significant part in determining whether or not a cathodic reaction is possible. The severity of galvanic corrosion is dependent on the conductivity of the electrolyte solution as it determines the distribution of corrosion across the surface of the anode material (Oldfield 1988) and (Zhang, 2011).

- *Total Geometry;*

The area ratio between the cathode and anode materials is an extremely important factor in galvanic corrosion. The larger the cathode when compared to the anode, the more oxygen reduction that can occur and hence the greater galvanic current and rate of corrosion. Also important are the shape and condition of the surface (Oldfield 1988).

- *Type of Join;*

The method by which the two different materials are coupled together also plays an key role in galvanic corrosion. We would expect a different rate of galvanic corrosion to happen between welding two materials together as opposed to joining them in a

manner in which they are insulated i.e. via a gasket or insulating washer and top hat, but electrically connected somewhere else in the system (Oldfield 1988).

2.2.1.1 EMF and Galvanic Series:

The electromotive force series (EMF series) is an arrangement of various metals in the order of their standard electrochemical potential and can be seen below in Table 1. The metals at the top of the list have a higher positive electrochemical potential and are considered the most noble, whereas those located at the foot of the sequence are found to be the most active and contain the higher negative electrochemical potential. Metals which are higher up in the series will displace those metals that are lower in the series, which when coupling two metals together, the metal with the lower potential will corrode. The metal with the lower negative potential is the cathode in the connection and remain unchanged, however the metal with higher negative electrochemical potential will act as anode and corrode.

	Metal/Metal-Ion Equilibrium	Electrode Potential vs. SHE at 25 °C (V)
Noble or Cathodic	Au^{3+}/Au	1.50
	Pt^{2+}/Pt	1.20
	Cu^{2+}/Cu	0.34
	H^{+}/H_2	0.00
	Sn^{2+}/Sn	−0.14
	Ni^{2+}/Ni	−0.25
	Cd^{2+}/Cd	−0.40
	Fe^{2+}/Fe	−0.44
	Zn^{2+}/Zn	−0.76
	Al^{3+}/Al	−1.66
Active or Anodic	Mg^{2+}/Mg	−2.36

Table 1 Standard emf Series for Metals (Popov, 2015)

The galvanic series shown below in Figure 3 provides guidance on the galvanic relationship of the different metals and alloys. The galvanic series is valuable when selecting metals to be connected together, although it does not provide information on the galvanic corrosion rate that will arise it is still a useful decision making tool. The list below begins with the least active (cathode) metal and proceeds down to the more active (anodic) metal of the galvanic series. Also included in the list is a selection of some commonly used alloys. In general the metals that are close to one another in the chart do not typically have a strong effect on one another, however as the distance between the metal (and alloy) increases so does the rate of corrosion.

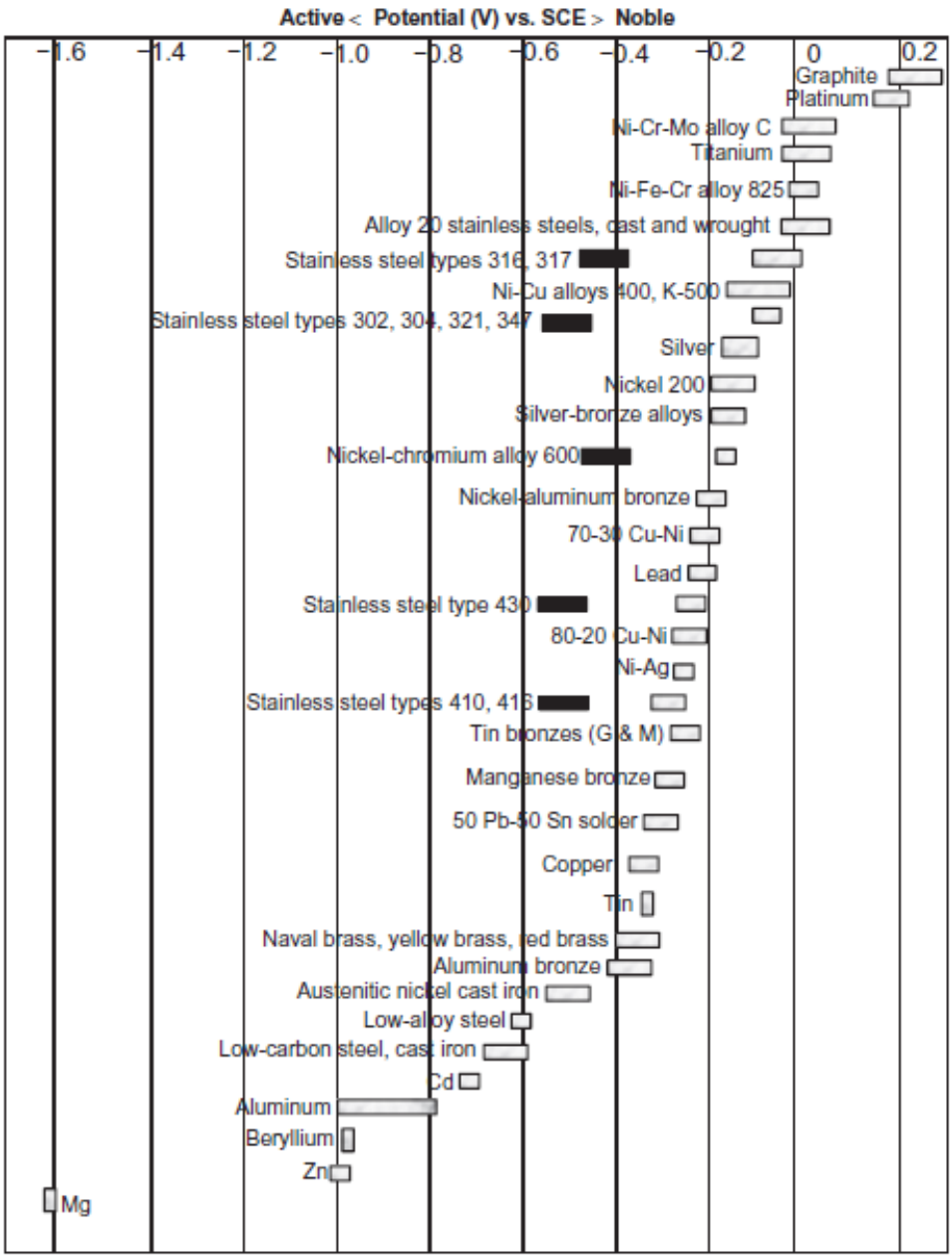

Figure 3 Galvanic Series (in Sea Water) (Popov, 2015)

Data on corrosion caused by contact of dissimilar metals has been taken from the British Standards PD6484 1979(1998) and is summarised below in Tables 2 and 3. The ratings that were used in the tables are:

0. No Corrosion

1. Slight Corrosion

2. Fairly Severe Corrosion - typically protection required

3. Severe Corrosion - Contact to be avoided

by: / Corrosion of :	Stainless Steel	Carbon Steel	Cast Iron	Galvanized (Zinc)	Copper	Bronze (Gunmetal)	Brass (HT)
Stainless Steel		0	0 to 1	0	0	0	0
Carbon Steel	2		0 to 1	0	3	3	3
Cast Iron	2	0		0	2	1 to 2	2
Galvanized (Zinc)	0 to 2	1 to 2	1 to 2		1 to 2	1 to 2	1 to 2
Copper	1	0	0	0		0	0
Bronze (Gunmetal)	0 to 1	0	0	0	0		0
Brass (HT)	1	0	0	0	0	0	

Table 2 Immersed in fresh water (i.e. inside pipework)

by: / Corrosion of :	Stainless Steel	Carbon Steel	Cast Iron	Galvanized (Zinc)	Copper	Bronze (Gunmetal)	Brass (HT)
Stainless Steel		0 to 1	0	0	0 to 1	0 to 1	0 to 1
Carbon Steel	1		0 to 1	0	1 to 2	1 to 3	2 to 3
Cast Iron	1 to 2	0		0	1 to 2	1 to 2	1 to 2
Galvanized (Zinc)	0 to 1	1	1		1 to 2	1	1
Copper	0	0	0	0		0	0
Bronze (Gunmetal)	0	0	0	0	0		0
Brass (HT)	0	0	0	0	0	0	

Table 3 Industrial Atmosphere

It is noted that these ratings are highly dependent on the relative areas of the two materials. A generalised observation is that if the area of the metal corroding is smaller in comparison to the other metal then the corrosion occurring will be more severe.

2.2.1.2 Prevention:

The following is a collection of guidelines on how to minimise or prevent galvanic corrosion (Popov, 2015):

- Select materials similar in galvanic series; ideally metals should be selected that are near to each other in the galvanic series however often due to

engineering requirements this is not always possible as different material properties are regularly needed in various parts of equipment

- Minimise the cathode-anode area ratio; this will reduce the galvanic coupling and galvanic current density. Whereas a larger cathode compared to the anode will result in the possibility of more oxygen occurring leading to a greater galvanic current and therefore corrosion
- Apply a cathode coating to decrease available area for cathodic reactions
- Do not coat the anode only; treating only the anodic metal increase the risk of severe localised corrosion on coating defects
- Insulate dissimilar metals to eliminate galvanic coupling; by insulating the metals the electrical path between the metals is broken
- Use environmentally friendly sacrificial materials such as zinc or tin to protect the galvanic assembly. It is noted that replaceable anodes are advised using this approach and only the corroded anodes needs to be replaced
- Use cathodic inhibitors to combat cathodic depolarisation reactions caused by oxygen

2.2.1.3 Examples of Galvanic Corrosion

Shown below in Figure 4 is an example of a recent pipework installation at a refurbished power station in the West of Scotland. To monitor pressure levels in the penstock, stainless steel 316L pipework and fittings have been fitted directly into the mild steel penstock pipe. The installation is only a matter of months old and looking at the image below you can see the early stages of what appears to be galvanic corrosion.

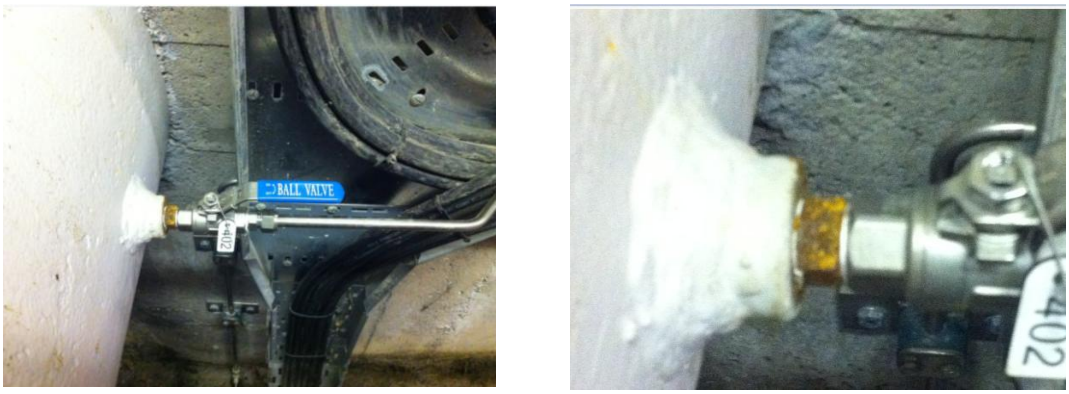

Figure 4 Galvanic Corrosion - Example 1

A further example of the problems associated with galvanic corrosion is revealed below in Figure 5. Shown are the threads of a carbon steel valve that was screwed into a stainless steel boss on the spiral casing - spiral shaped pipe. As you can see the threads have almost totally been eaten away and were very close to failure.

Figure 5 Galvanic Corrosion - Example 2

2.2.2 Crevice Corrosion

Crevice corrosion is a form of localised corrosion on the surface of a metal either at the gap or crevice between two connected surfaces which can be formed between two metals or a metal and non-metallic material. (Yang and others, 2013). The cause of crevice corrosion is a result of the potential difference in the concentration of materials inside and outside the crevice restricting the free flow of the environment between the surfaces, often caused by a design fault. (Singh, First Edition) The severity of the corrosion is very dependent on the geometry, if the crevice is narrow and deep then you would expect more severe corrosion to occur.

As explained by (Yang and others, 2013) initiation of crevice corrosion, uniform corrosion is witnessed both inside and outside of the crevice. The main anodic reaction is:

$$i. \quad M \rightarrow M^{n+} + ne^{-}$$

where M corresponds to the metal and M^{n+} relates to the metal ions. The possible cathodic reactions are:

- Reduction of oxygen,

$$ii. \quad O_2 + 2H_2O + 4e^{-} \rightarrow 4OH^{-}$$

- and/or hydrogen evolution reaction,

$$iii. \quad 2H^{+} + 2e^{-} \rightarrow H_2$$

(Yang and others, 2013) go on to discuss that the excess positively charged metallic ions released are electrostatically counter balanced by negatively charged ions such hydroxide (H^{+}) and chloride (Cl^{-}) migration into crevice from the bulk solution. Separation of the anodic and cathodic reactions and net anodic metal dissolution in the crevice occurs due to the reduction of oxygen continuing on the outer surface of the crevice even although the oxygen inside of the crevice has been depleted. Metal ions hydrolysis and electro-migration increase the $H^{+}$and Cl^{-} concentration in the crevice by:

$$iv. \quad M^{n+} + nCl^{-} \rightarrow MCl_n$$

$$v. \quad MCl_n + nH_2O \rightarrow M(OH)_n + nH^{+}nCl^{-}$$

$$vi. \quad M^{n+} + nH_2O \rightarrow M(OH)_n + nH^{+}$$

The crevice wall is changed from its passive state to an active state as $H^{+}$and Cl^{-}in the electrolyte attack and destroy the passive film on the crevice wall. The basic rule is that an increase in the concentration of reactants will further drive the reaction process, resulting in a build-up of reaction product that will stifle the reaction. In other words, the build up of corrosion product will stifle the corrosion process in the crevice. (Singh, First Edition)

The onset of corrosion can be delayed or instant, it is initiated once the crevice solution reached the chemical (or electrochemical) condition in which the crevice can be locally activated. Once the passive oxide film that is protecting the surface of the metal inside the crevice is broken for some reason, the rate of active corrosion is increased as is the dissolution rate of metal ions (Chang and others, 1998)

2.2.2.1 Examples of Crevice Corrosion

Two images of crevice corrosion are shown below in Figure 6 and 7. The first example shows the occurrence of crevice corrosion as a result of the gap between the type 316 stainless steel tube and tube sheet in a seawater reverse osmosis desalination plant. The second example illustrates a full brown crevice in an otherwise highly resistant to seawater material.

Figure 6 Crevice Corrosion Example 1

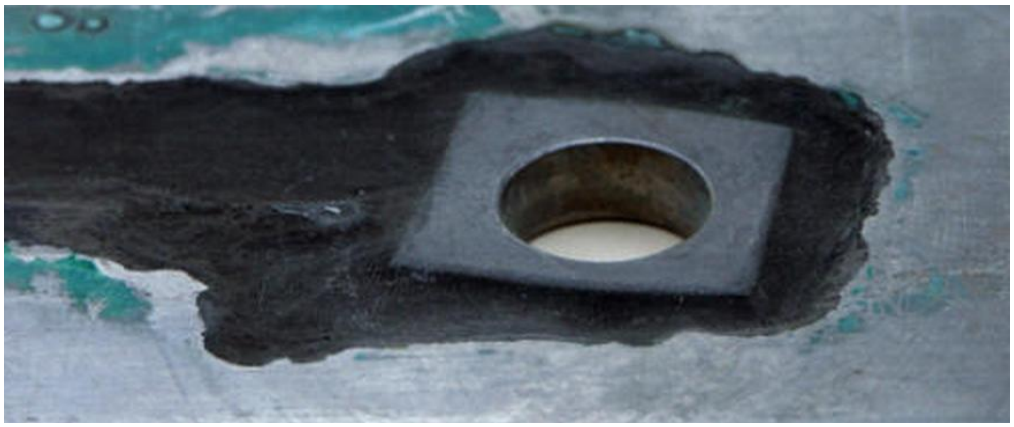

Figure 7 Crevice Corrosion Example 2

2.2.3 Pitting Corrosion

Similar to crevice corrosion, pitting corrosion is a localised form of corrosion, which occurs as a result of a breakdown of the otherwise protective passive film on the metal surface. Pitting corrosion is commonly found on passive metals and alloys, such as aluminium alloys and stainless steel alloys, when the ultra thin passive film is damaged either chemically or mechanically. The resulting pits can often appear rather small at the surface but in reality they may have larger cross section areas deeper inside the metal. The profile of the pit in terms of its shape, size and depth of penetration is found using metallography on a cross sectional sample. The American Society for Testing and Materials (ASTM) has a standard visual chart for rating of pitting corrosion which is shown in Figure 8 below (Zhang and others, 2015) describe the pitting process as being random, sporadic and stochastic in nature, and the prediction of the time and location of events extremely difficult. Pitting generally is focussed on a on a small section of the metal surface, and always causes failure by perforation or by starting stress corrosion cracks. It can be one the more destructive and undetectable forms of corrosion in metals (Tian and others, 2014) .

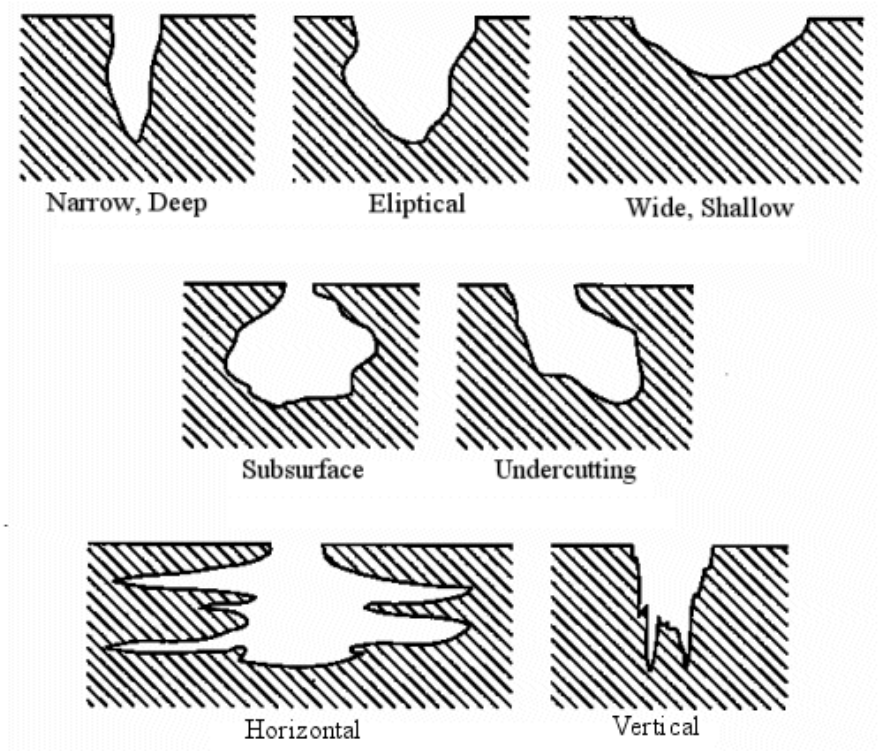

Figure 8 ASTM visual chart for rating pitting corrosion

Singh (First Edition) breaks the pitting corrosion into 4 main stages, these are indentified as:

- Initiation; Onset of pitting at the locations due to defects, imperfections in protective coating or at the local loss of passive films (as in stainless steels). Once started the corrosion activity is rapid

- Propagation; corrosion is driven by the potential difference between the anodic pit and the external metal surface surrounding the pit.

- Termination; Once the pit has stopped being an anode the corrosion is terminated, this is typically caused by filling the pit with corrosion product itself or by elimination of the corrosive environment

- Reinitiating; A pit can resume if the corrosion product is removed or the terminated pit is rewetted

The severity of pitting corrosion is controlled by factors such as the corrosive environment, chloride concentration, acidity of the electrolyte, concentration of the oxidiser, temperature, structural characteristics, and the material composition of metal or alloy. In addition localised damage to a passive oxide either mechanically or chemically, insufficient inhibitor coverage, and lack of uniformity in the structure of the metal due to impurities, can all contribute to pitting corrosion. (Popov, 2015)

2.2.3.1 Examples of Pitting Corrosion:

Some commonly seen examples of pitting corrosion are shown in the Figures 9 to 12 underneath. The first image (Figure 9) is of pitting corrosion in the bronze layer underneath chromium plating which has been removed. The second picture (Figure 10) shows corrosion pitting taking place on the blades of a steam turbine. Figures 11 and 12 show CO_2 and H_2S pitting respectively. Pitting in the CO_2 environment produces pits that are generally small with sharp edges and smooth rounded bottoms whereas in the sour H_2S system the pitting observed are more shallow round depressions with etched bottoms and sloping sides.

Figure 9 Pitting Corrosion Example 1

Figure 10 Pitting Corrosion Example 2

Figure 11 Pitting Corrosion Example 3

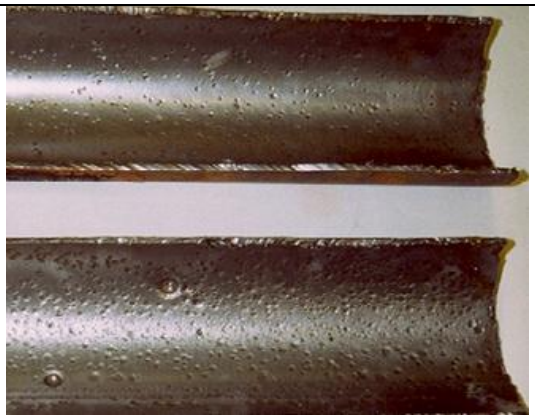

Figure 12 Pitting Corrosion Example 4

2.2.4 Erosion Corrosion

Erosion-corrosion is a form of material degradation encompassing mechanical wear together with electrochemical corrosion processes (Andrew and others, 2014). According to (Zeng and others, 2014) it is widely understood that during the erosion corrosion process the total material weight loss is greater than the sum of the pure mechanical erosion and electrochemical corrosion. This is a result of the erosion enhancing the corrosion and vice versa, commonly referred to as the synergistic effect. Although extensive investigation has be undertaken into achieving large knowledge levels of pure corrosion and pure erosion, the mechanism of synergy between erosion and corrosion is very complex and as such is not fully understood (Islam and others, 2013). Almost all metal alloys are at risk to some level of erosion corrosion, it can be particular destructive to alloys that passive by producing a protect film on the surface. In addition soft metals for instance copper and lead are also prone

to erosion-corrosion (Callister, Seventh Edition). Erosion can amplify the corrosion rate by removing the passive film, roughening the metal surface, increasing the mass transport process, whilst corrosion can promote erosion by weakening the grain and phase boundary, enhancing the surface roughness and/or dissolving the work hardened protective layer (Zeng and others, 2014). The onset of corrosion can be particularly harmful if the protective barrier of the alloy is not capable of rapid and continual reformation (Callister Seventh Edition). Erosion corrosion is often a common mode of failure in the oil and gas industries, power plants and petrochemical industries. Typical examples of failures that have occurred have been recorded in flow handling equipment where the fluid varies direction or the flow becomes turbulent, such as pipelines, valves and various rotating equipment (Wang and others, 2015).

Callister gives the following suggestions as ways to limit erosion corrosion:

- change the system design to eliminate the effects of impingement and turbulence on the material
- incorporate other materials that naturally resist the effects of erosion
- removing particulates and bubbles from the solution to reduce its ability to cause erosion

2.2.4.1 . Examples of Erosion-Corrosion:

The first erosion-corrosion example shown in Figure 13 is a bronze impeller from a centrifugal pump. The impeller was used in a chemicals transportation system and on studying the surface you can see the impeller has been attacked with a distinct flow pattern

Figure 13 Erosion-Corrosion Example 1

Shown in Figure 14, is the image of a carbon steel pipe used for transporting slurry at a mine. Looking at the picture the protective rubber lining has became delaminated which has led to the rapid onset of erosion-corrosion in the underlying steel pipeline.

Figure 14 Erosion-Corrosion Example 2

The final example of erosion-corrosion damage (Figure 15) is in a copper pipeline, where water swept pits similar to small horseshoe shaped features are present.

Figure 15 Erosion-Corrosion Example 3

2.2.5 Flow Assisted Corrosion (FAC)

Flow assisted corrosion (also referred to as flow accelerated corrosion) is a corrosion mechanism whereby the protective oxide layer on a metal surface dissolves into a stream of fast flowing water or a water-steam mixture. As the flow continues the oxide layer becomes thinner which as a result reduces the protective properties which in turn increases the corrosion rate. Eventually a steady state is reached as equal corrosion and dissolution rates develop and stable corrosion rates are maintained. It is possible that in some sections of the metal the oxide layer may be so thin as to expose the bare metal surface (Dooley and Chexal, 2000). The process of flow assisted corrosion can basically be split into three steps; (Gammal and others, 2010)

1. a series of electrochemical reactions at the metal-oxide interface
2. chemical erosion that dissolves the oxide layer of the metal.
3. mass transfer to the flow that is accelerated by the hydrodynamics of the fluid flow

Wall thickness reduction from corrosion due to flow is a particular problem facing carbon steel piping, tubing and vessels exposed to flowing water or wet steam (Dooley and Chexal, 2000). The corrosion can fracture the carbon steel piping in the most unpleasant of scenarios making it a major problem facing ageing power plants. As Ahmed (2010) discusses it can result in costly power station outages and expensive corrective actions and medical treatment injuries. (Dooley and Chexal, 2000) gives an example of what can go wrong when a pipeline ruptures in a nuclear power station due to FAC. In 1986 an elbow in the condensate system rupture caused four fatalities and tens of millions of dollars in repair costs and lost revenue. This is not a one off case where pipework has failed due to FAC:

"Over the years, FAC has caused hundreds of piping and equipment failures in all types of fossil, industrial steam, and nuclear power plants." (Dooley and Chexal, 2000)

In particular 90 degree piping elbows have been widely acknowledged as one of the most likely sections of pipe to fail due to FAC. This is due to the severe flow directional changes causing pressure drops along the elbow of the pipe and turbulent flows (Gammal and others, 2010). The location of the corrosion is typically localised due to the local high area of turbulence within the component (Ahmed, 2010)

The main factors causing FAC are classified by (Dooley and Chexal, 2000) as:

- Hydrodynamic, such examples include: flow velocity, pipe roughness, geometry of the flow path and steam quality
- Environmental, such examples include: temperature, pH, water impurities, reducing agent and oxygen concentration
- Metallurgical, such examples include: mainly the chemical composition of the metal. Chromium content is the steel is also an important factor. Where a

nominal content of chromium as low as 1% is found, the FAC rates will be negligible

2.2.5.1 Examples of Flow Assisted Corrosion:

Below is a sample of the problems that have been witnessed at numerous ageing power generation stations throughout the world. Image one (Figure 16 - top left image), shows the wall thickness of an 18" elbows that has decreased from 12.7mm to 1.5mm due to flow assisted corrosion. The second image (Figure 16 - top right image) is of an actual failure that occurred in a high pressure extraction line at Fort Calhoun nuclear power station in 1997. The final image (Figure 16 - bottom centre image) is also from a nuclear power station - Millstone Unit 2 - and shows the pipeline rupture at an 8 inch elbow of a moisture separator reheater in 1991. The flow assisted corrosion was not picked up due to the lack of condition monitoring such as ultrasonic thickness checks being missed on that section of pipe from the routine maintenance checks.

Figure 16 Examples of Flow Assisted Corrosion - (Ahmed, 2010)

2.2.6 Fretting Corrosion

Fretting corrosion is a wear process that is caused by small movements of one contacting face against another in a corrosion medium. The amplitude of the movement often falls in the range 1 - 100μm (Ren and others, 2015). It is a leading root cause in the reduction of the lifetime of mechanical assemblies, such as wind turbine gearbox bearings and in aeronautics, car industry and biomedical field sectors. The material wear rate is enhanced in the presence of a corrosive medium (Geringer and others, 2005). According to (Geringer and MacDonald, 2012), depassivation is induced due to mechanical friction destroying the protective oxide layer at a faster rate than the barrier layer can grow into the metal at zero barrier layer thickness. The key particulars for fretting corrosion include contact pressure between the two surfaces, displacement, relative velocity of the two surfaces and the presence of a crevice (Geringer and MacDonald, 2012). Chemical compositions and microstructures of the contact surface, rigidity, porosity of the contact surface and surface hardening are also important factors in fretting corrosion (Ren and others, 2015). The surface damage resulting from fretting corrosion is broken down by (Vingsbo and Soderberg, 1998) into three different regimes; Stick, Mixed Stick-Slip and Gross Slip. Stick conditions can be obtained through fretting at extremely low displacement amplitudes and topography of the scar shows very limited surface damage due to oxidation and wear, with no fatigue crack formation witnessed. Where the mixed stick-slip regime is observed the wear and oxidation effects are small. A mildly worn central area due to the sticking of the counterface surface and a highly worn area where the slipping of the counterface occurs is witnessed. Fatigue life may be significantly reduced as crack growth quickens. The fretting scar in gross slip regimes are characterised by sliding wear marks in the direction of the fretting. Severe surface damage as a consequence of extensive wear, with oxidation an integral part of this process are evident in the gross slip regime.

2.2.6.1 Examples of Fretting Corrosion:

Figure 17 shows an example of fretting corrosion on the outer diameter of a spherical roller. The cause of the fretting was a result of micro movement between the bearing and mating housing bore. More extensive corrosion is shown in Figure 18 on the outer race of a deep groove ball bearing.

Figure 17 Fretting Corrosion Example 1

Figure 18 Fretting Corrosion Example 2

2.2.7 Stress Corrosion Cracking (SCC)

Stress corrosion cracking (SCC) is the brittle failure of an alloy in the presence of a low constant tensile stress exposed to an environment. For SCC to occur the simultaneous presence of a corrosive environment and tensile stress on the material is necessary (Kain, 2011). This is further clarified by (Popov, 2015) when he explains that alongside the lasting tensile stresses to start SCC, the metal requires to be in contact with a corrosive environment such as water, chloride ion and oxygen. A major issue with SCC is that it is extremely difficult to detect until extensive corrosion has begun develop which in some cases can lead to catastrophic failures. (Popov, 2015). The three main factors that are necessary to cause SCC are shown in Figure 19. Material chemistry and microstructures due to alloy compositions and forming methods can significantly affect SCC. As (Shoji and others, 2011) details the composition of bulk alloy can change the passive film stability and phase distribution, he gives chromium in stainless steels as an example. Further to this, minor elements such as the carbon content in stainless steels can create variations in the passive film causing sensitisation – loss of alloy integrity. Differences in the oxidation rate can also be affected by impurity elements. Tensile stresses can be in the form of residual stress, directly applied stress via applied loads or low amplitude cycling. Stresses can also be introduced from welding, machining, grinding and heat treatment works. (Popov, 2015). (Kain, 2011) gives examples of how some alloys can experience SCC in certain environments, such as, austenitic stainless steels have been known to undergo SCC in the following environments; hot concentrated chloride solutions,

chloride contaminated steam, oxidising high temperature high purity water and polythionic acid.

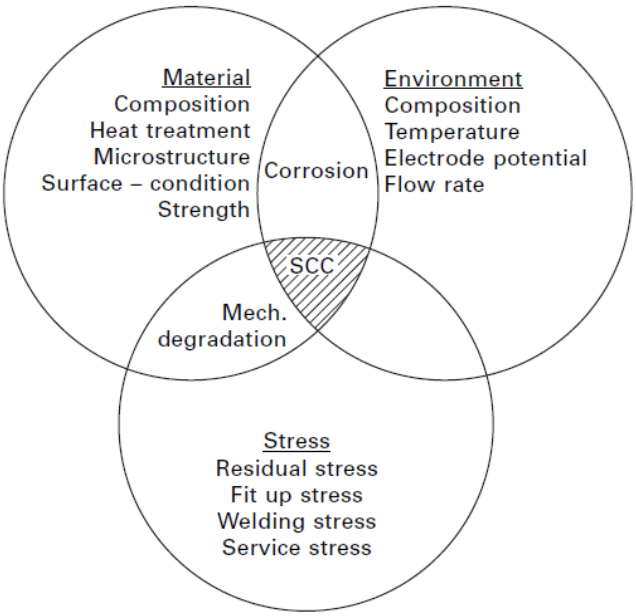

Figure 19 SCC Factors Required (Kain, 2011)

2.2.7.1 Examples of Stress Corrosion Cracking:

The example shown in Figure 20, is of a stress corrosion crack in an aluminium alloy used in an aircraft structure. The photomicrograph shown Figure 21 is of a crack initiation from the pit at the weld fusion line and its localised propagation in a tree root shape.

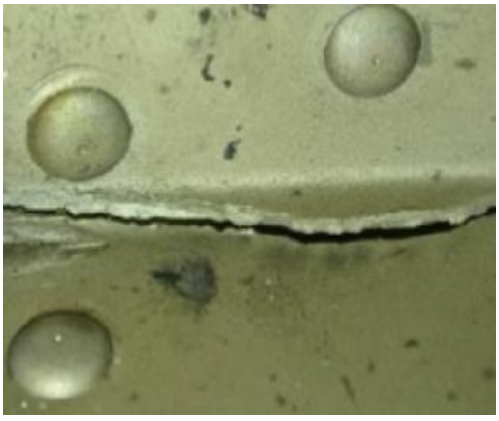

Figure 20 SCC Example 1 (Popov, 2015)

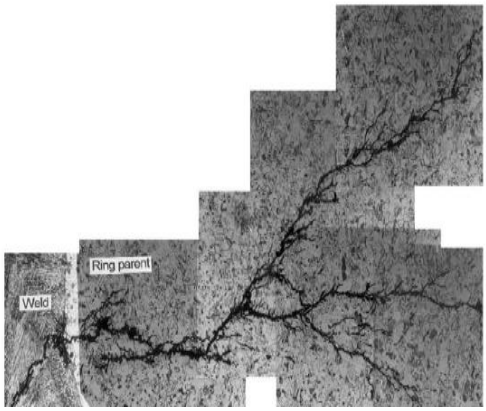

Figure 21 SCC Example 2 (Popov, 2015)

2.3 Stainless Steels

A large proportion of this project involves the testing and analysing of stainless steels corrosion resistant properties in various solutions. However before this can be undertaken an understanding of what they are, the difference between the various types and their changing compositions is required. The main quality of stainless steel is its resistance to corrosion, which can vary depending on the grade of stainless steel used, where the formation of a passive chromium oxide film (passivation) can protect the material (Holmes, Sharifi and Stack, 2014). The consumption of stainless steel has exceeded many other similar materials and grown at a compound growth rate of 5% over the last 20 years. Particular growth increases have been due to its increasing use in the construction industry and the rapid developments seen in China (Baddoo, 2008). Estimations by (Baddoo, 2008), show that in 2006 in the region of 4 million tonnes of stainless steel were used in some sort of construction application worldwide, this equated to 14% of the total quantity of stainless steel consumed. Stainless steels are iron base alloys that contain as a minimum 11% of chromium to provide adequate resistance to corrosion. The addition of nickel and molybdenum can also enhance the corrosion resistance of the stainless steel material (Callister, Seventh Edition). The three main classifications of stainless steel based on their crystalline microstructure resemblance are: Austenitic, Ferritic and Martensitic.

As a result of their higher chromium content and nickel additions austenitic stainless steels are the most corrosion resistant of the three main stainless steel classification (Callister, Seventh Edition). (Loto and others, 2012) describes austenitic stainless steels as having a wide spectrum of resistance to corrosion in chemical environments. If the very thin self healing film that protects the core metal from attack is damaged either mechanically or chemically it will reform exceptionally fast. Austenitic steels cannot be hardened by heat treatment but can be hardened significantly by cold working and are frequently referred to as non magnetic as their response to a magnet (hand held) is insignificant. Good formability, weldability and toughness particular at lower temperature are some of the reasons why austenitic stainless steels are the most widely used grade of stainless steel.

Similarly to austenitic stainless steels, ferritic stainless steels can't be heat treated so are hardened and strengthened by cold workings (Callister, Seventh Edition). Due to low carbon contents these types of steel are limited in strength at high temperatures when compared to other classifications, and typically have annealed yield strengths in the region of 275 to 350MPa (BSSA). A significant benefit of ferritic grade stainless steels is the lower and more stable cost which is a direct result of them not being alloyed with nickel. Ferritic steels are magnetic and display lower thermal expansion properties when compared to austenitic stainless steels (Baddoo, 2008). The main disadvantages of ferritics as described by the British Stainless Steel Association (BSSA) are:

- inadequate toughness - unacceptable at temperature below zero
- formability - due to lower ductility it is poor in stretch forming processes
- weldability - poor weld toughness when compared to austenitics are rapid grain growth in thick material sections are observed

Particular applications of ferritic stainless steels are in emergency housing, factories, roofs and their supports, cladding and tunnel lining (Baddoo, 2008)

Martensitic stainless steels are comparable to carbons steels. As a result of their high carbon content they are capable of being heat treated to improve hardening and strength properties of the material, however a consequence of this is the ductility and toughness of the alloy is decreased. These steels have a lower chromium content, typically in the region of 12-15%, than the others and as such they generally have a lower resistance to corrosion. Martensitic stainless steels are similar to ferritic in that they are magnetic. Due to the high strength and reasonable corrosion resistance the martensitic stainless steels are used in range of applications, such as gears, blades, surgical instruments and bearings. However when compared to austenitic and ferric classifications their use is not as great or widespread (BSSA) and (Callister, Seventh Edition).

A broad array of mechanical properties coupled with excellent corrosion resistance make stainless steels adaptable in their application. To summarise and allow contrasts to be made a list of commonly found stainless steels, arranged by classification, along

with the associated composition, mechanical properties and their typical applications are shown below in Figure 22 (Callister, Seventh Edition):

Table 11.4 Designations, Compositions, Mechanical Properties, and Typical Applications for Austenitic, Ferritic, Martensitic, and Precipitation-Hardenable Stainless Steels

AISI Number	UNS Number	Composition (wt%)[a]	Condition[b]	Mechanical Properties: Tensile Strength [MPa (ksi)]	Mechanical Properties: Yield Strength [MPa (ksi)]	Mechanical Properties: Ductility [%EL in 50 mm (2 in.)]	Typical Applications
			Ferritic				
409	S40900	0.08 C, 11.0 Cr, 1.0 Mn, 0.50 Ni, 0.75 Ti	Annealed	380 (55)	205 (30)	20	Automotive exhaust components, tanks for agricultural sprays
446	S44600	0.20 C, 25 Cr, 1.5 Mn	Annealed	515 (75)	275 (40)	20	Valves (high temperature), glass molds, combustion chambers
			Austenitic				
304	S30400	0.08 C, 19 Cr, 9 Ni, 2.0 Mn	Annealed	515 (75)	205 (30)	40	Chemical and food processing equipment, cryogenic vessels
316L	S31603	0.03 C, 17 Cr, 12 Ni, 2.5 Mo, 2.0 Mn	Annealed	485 (70)	170 (25)	40	Welding construction
			Martensitic				
410	S41000	0.15 C, 12.5 Cr, 1.0 Mn	Annealed Q & T	485 (70) 825 (120)	275 (40) 620 (90)	20 12	Rifle barrels, cutlery, jet engine parts
440A	S44002	0.70 C, 17 Cr, 0.75 Mo, 1.0 Mn	Annealed Q & T	725 (105) 1790 (260)	415 (60) 1650 (240)	20 5	Cutlery, bearings, surgical tools
			Precipitation Hardenable				
17-7PH	S17700	0.09 C, 17 Cr, 7 Ni, 1.0 Al, 1.0 Mn	Precipitation hardened	1450 (210)	1310 (190)	1–6	Springs, knives, pressure vessels

[a] The balance of the composition is iron.
[b] Q & T denotes quenched and tempered.

Figure 22 Designations, Compositions, Mechanical Properties and Typical Application for Stainless Steels (Callister)

2.3.1 Difference between types 304 and 316

The two types of stainless steels that will be tested during the project are austenitic type 304L and 316L. The letter "L" after a stainless steel number indentifies the steel as being a low carbon grade, for example looking at Figure 23 below, the 316 series of stainless steel contains a max carbon content of 0.08 whereas 316L has a 0.03 max content. The main reason for using a lower carbon grade of stainless steel is during welding as it reduces the tendency of the material to crack. In some cases the welds of

stainless steel with higher carbon contents have been seen to crack spontaneously as they cool down from the welding process.

(Composition in Weight Per Cent - Balance Iron)

UNS Number	EN Number	AISI Type	ACI Type	C	Cr	Mo	Ni	Structure[3]
517400[1]	1.4542	17-4PH[2]	CB-7CU-1	.07max	15.0-17.5	-	3.0-5.0	PH
541000	1.4006	410	CA-15	.15max	11.5-13.5	-	-	Mart
S43000	1.4016	430	-	.12max	16.0-18.0	-	-	Ferr
S30400	1.4301	304	CF-8	.08max	18.0-20.0	-	8.0-10.5	Aus
S30403	1.4306	304L	CF-3	.03max	18.0-20.0	-	8.0-12.0	Aus
S31600	1.4401	316	CF-8M	.08max	16.0-18.0	2.0-3.0	10.0-14.0	Aus
S31603	1.4404	316L	CF-3M	.03max	16.0-18.0	2.0-3.0	10.0-14.0	Aus
S31703	1.4438	317L	CG-3M	.03max	18.0-20.0	3.0-4.0	11.0-15.0	Aus
N08904	1.4539	904L[2]	CN-3M	.02max	19.0-23.0	4.0-5.0	23.0-28.0	Aus
S31803[1]	1.4462	2205[2]	CD3MN	.03max	21.0-23.0	2.5-3.5	4.5-6.5	Dup
S32205	1.4462	2205N[2]	CD3MN	.03max	22.0-23.0	3.0-3.5	4.5-6.5	Dup

Figure 23 Chemical composition of some common stainless steels (Covert and Turthill, 2000)

(Loto and others, 2012) refers to stainless steel type 316 having a higher level of corrosion resistance than that of the type 304. (Loto and others, 2012) draws on the detail that as type 316 consists of approximately 2% Molybdenum (Mo) the passive film is strengthened which consequently improves resistance to pitting corrosion attacks in reducing acids. This is reiterated by (Olsson and Landolt, 2003), whom describes Mo as an element with a strong beneficial influence on the pitting resistance of a stainless steel. The type 304 austenitic iron-chromium-nickel alloy and low carbon content is the most widely used of all the stainless steels, its applications are diverse and can be seen from a wide variety of industries such as beverage, electric power, architecture and petroleum refining. The obvious features that make type 304 so appealing are to do with its strong corrosion resistance across numerous environments, good formability, weldability and reasonable cost (Covert and Turthill, 2000). Type 316 is an austenitic iron-chromium-nickel-molybdenum stainless steel with superior corrosion resistance to that of type 304 and other chromium nickel steels when exposed to corrosive environments such as sea water. It is similar to the type 304 family in that is durable, easy to form and weld however it is slightly more expensive and contains less chromium. Where welding is required and improved

corrosion resistance a necessity type 316L is often recommended (Covert and Turthill, 2000).

2.4 Peat

Peat can be defined as the partially decomposed remains of plants and soil organisms which have accumulated in a water saturated environment in the absence of oxygen. Its primary uses is as a fuel source and a fertiliser. The build up of peat is increased when the new organic material on the surface surpasses the rate of decomposition and 'turn-over' of the surface material. Typically in the UK this occurs seasonally or year round due to the UK climate being wet and cold. The Scottish National Heritage (SNH Report) refer to peat as being far less dense than other soil materials, and it having the majority of its volume taken up by water when wet. The typical carbon content of peat found in the UK is approximately 52% by dry weight, further to this, the ratio of organic matter in peat is very high, typical percentages found are above 20-25% for 'peaty' soil and more than 50-60% organic matter for 'peat' (SNH Report). Peat has been portrayed as having some very unique characteristics for instance it acts as a water repellent barrier when very dry. These features of peat are as a result of the variety of organic compounds that are formed during the decomposition of living organisms. A photograph of the peat used during the testing phase of the project is shown below in Figure 24. The peat sample was taken from the inside surface of the main tunnel pipe at a hydro power station after the pipeline had been dewatered.

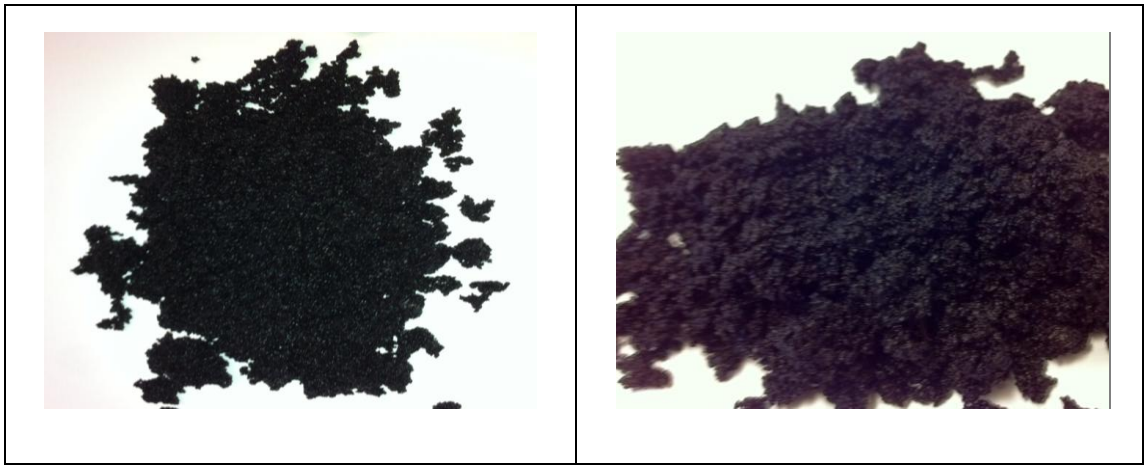

Figure 24 Peat Sample

2.4.1 Peat Location Maps

Shown below in Figure 25 is the map highlighting the depths of peat across Scotland. The historical data was collected during the 1980's. Whilst reviewing the map it is evident that the depth of peat is deeper in the North of Scotland than in the South-West, it is hoped that as two different solution samples have been taken from power stations in the North and South of Scotland for testing conclusions can be made to the peat depth and its effects. A further 1:250,000 scale map showing the location and extent of peat soils across Scotland is shown in Figure 26. Similar conclusions can be drawn to those above as the extent of 'peat soil' (dark purple) with organic matter of more than 50-60% is more evident in the North as Scotland than in the South-West where it is more likely that 'peaty soils' will be observed.

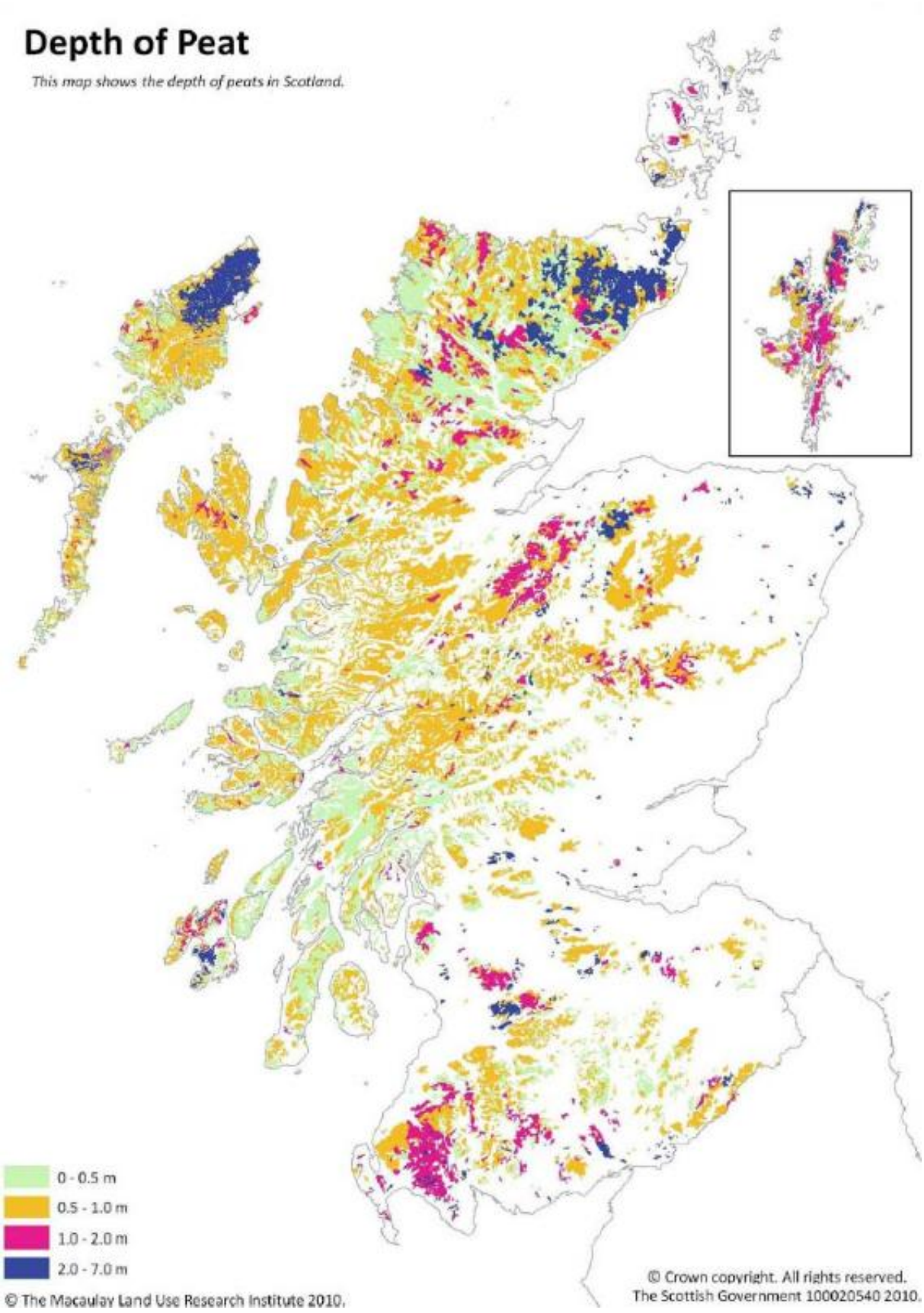

Figure 25 Depth of Peat in Scotland- (SNH Report)

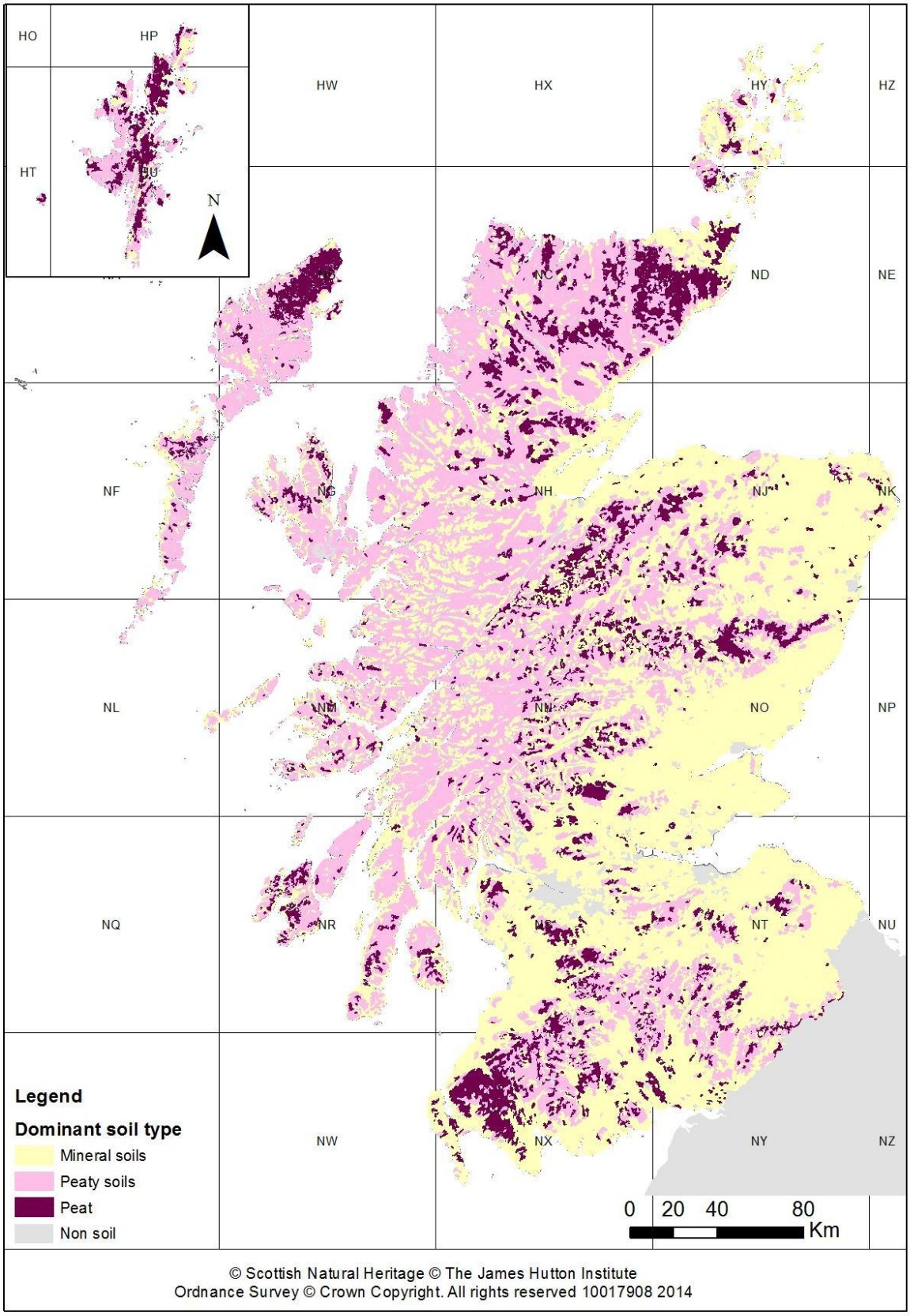

Figure 26 Location and extent of peat soils in Scotland- (SNH Report)

3 Hydro Power Station Site Inspection

To try and glean an understanding of the problems of peat contamination within hydro power stations across Scotland several site visits and discussions with local engineers were undertaken. However due to operational demands it proved difficult at times to get an intrusive inspection of the pipework systems. Fortunately, during one site visit planned routine maintenance was being performed by the local staff and the opportunity to witness the issues of peat contamination first hand was presented. As shown below in Figure 27 you can see pockets of peat sticking to the mesh of a control water rotary filter for the Main Inlet Valve (MIV) – a valve used as a safety device located upstream of the turbine within the power station building - the role of the rotary filter is to provide clean control water to the water operated actuator that is used to stroke the MIV. The MIV actuator requires reliable, stable and controllable supply to allow it to operate the valve appropriately, therefore any constraints to the flow can be a major problem. From speaking with the local staff this is a common issue and they regularly have to pressure wash the filter basket to remove the peat deposits.

Figure 27MIV Control Water Rotary Filter

During the visit maintenance on the cooling water system for the 2 main rotor shaft bearings was also being undertaken. Discussions with the local engineer highlighted

the problems he had with maintaining the required cooling water flow – to keep the bearing oil temperatures within their operating parameter - to the rotor shaft bearings as peat would over time choke sections of the pipework and valves that made up the system. Shown below in Figures 28 to 31 are a selection of the cooling water system photos that were taken throughout the day. Looking at them you can see clear evidence of peat build up which will restrict the flow. It is not entirely clear why the peat sticks to the carbon steel material but it can usually be removed from the cooling system by increasing the system water pressure, however this has an operational problem once the flows to the bearings are altered. A further problem that was discussed with the hydro engineer was to do with the cooling water flow control relay shown in Figure 29. The problem being the peat contamination prevents the intrusive disk in the flow from changing over the electric switch accurately therefore the software in the control room of the power station could be showing healthy or unhealthy flow when it is actually the opposite.

Figure 28 Cooling Water Isolating Valve

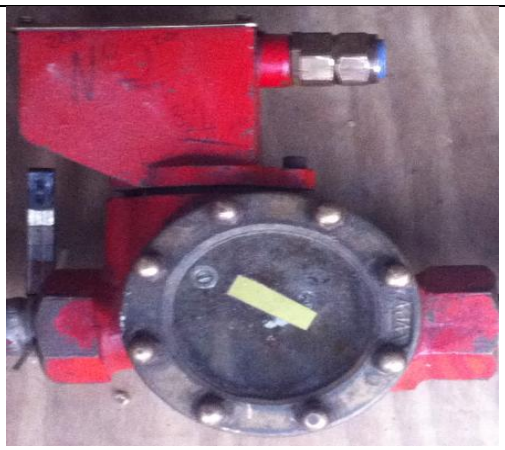

Figure 29 Cooling Water Flow Control Relay

Figure 30 Cooling Water Isolating Valve

Figure 31 Cooling Water Isolating Valve Close Up

Furthermore on further inspection at a different power station the flange shown in Figure 32 was found. Although no longer in service, conversation with the hydro engineer on site provided some interesting information on its history. The flange material is carbon steel and it has been welded onto the stainless steel pipework in the past. This method was attempted in the late 1980's to try and tackle the issue of galvanic corrosion whilst minimising the cost implications as it prevented the need to supply expensive stainless steel flanges that were suitably pressure rated. Although the weld was undertaken using dissimilar metal rods, you can see clear evidence of material wear due to galvanic corrosion along the weld. Looking at the image it is clear to see why this method is no longer standard in the hydro industry.

Figure 32 Flange from Power Station Visit – Galvanic Corrosion

4 Materials and Methodology

4.1 Experimental Variables Used

4.1.1 Material

Throughout the testing stage of the project three material samples in total were used and analysed. They are shown below in Table 4 alongside their % chemical composition. The main drivers for their selection was availability and cost in acquiring the material. Furthermore in the case of the two stainless steel samples they were chosen due to their frequent use within the hydro power industry.

Stainless Steel 316L									
C	Mn	Si	P	S	Cr	Mo	Ni	N	Fe
0.03 max	2.00 max	0.75 max	0.03 max	0.03 max	17 - 20	2 - 4	12 - 14	0.1	Bal
Stainless Steel 304L									
C	Mn	Si	P	S	Cr	Mo	Ni	N	Fe
0.03 max	2.00 max	0.75 max	0.045 max	0.03 max	18 - 20		8 - 12	0.1	Bal
Steel Gauge plate (A.I.S.I 0-1- Ground Flat Stock)									
C	W	Cr	Mn	V	Si	S	P	Fe	
0.95	0.5	0.5	1.2	0.2	0.25	0.035	0.035	96.37	

Table 4 Project Material Samples

4.1.2 Test Solutions -

The solution that the three metals were immersed in was changed during each test. In total eight samples were taken and used during the experimentation phase. The solutions used are listed below in Table 5.

Sample Number	***Solution Name***	***Comments***
1	De-ionised Water	Taken from University of Strathclyde Advanced Material Research Laboratory

2	Power Station A	Sample taken from the tailrace* of a hydro power station in the North of Scotland
3	Power Station B - Sample 1	Sample taken from the tailrace of a Power Station in the South-West of Scotland. Unfortunately at the time of taking the sample the machine was not running at the time so it is not entirely reflective of the solution going through turbine.
4	Power Station B - Sample 2	Sample taken from the same station in the West of Scotland. However the location of where the sample was taken was inside the pipeline upstream of the turbine house.
5	20% Peat	Solution was made up of 20% Peat and 80% De-ionised Water
6	40% Peat	Solution was made up of 40% Peat and 60% De-ionised Water
7	5% Peat	Solution was made up of 5% Peat and 95% De-ionised Water
8	10% Peat	Solution was made up of 10% Peat and 90% De-ionised Water

Table 5 Project Solution Samples

*tailrace is the path through which water is discharged out of the hydro power plant after power generation

4.2 Testing Methodology

4.2.1 pH Testing

To determine the degree of acidity/alkalinity of the eight solutions a pH test was performed. Prior to any testing taking place and to ensure the accuracy of results the pH meter had to be calibrated. Calibration was achieved through the use of buffer solutions containing 7.01 and 4.01 solutions that were purchased from RS components. Once calibrated, 100ml of each sample was tested individually for 30

minutes with readings reviewed every 5 minutes. The final results of the testing can be seen below in Table 6.

Sample Number	***Solution Name***	***pH Result***
1	De-ionised Water	6.51
2	Power Station A	5.97
3	Power Station B - Sample 1	7.62
4	Power Station B - Sample 2	6.14
5	20% Peat	5.12
6	40% Peat	4.17
7	5% Peat	5.42
8	10% Peat	5.38

Table 6 pH Test Results Samples A - H

It is expected that the solutions lower in pH value will enhance the corrosion rate whereas those higher in pH will reduce the rate of corrosion. These observations have been drawn from (Fattah-alhossenini and Vafaeian, 2014) who studied the effect of solution pH on the electrochemical behaviour of AISI 304 and AISI 430 ferritic stainless steels and drew the following conclusion:

1. Potentiodynamic polarization curves showed that the corrosion current density of both AISI 304 and AISI 430 stainless steels increased with decreasing pH

2. Increasing the solution pH offers better conditions for forming passive films with higher protection behaviour, due to the growth of much thicker and less defective films.

4.2.2 Electrochemical Testing - Polarisation Curves

Electrochemical experimental methods are used to quantify the corrosion properties of metals under various conditions. A potentiodynamic approach where the applied potential is increased with time while the current is continually monitored was favoured over other possible approaches. During the testing polarisation curves where produced, showing a plot of current density (or log |i|) versus electrode potential (E)

for the specific electrode-electrolyte combination. Interpretation of the curve will provide information on, the kinetics of the corrosion reactions, whether active/passive and/or passive/transpassive transitions have taken place, and the measured corrosion current allowing corrosion rates to be calculated.

4.2.2.1 Test Apparatus

The electrochemical tests were conducted in a corrosion cell with three-electrode system using a Gill AC electrochemical potentiostat (ACM instrument, UK), as shown below in Figure 33. The potentiostat was linked to the Core Running/Sequencer software located on a nearby computer which allowed for the polarisation curves to be produced. To ensure a stable and reproducible potential in the solution the working electrode (WE) was measured against the reference electrode (RE) by the means of a voltmeter. A saturated calomel electrode (SCE) was used as the reference electrode which consisted of mercury covered with a paste of mercurous chloride and mercury in a chloride solution. The Auxiliary Electrode (AE) was of a Platinised-Titanium (Pt-Ti) mesh formation.

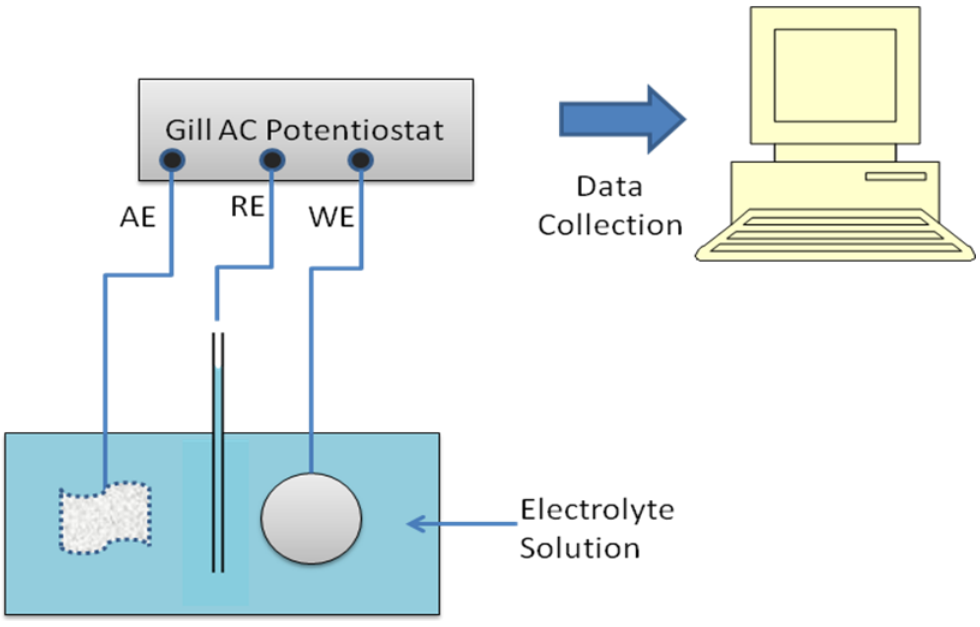

Figure 33 Test Set-up

4.2.2.2 Test Parameters

In total twenty four experiments were undertaken - three material samples x eight solutions of varying pH - which will be analysed in the results section. Where possible

the only variable changed during each test was the solution the metal was submerged in. To prevent any cross contamination between samples the testing apparatus was thoroughly cleaned after each test. The exposed surface area of the material was set to 1cm² with the remaining material suitably insulated. A sweep rate of 33.33mV/min was kept constant throughout the testing, as a reminder the sweep rate is the process by which the cyclic sweep from the start potential to reverse potential over a set number of cycles is controlled. It was hoped that the start potential and reverse potential would be set at -500mV and 500mV respectively for all test conditions, however due to reasons that will be discussed later this was not possible for the AISI 0-1 steel gauge plate material. Subsequently the AISI 0-1 material start potential was set at -750mV, the reverse potential remained at 500mV. Varying the start potential whilst maintaining similar sweep rates had a direct effect on the exposure time of the materials, both the stainless steel samples had a test duration of 30 minutes whereas the steel gauge plate was slightly higher at 37.5 minutes.

5 Results and Discussion

5.1 pH Results

When reviewing the pH test results the value for de-ionised water is as expected, however the two samples taken from the tailrace of Power Station A (sample 2) and B (sample 3) are noticeable different. The acidity of sample 2 is just less than 100 times more acidic than that of sample 3. A possible reason could due to the differing depths and extent of peat soils found in the North and South-West of Scotland having an effect on the water solution going through the power station. A further possibility could be that the sample of Power Station B was taken whilst the station was out for major refurbishment work and the solution is more likely to be a reflection of the rain water and foreign matter mix, whereas the water solution from Power Station A was collected whilst the machine was operational. A general statement can be made that the increasing addition of the peat compound produces an increasing acidic solution when comparing the four peat and de-ionised water mixtures.

5.2 Polarisation Curves

The individual polarisation curves for the material 316L, 304L and AISI 0.1 Ground Flat Stock can be found in Appendix 1.

5.2.1 Stainless Steel 316L Results

The polarisation curves for electrochemical tests 1 to 4 performed on the stainless steel 316L material are shown below in Graph 1. The trend colours shown in the graph relate to the following test solutions that the material was submerged in for the duration of the test: blue = de-ionised water solution (Test 1), red = power station A sample (Test 2), green = power station B - sample 1 (Test 3), and purple = power station B - sample 2 (Test 4)

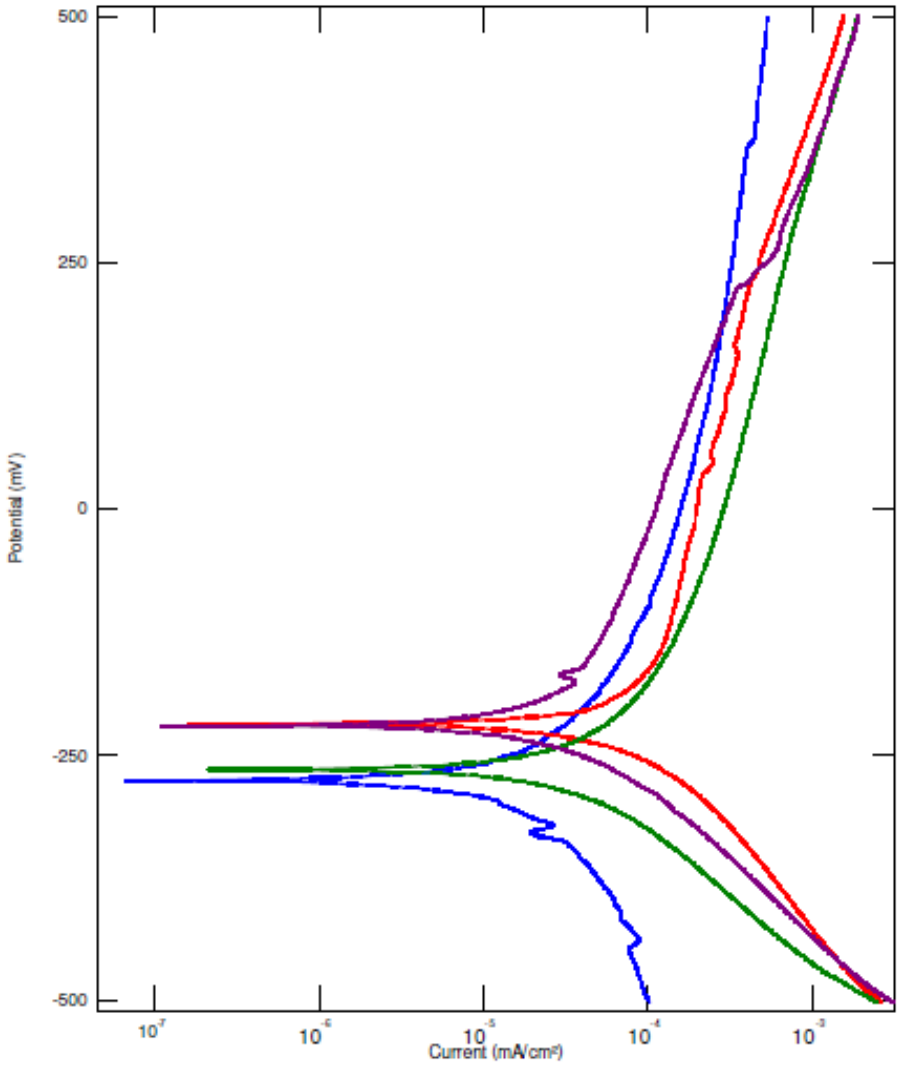

Graph 1 Stainless Steel 316L - Combined Test 1 to 4

Interpreting the graph it looks as though a dip has occurred during the testing of the stainless steel 316L sample in the cathodic region whilst in a solution of de-ionised water, which may indicate an active/passive transition occurring. However this appears to be too small of a dip and could in reality be the result of a lack of smoothing of the results after testing. When the trend of the Power Station B Sample 2 is analysed, a rapid increase in current density at 250mV is observed. It is possible that this increase could suggest the presence of pitting corrosion forming on the material surface. The rate of corrosion is lowest in the de-ionised solution which is as expected. From taking a closer look of the effects of the two water solutions taken from the North and South-West of Scotland, shown in Graph 2 below, we see that both trends show slight linearity in the cathodic region. The corrosion appears to be uniform with only activation polarisation occurring and no clear signs of surface films

forming. A difference in the corrosion potential is seen, Power Station B corrosion potential has shifted in the cathodic direction by 10mV. A possibility for this could be due to the difference in the pH of the two test solutions.

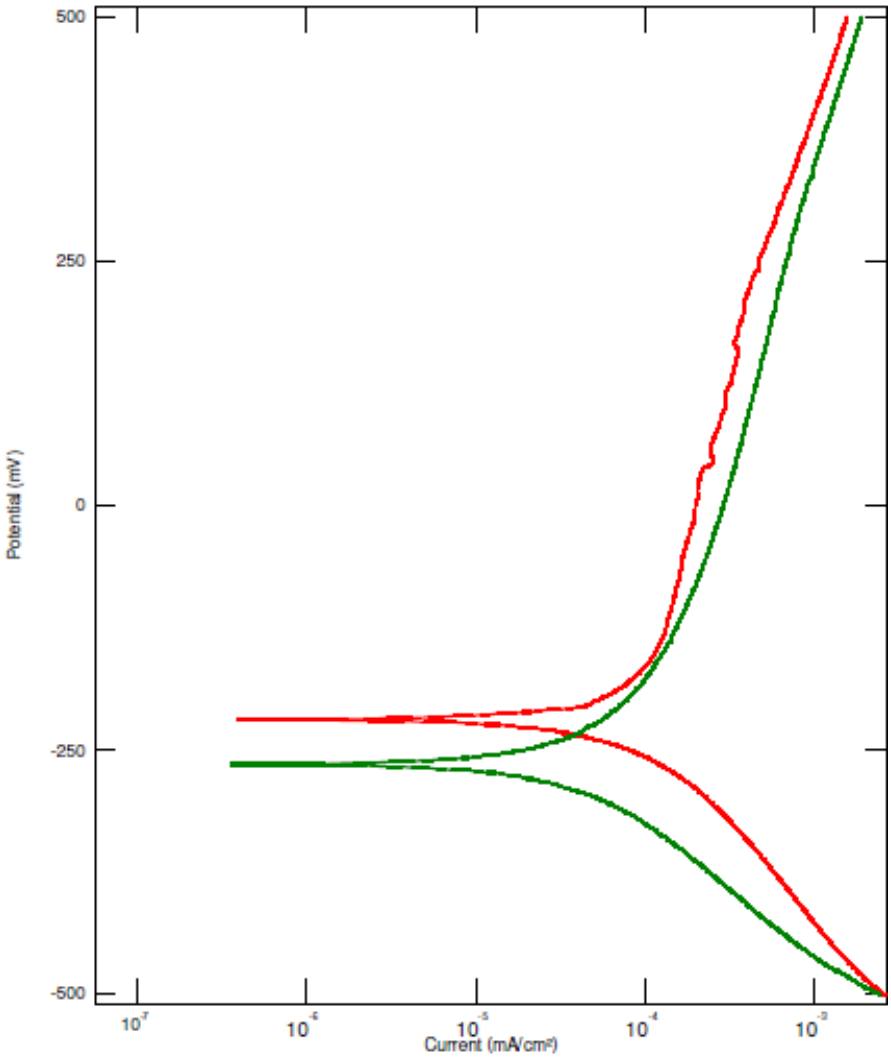

Graph 2 Stainless Steel 316L - Combined Tests 2 and 3

The stainless steel 316L polarisation curves for the varying peat and de-ionised water solutions (tests 5 to 8) are shown in Graph 3 below. The trend colours shown in the graph relate to the following test solutions that the material was submerged in for the duration of the test: blue = 20% peat and 80% de-ionised water solution (Test 5), red = 40% peat and 60% de-ionised water solution (Test 6), green = 5% peat and 95% de-ionised water solution (Test 7), and purple = 10% peat and 90% de-ionised water solution (Test 8). Looking at the graph as a whole we can see the corrosion potential was approximately the same for all results up to 20% peat, however in the case of the

40% test solution the corrosion potential drops by approx 30mV in the cathodic direction. This may be the result of the more acidic solution making the material less corrosion resistant. The corrosion current with the varying peat concentrations draws a similar conclusion to that above as the current density for the 40% peat is approximately one order of magnitude higher, highlighting a higher rate of corrosion. All four trends appear to show some forms of active/passive transitions although far less obvious in 10% peat results. The active/passive transitions appear to be more severe in 20% peat solution with rapid increases in current density observed which could mean the likelihood of pitting is greater with more pits propagating.

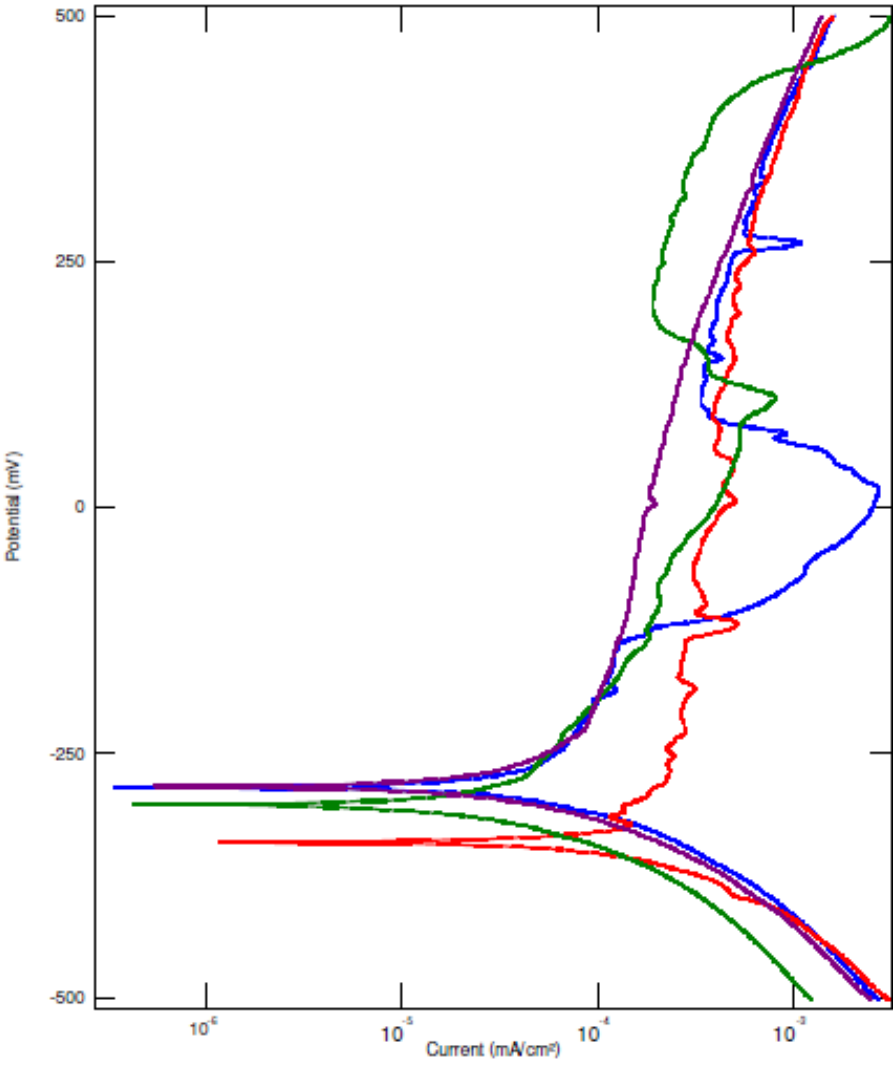

Graph 3 Stainless Steel 316L - Combined Test 5 to 8

5.2.2 Stainless Steel 304L Results

The 304L material polarisation curves for the test solutions used in experiments 1 to 4 are shown in Graph 4. The tests are equivalent to the following colours shown on the graph: blue = de-ionised water solution (Test 1), red = power station A sample (Test 2), green = power station B - sample 1 (Test 3), and purple = power station B - sample 2 (Test 4). Looking at the graph it can be seen that the current density of tests 2 to 4 are almost identical whereas the de-ionised water solution is approximately one order of magnitude less thus highlighting a reduced corrosion rate in the de-ionised water case. The anodic region is noticeable higher in the de-ionised solution with a corrosion potential of ~0mV, this typically shows that the material is more corrosion resistant, however as the material was the same for all four test cases the only probabilistic conclusion that can be drawn is that the de-ionised solution is less corrosion effect on the material when compared to the other three.

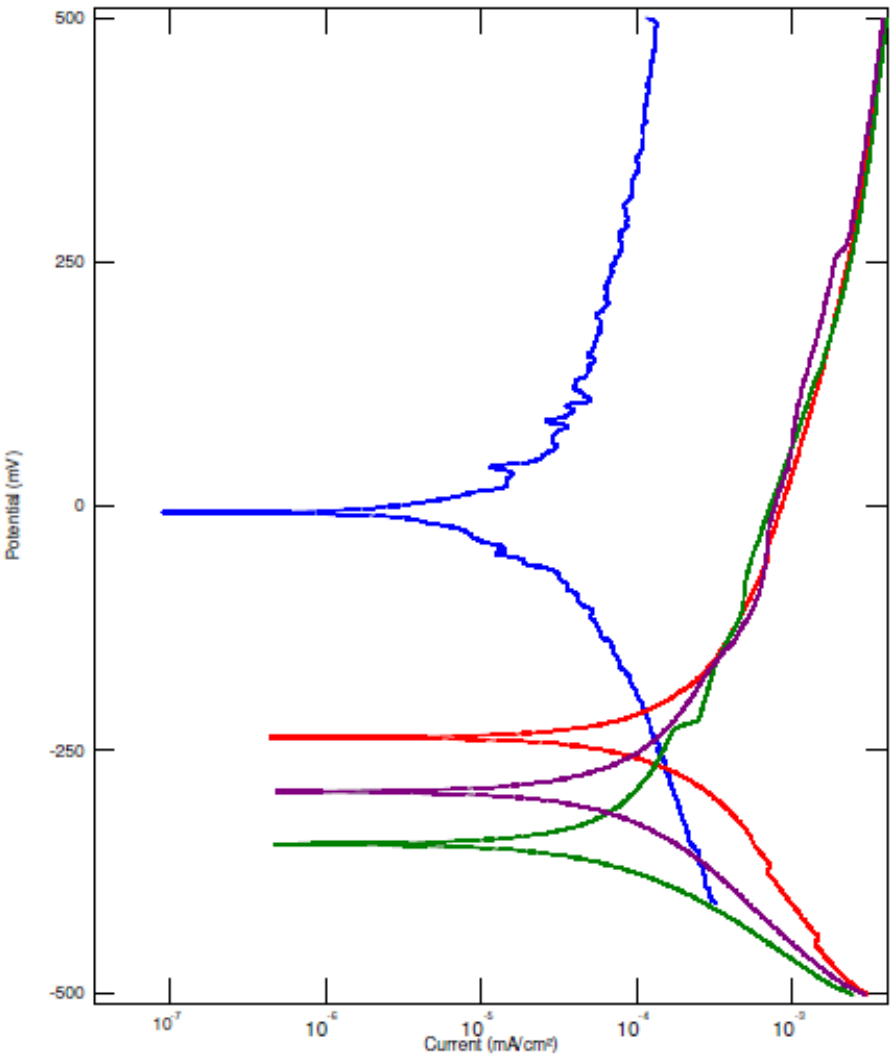

Graph 4 Stainless Steel 304L - Combined Test 1 to 4

Similarly to stainless steel 316L, a more in-depth investigation of the two power station samples is undertaken for the 304L sample, the results are shown in Graph 5. There is a short rapid rise in the current density at -250mV for the power station B sample, this could be highlighting a change in the material surface. On close inspection a similar occurrence appears to happen for the power station A solution at ~0mV, however this is somewhat less severe and may actually be the result of noise in the environment affecting the result. We can also determine from the graph that the passivation of power station A occurs at a higher potential than that of power station B.

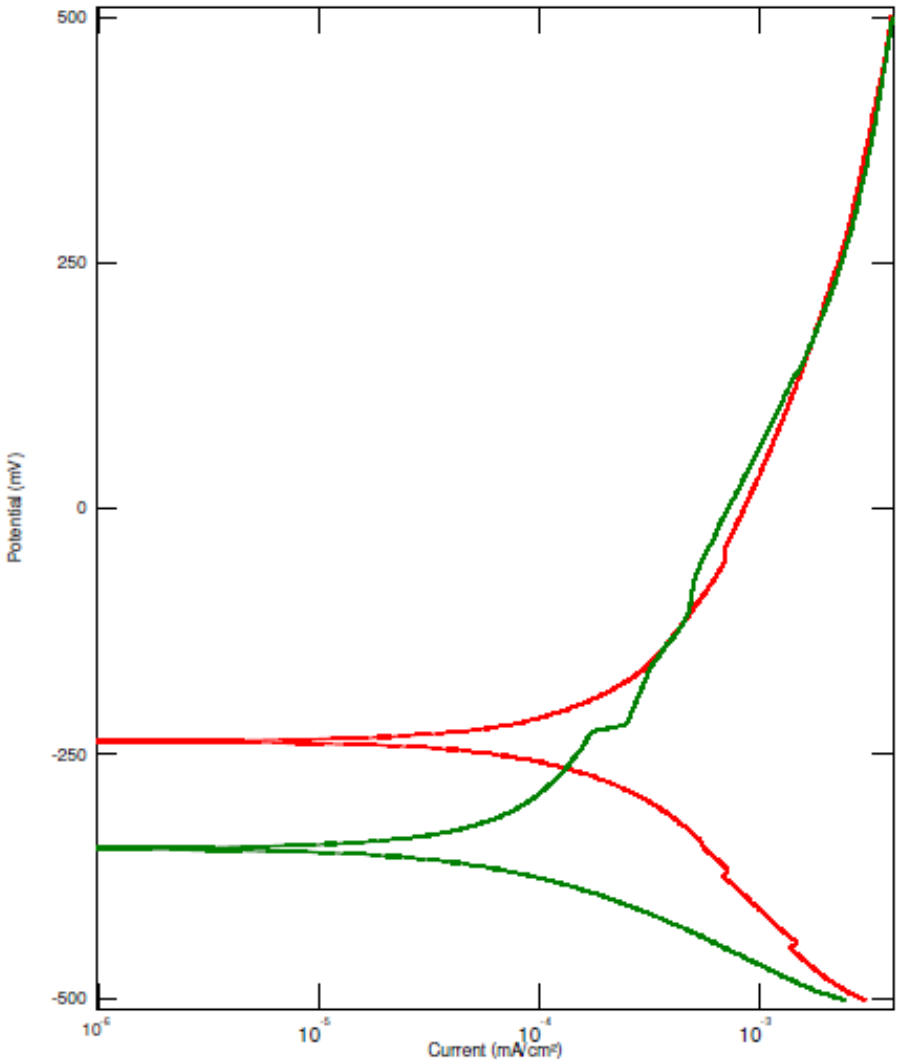

Graph 5 Stainless Steel 304L -Combined Tests 2 and 3

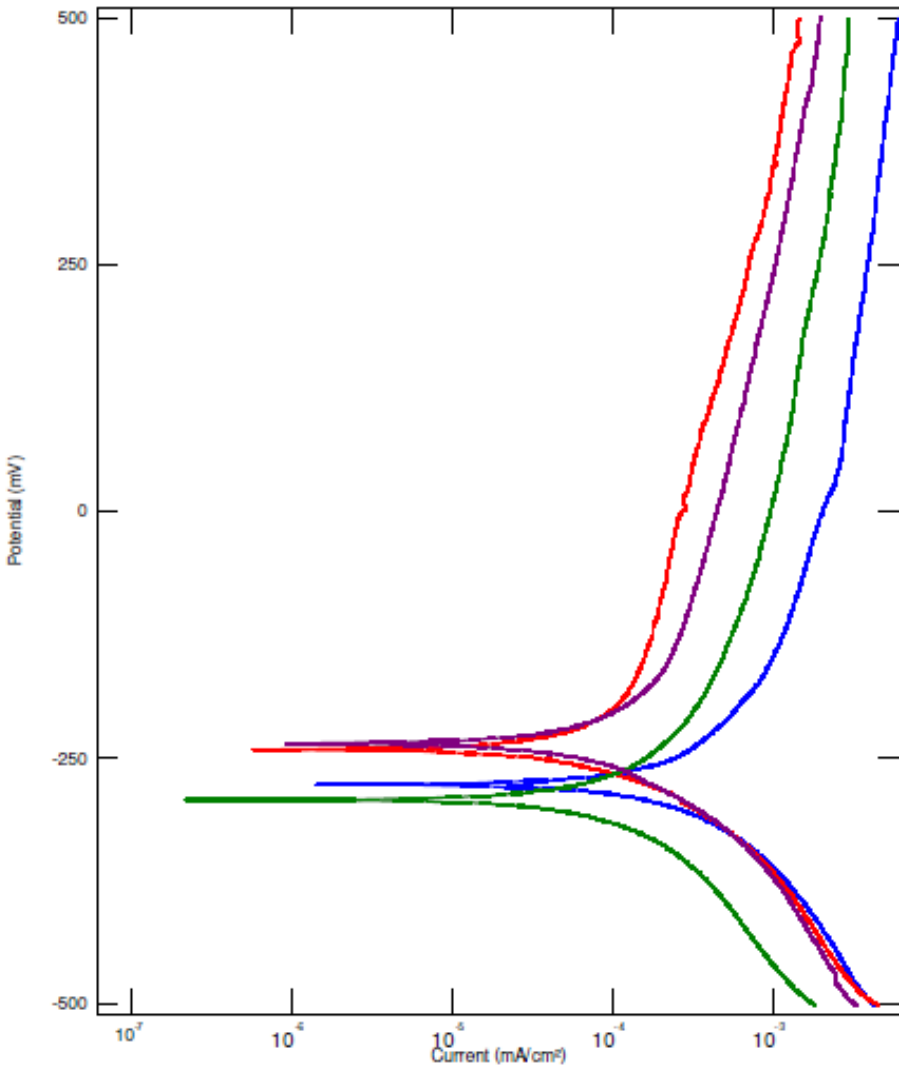

Graph 6 Stainless Steel 304L - Combined Tests 5 to 8

Graph 6 above shows the combined polarisation curves that have been created for the changing peat and de-ionised water concentrations (tests 5 to 8) for the stainless steel 304L material sample. The trend colours shown in the graph relate to the following: blue = 20% peat and 80% de-ionised water solution (Test 5), red = 40% peat and 60% de-ionised water solution (Test 6), green = 5% peat and 95% de-ionised water solution (Test 7), and purple = 10% peat and 90% de-ionised water solution (Test 8). The evaluation of the graph does not highlight any significant observations, however a wider conclusion that could be made is the higher chromium content in the 304L material is providing more of a corrosion resistance to the differing peat solutions than that of the 316L material. This is highlighted by the lack of corrosion signs being observed in the anodic region of the polarisation curves.

5.2.3 Combined 304L and 316L Results

A selection of polarisation curves for the testing of both stainless steel 304L and 316L are shown below in the following graphs, the rest can be found in Appendix 1. Where a direct comparison is made between the two iron based alloys in a single solution the blue line of graph is a representation of the 316L material and the red line that of the 304L material.

Evaluating the polarisations curves in Graph 7 below for the two power station tailrace samples for the two different stainless steels we notice that corrosion rates for all four tests are almost identical. The only significant observation is found when comparing at the corrosion potential of the stainless steel 304L with power station B (purple trend) against that of the rest (red trend = 316L with power station A, blue = 316L with power station B, and green = 304L with power station A). The corrosion potential of 304L (power station B) is at approximately -350mV whereas the others are approximated -250mV, this decrease in passivation characteristic could be a result of the solution penetrating the passive film causing the film to breakdown.

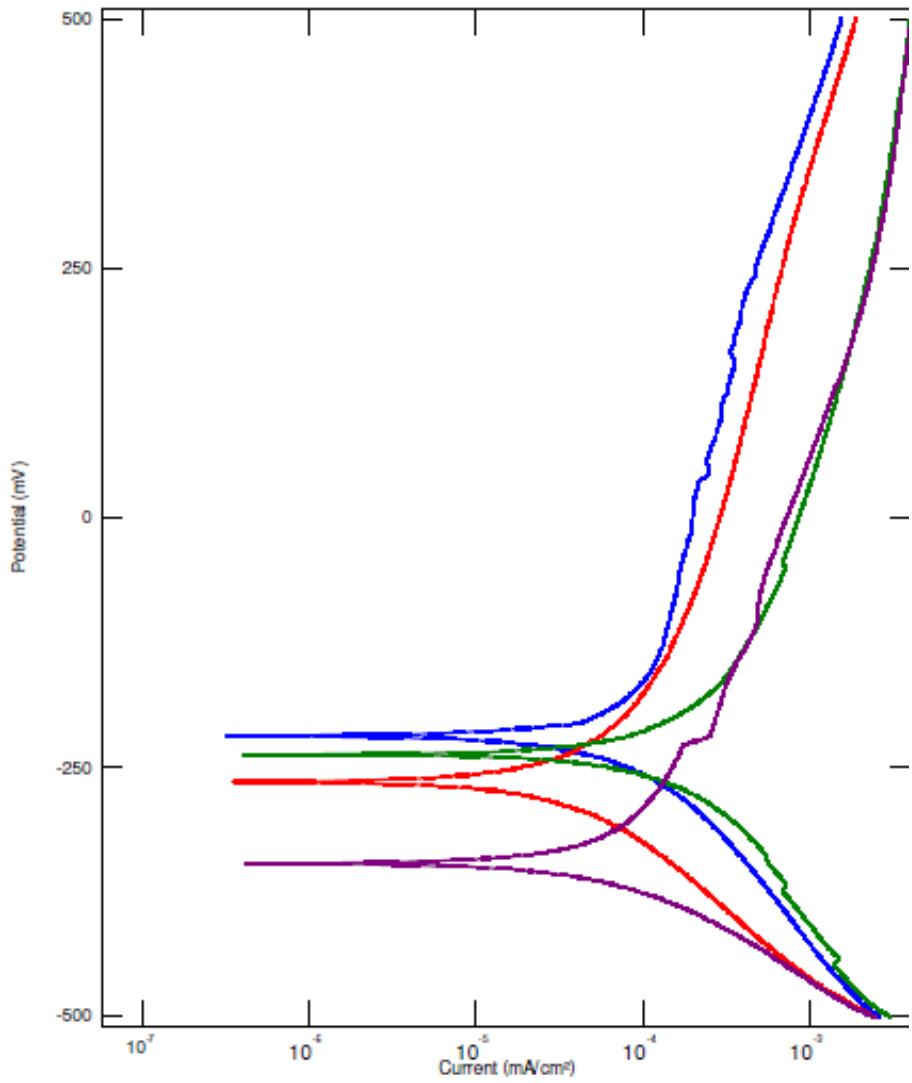

Graph 7 Stainless Steel 304L and 316L - Tests 2 and 3

To allow for a comparison to be made between the stainless steel type 304L and 316L materials in the differing peat concentration scenarios Graphs 8 to 10 have been produced. The graphs show the peat concentrations at 20%, 40% and 5% respectively. Reviewing the results for the 20% peat concentration in Graph 8, we can see that two different trends have been created. The 316L material appear to be showing active/passive transitions whereas the 304L results looks relatively uniform. A similar trend continues with the 40% peat in Graph 9, although the active/passive transition is less severe than that discussed above. Further to this the corrosion potential is approximately 100mV lower in the 306L result, highlighting that the 304L material may be more corrosion resistant. The tendency of the 316L material to show an active/passive transition in the anodic region is shown again with 5% peat solution in Graph 10 below. A final observation that can be made when looking at the 3 graphs is

that in each of the peat solutions the 304L material appears to have experienced only activation polarisation only with no surface films being formed.

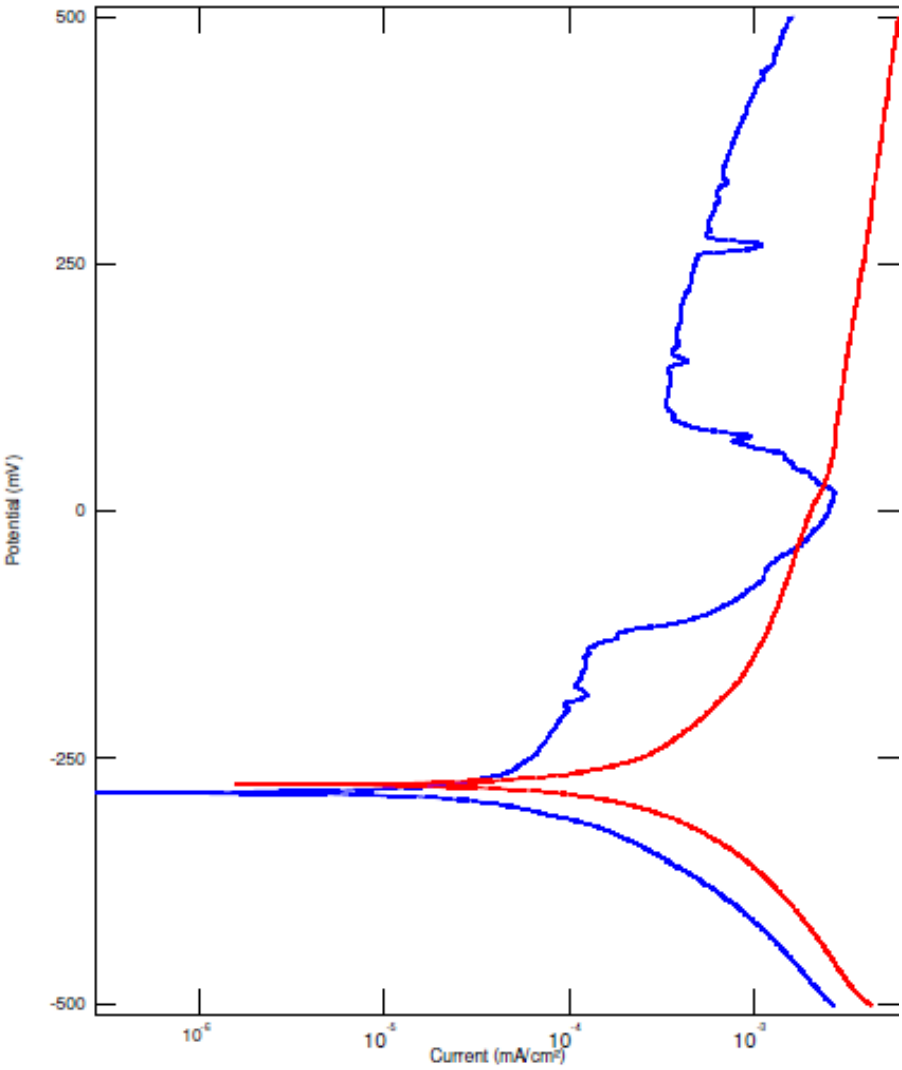

Graph 8 Stainless Steel 304L and 316L - Test 5 20% Peat

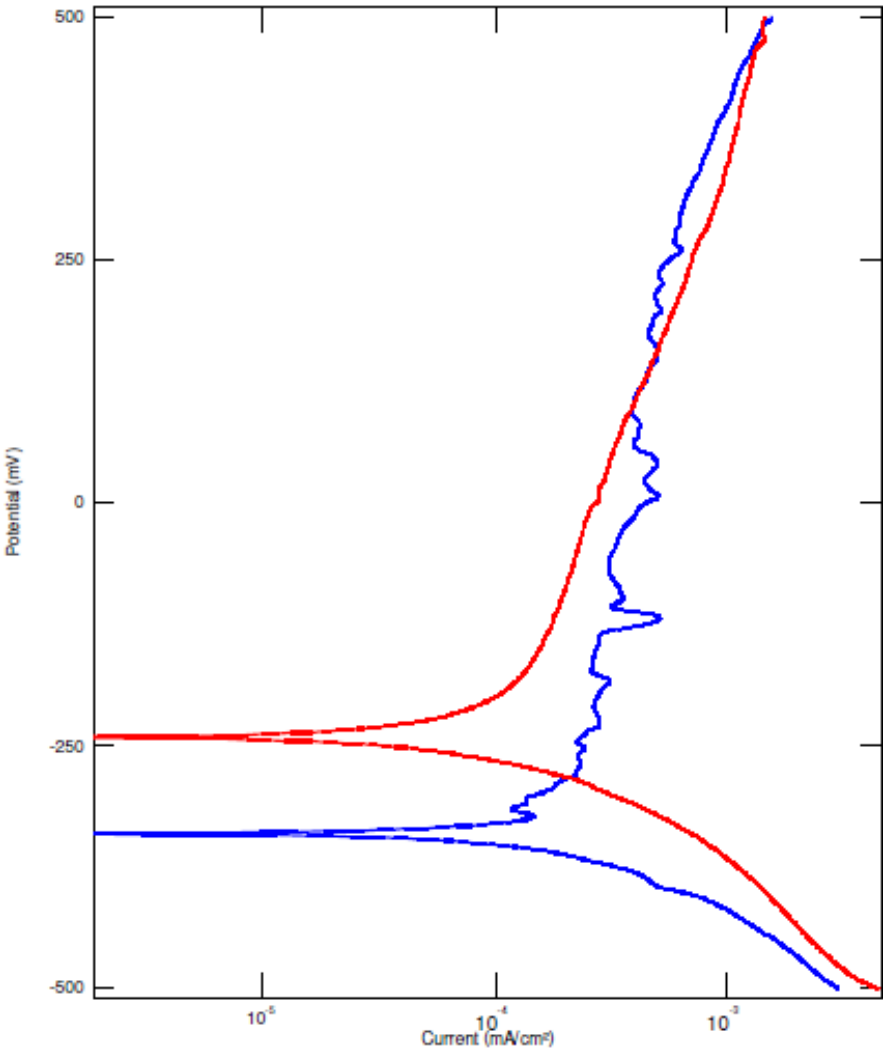

Graph 9 Stainless Steel 304L and 316L - Test 6 40% Peat

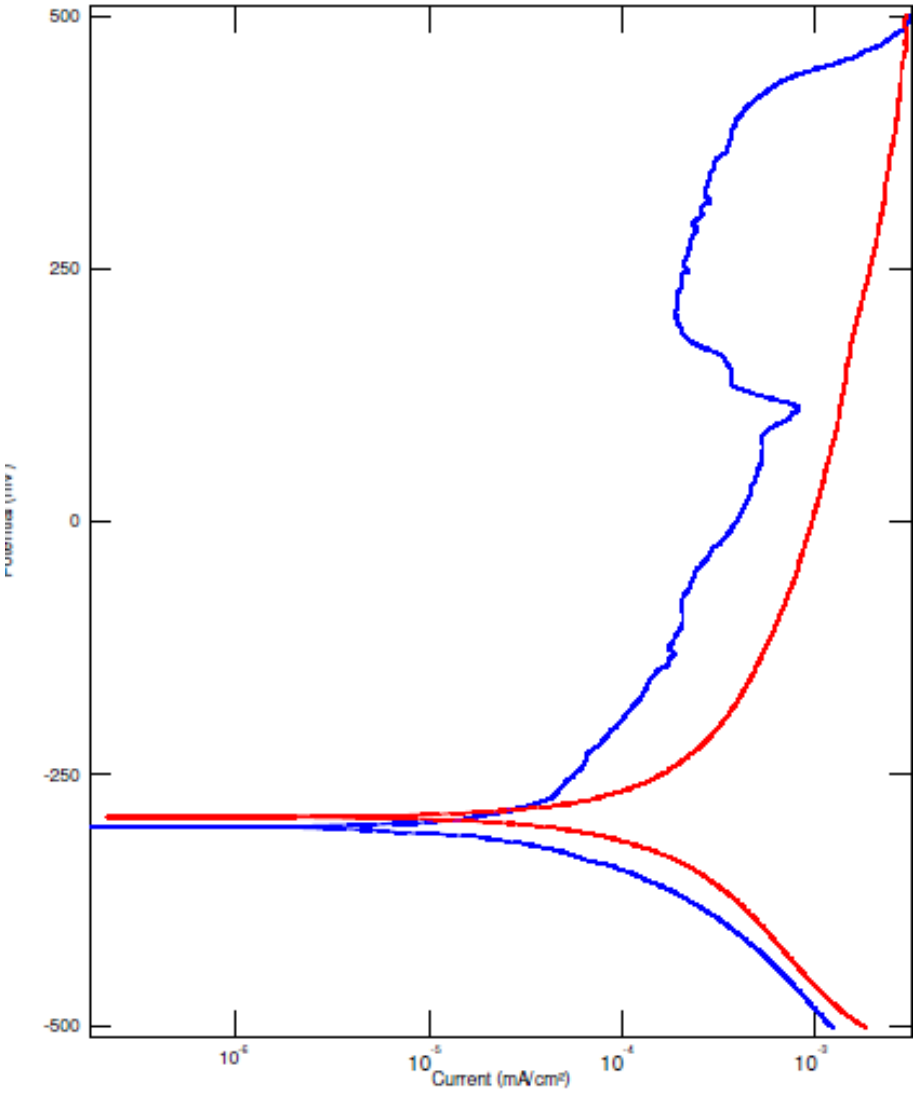

Graph 10 Stainless Steel 304L and 316L - Test 7 5% Peat

5.2.4 Combined 304L, 316L and AISI 0.1 Ground Flat Stock Results

A collection of polarisation curves showing a comparison of the testing undertaken for both stainless steels 304L and 316L and the AISI 0.1 Ground Flat Stock are shown below in the following graphs, the rest can be found in Appendix 1. In each of the cases the blue line of graph is a representation of the 316L material, the red line that of the 304L material and the green AISI 0.1 Ground Flat Stock.

The polarisation curves for when the three materials are in a solution from power station B (sample 2) are shown in Graph 11 below. We can see that the AISI 0-1 corrosion potential appears at a lower value than the 304L and 316L materials, with a noticeably higher current density, which is indicating that the material is being less resistant to corrosion.

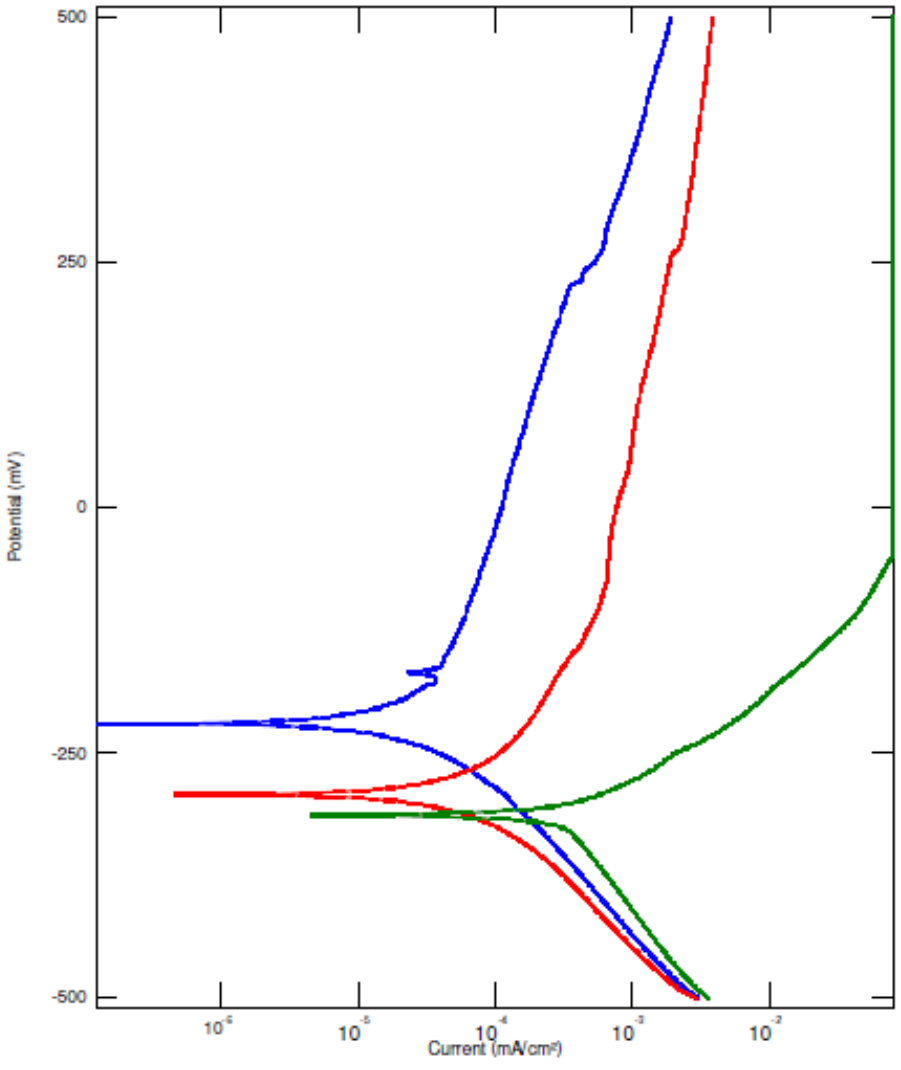

Graph 11 Combined 304L, 316L and AISI 0.1 Ground Flat Stock - Power Station B Sample 2

Comparison of the three materials with the changing peat concentrations are shown below in Graphs 12 to 15. It is worth noting that the start potential for AISI 0-1 ground flat stock was altered from -500mV to -750 as the passive region of the sample was being broken straight away during testing. Subsequent research has shown that typically potentiodynamic tests normally have a start potential of at least -1000mV (often lower), this is to cover the cathodic protection section in the majority of materials. Reviewing the results for the 20% peat solution as shown in Graph 12, we can see the corrosion potential is at -700mV for the AISI 0.1 material whereas the stainless steel samples are much higher at -250mV. Further to this the current density is higher signifying poorer corrosion resistance. With the 40% curve in Graph 13, we can see the passive region for the ground flat stock is almost broken straight away at -750mV. There appears to be no protective film that is formed as a rapid increase in current density is seen resulting in a higher corrosion rate. Reducing the peat concentration from 40% to 5% in Graph 14, raises the corrosion potential of AISI 0-1 to -400mV which is closer to the stainless steel materials, however the corrosion rate is still observed as been higher in the ground flat stock material. The anodic oxidation curve is almost linear showing higher active corrosion. The final graph of 10% peat is revealed in Graph 15. Analysing the graph in a similar way to the other 3 highlights that the stainless steel materials are providing more resistance to corrosion than that of the AISI 0-1 steel as they passivate at a higher potential. The stainless steel type 304L sample in particular appears to be showing uniform corrosion with no surface films needing to be formed.

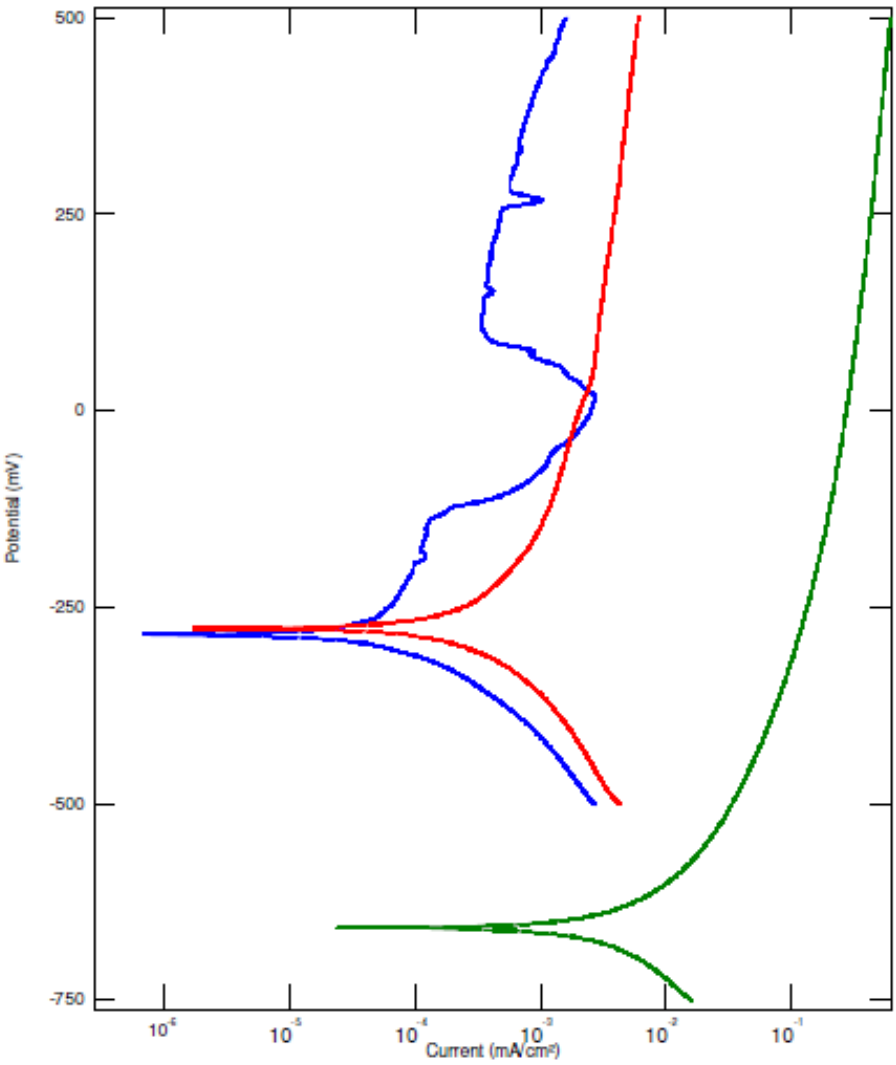

Graph 12 Combined 304L, 316L and AISI 0.1 Ground Flat Stock - 20% Peat

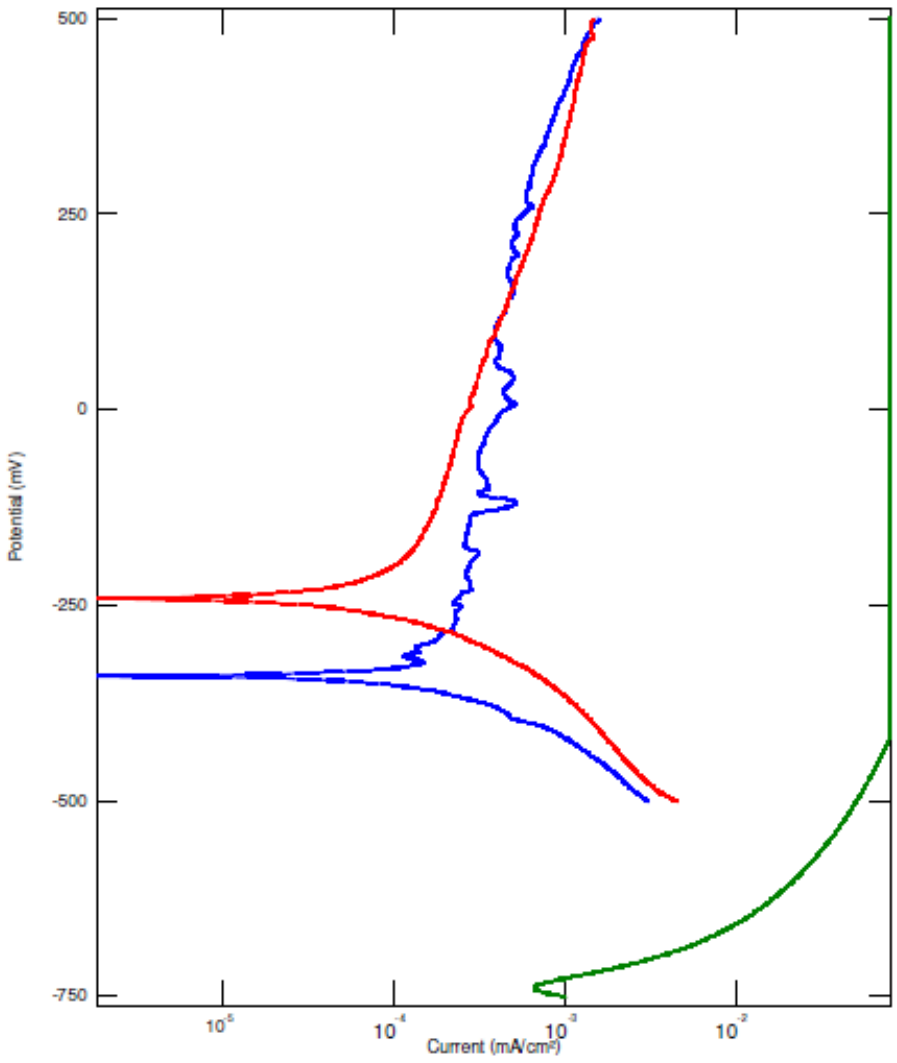

Graph 13 Combined 304L, 316L and AISI 0.1 Ground Flat Stock - 40% Peat

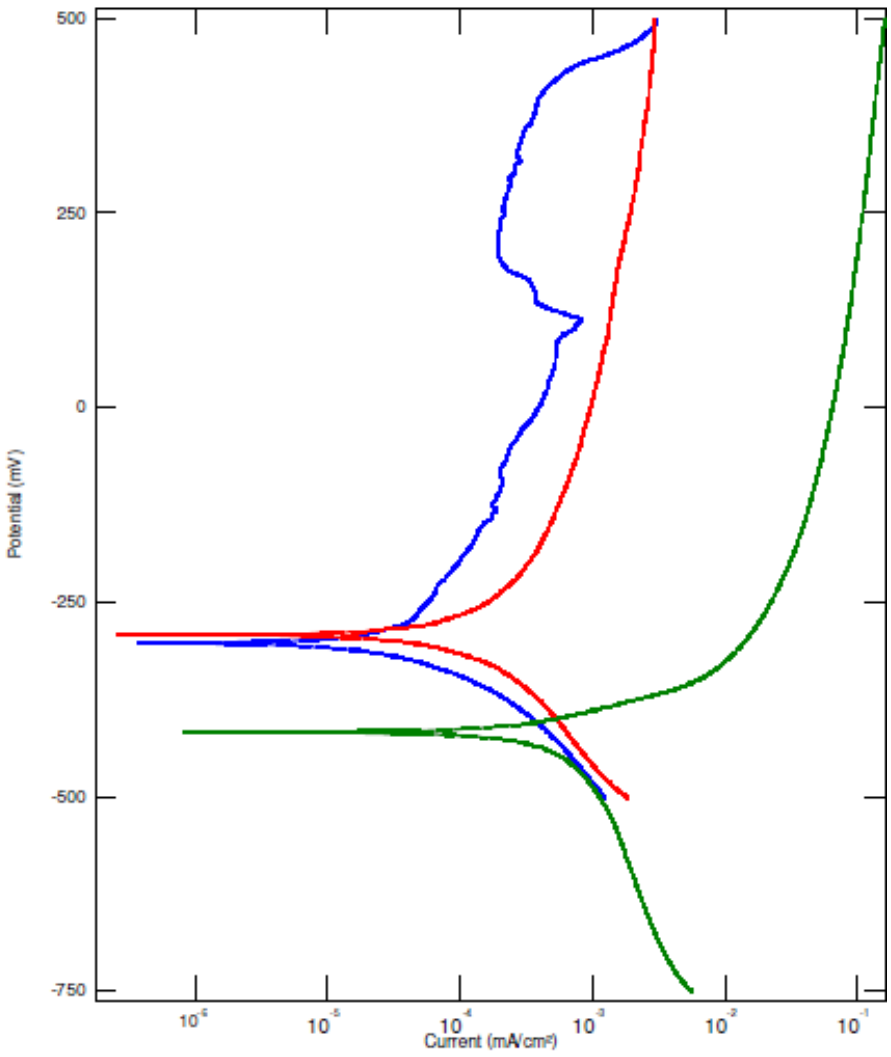

Graph 14 Combined 304L, 316L and AISI 0.1 Ground Flat Stock - 5% Peat

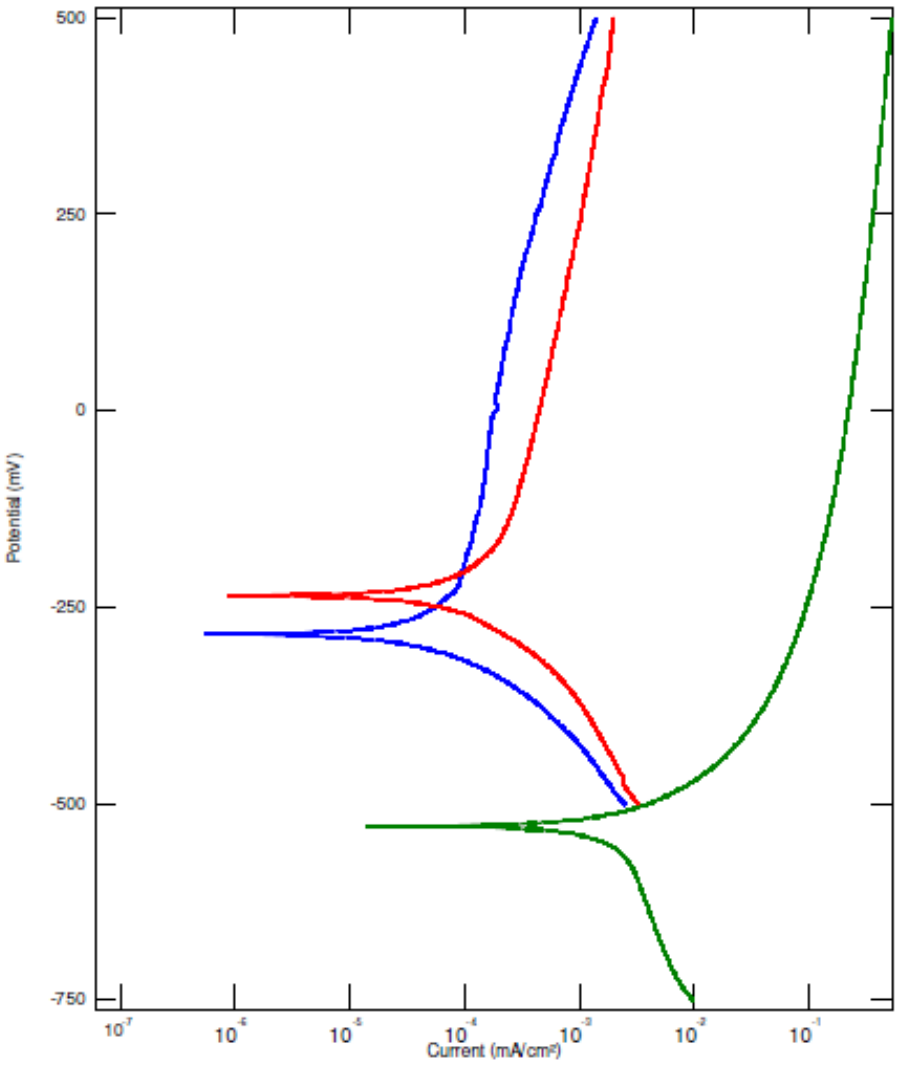

Graph 15 Combined 304L, 316L and AISI 0.1 Ground Flat Stock - 10% Peat

5.3 Corrosion Rate Maps

To increase the understanding of the contributing factors, and provide a visual representation of the corrosion observed during the testing process, corrosion rate maps were constructed with various parameters. The corrosion maps are shown in Figures 34 to 37. The corrosion rates for each of the five peat sample were calculated using the formula:

$$Kc = \frac{Mlt}{ZF}$$

Equation 1: Corrosion Rate (Stack, Mathew and Hodge 2011) [1]

Where,

K_c is the corrosion rate

M is the atomic mass of the material

I is the measured corrosion current

t is the exposure time

Z is the valence electrons involved the corrosion of the steel

F is Faradays constant

The final results of the corrosion rates calculated for the five solutions are shown in Table 7 below. Information on the data used and the calculation method can be found in Appendix 2.

Solution	**Material**		
	316L	*304L*	*Steel Gauge Plate (AISI 0-1)*
0% Peat	6.46469E-08	1.7453E-07	5.15171E-05
5% Peat	1.43479E-07	1.46231E-06	0.000130876
10% Peat	1.34221E-07	1.13381E-06	0.000406339
20% Peat	8.29244E-07	3.05992E-06	0.000462199
40% Peat	1.34499E-07	9.86432E-07	7.20202E-05

Table 7 Calculated Corrosion Rates

The boundaries used to determine the levels of corrosion were set after discussions with my supervisor and other academic staff. These were defined as four categories;

low, medium, high and severe, the categories were defined as follows based on the maximum corrosion rate calculated:

- *Severe Corrosion* ≥80% of maximum corrosion rate
- 50% of maximum corrosion rate ≤ *High Corrosion* < 80% of maximum corrosion rate
- 25% of maximum corrosion rate ≤ *Medium Corrosion* < 50% of maximum corrosion rate
- *Low Corrosion* > 25% of maximum corrosion rate

The boundaries were shaped using extrapolation between the above limits for the classifications. Whilst reviewing the corrosion map produced for stainless steel types 304L and 316L (Figure 34), we can see that the 304L material is more affected by the peat solution. This is somewhat backed up by the literature study as the corrosion resistance of 304 is generally lower than that of 316 as a result of the 2% molybdenum content. Interestingly, in both cases a minimum corrosion resistance was observed at 20% peat and 80% solution, although it was more severe for the 304L material. It was expected that due to the more acidic nature of the 40% peat concentration would produce a poorer result. One possibility could be the surface finish on the two materials being different, however as it is the same trend for both 304 and 316 this may not be justifiable.

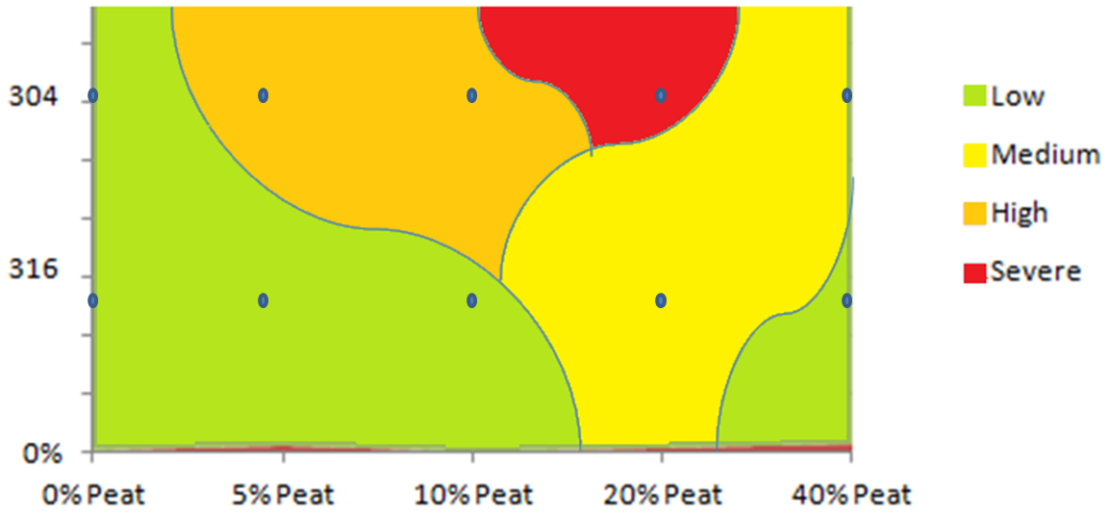

Figure 34 Corrosion Rate Map for SS316L and SS304L

Investigating the results for the corrosion rate map with all 3 test materials shown (Figure 35), it is clearly visible that the AISI 0-1 ground flat stock disk is suffering more with corrosion than the two stainless steel material samples. Both corrosion are showing low corrosion rates in each of the five test solutions when compared to the AISI 0-1 material. The flat stock material is particularly severe between 10 and 20% peat concentrations. An initial thought is that the lower chromium content in the AISI 0-1 material will be making the corrosion resistance generally lower.

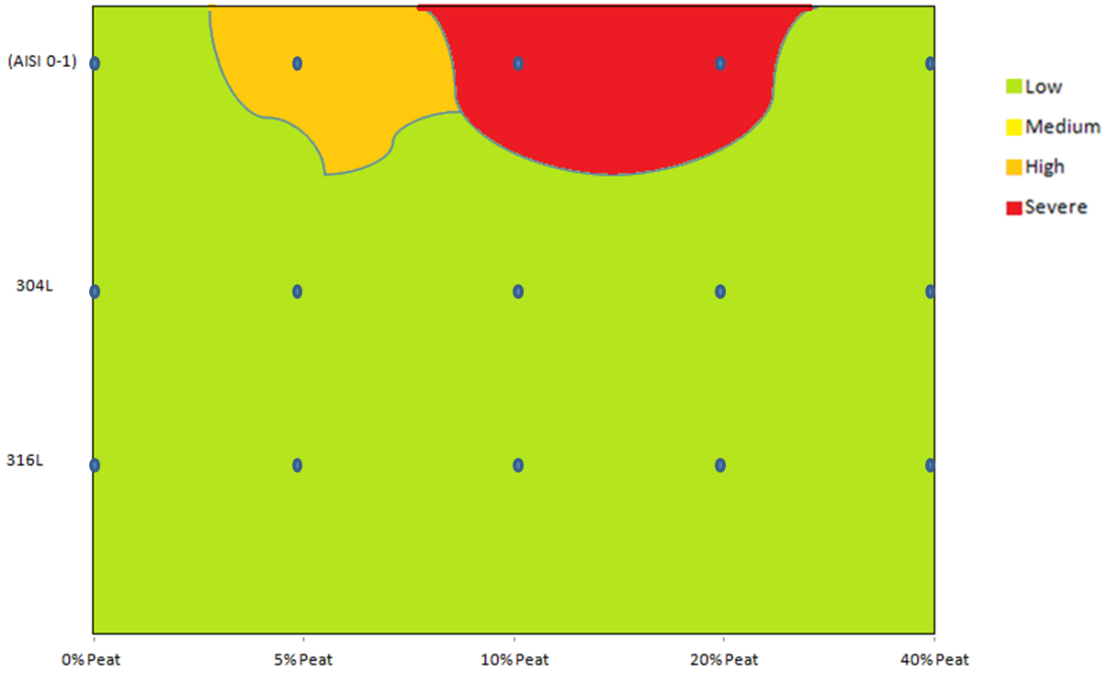

Figure 35 Corrosion Rate Map for all 3 Materials

The discussion point raised above that the lower chromium content could be having an effect on the corrosion resistance is evident in the corrosion rate map of chromium content against pH below in Figure 36. By undertaking an assessment of the map we can detect that at the higher chromium percentage composition the rate of corrosion seen is low across the range of pH values, whereas for the lower chromium percentages severe and high corrosion rates are observed at pH values 4.8 to 5.6. A possible test that is recommended for the future works is for further testing to be carried out on a greater range of chromium ranges to determine the point at which the percentage composition changes the corrosion rate state from severe to low.

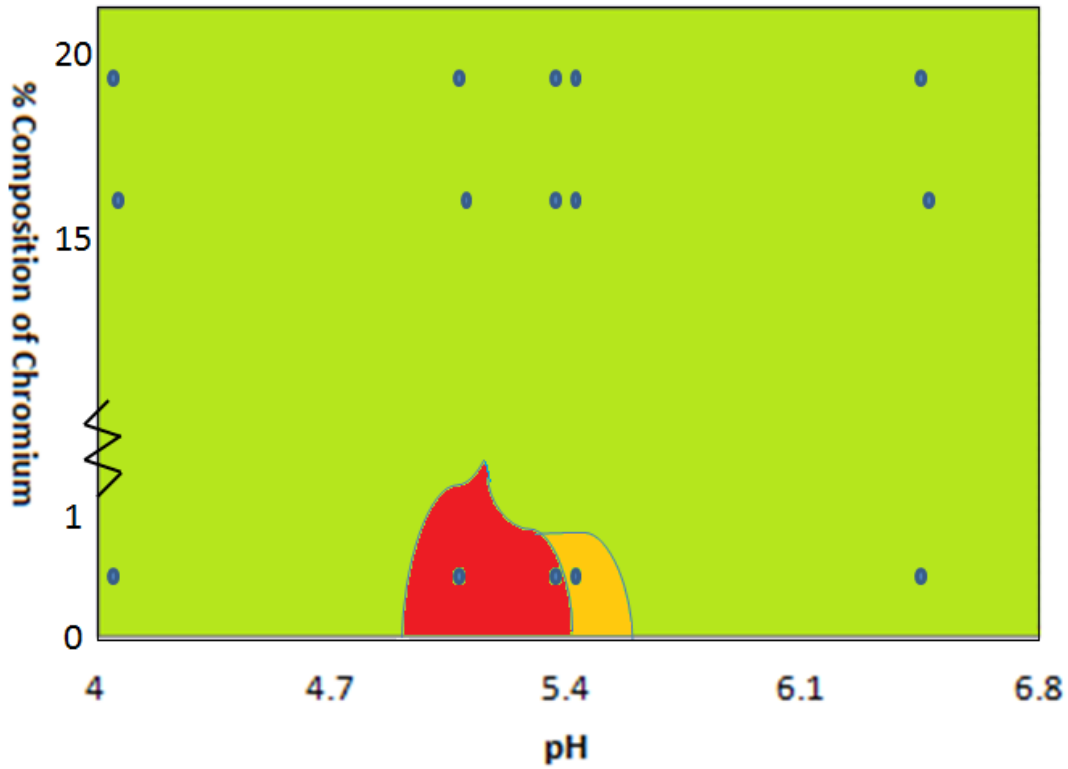

Figure 36 Corrosion Rate Map Chromium Content v pH value

Reducing the percentage composition of the chromium from that seen above in Figure 36 to a condensed chromium content range of between 17 - 20% shown in Figure 37 we can determine further conclusions. It is evident that the pH value is having an effect on the rate of corrosion, further to this the more neutral pH solution is giving a lower corrosion rate category across the whole range of chromium content. Interestingly the higher chromium value at a reducing pH value is presenting higher corrosion rates. A severe rate of corrosion is seen between 19 - 20% composition of chromium and at a pH value of 4.7 to 5, whereas at this same point only a medium rate is seen at the smaller chromium content. One possible reason could be that at the lower chromium values, higher contents of transition metals such as nickel and molybdenum are present in the overall composition which are enhancing the corrosion resistance far more than that of the higher chromium content. In most cases any addition of molybdenum will strengthen the passive film that is formed during the corrosion attack.

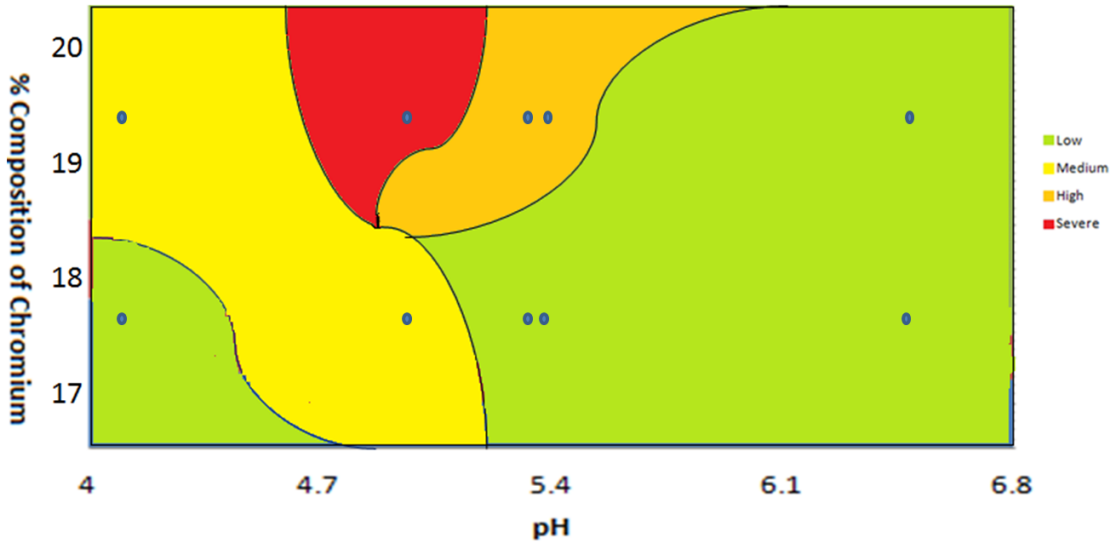

Figure 37 Corrosion Rate Map - Reduced Chromium Content Range vs. pH

5.4 SEM Analysis Results

To identify any signs of corrosion such as pitting formation that occurred during the experiments Scanning Electron Microscope (SEM) was undertaken on the 1cm² exposed surface section of the material samples. The SEM used was an S-3700N model Tungsten Filament SEM (Hitachi High Technologies Europe) and undertaken in the University of Strathclyde Advanced Material Research Laboratory. A sample of the inspections under the high magnification are shown below in Figures 38 to 41. The first SEM analysis is from the AISI 0-1 material in a test solution taken from power station B (Figure 38). We can see the emergence of an oxide forming on the surface of the material, this is evident by shape and the high oxygen content (approximately 33% of total) when analysed.

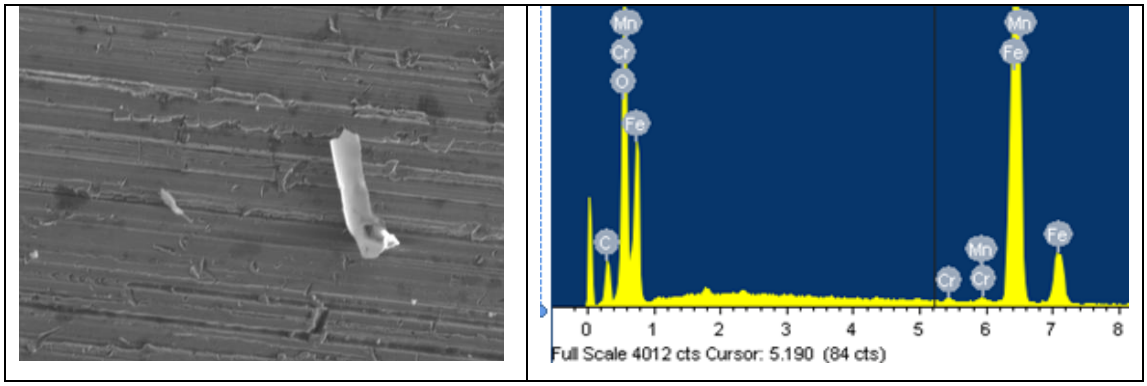

Figure 38 SEM Analysis - AISI 0-1 Material with Power Station B - Sample 2 Solution

The second image that was captured using SEM was found whilst reviewing the surface of the AISI 0-1 material in a test solution containing 20% peat, Figure 39. We can see several black spots on the exterior of the material surface. On analysis of the content it is found that the black spots contain higher than expected nitrogen and sodium contents, 12 and 13% of total respectively, this could signify the presence of an organic matter which could be realistic of the peat compound.

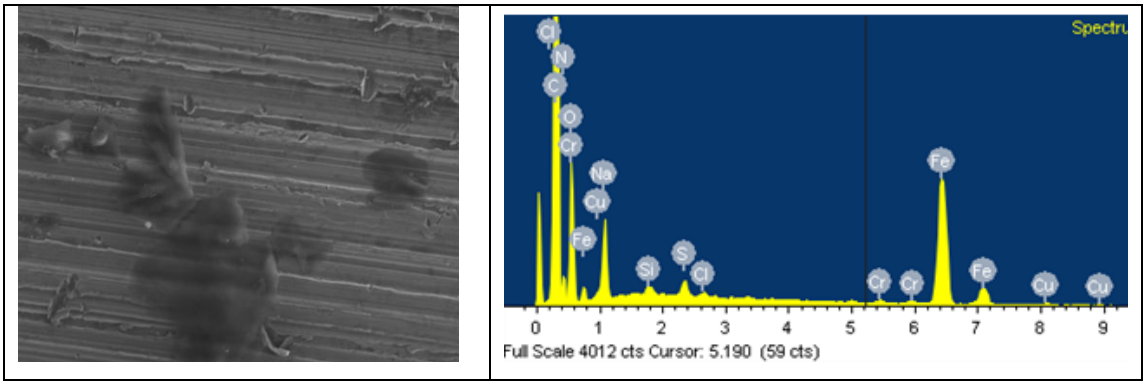

Figure 39 SEM Analysis - AISI 0-1 Material with 20% Peat Solution

Unfortunately as can be seen in Figures 40 and 41 below, the material surface preparation prior to the experiments being undertaken was making assessment via SEM difficult to perform. In Figure 40 we can make out a white dot in the crevice of the material, on review this appears to be a salt crystal which could suggest a possible contamination issue caused possible with the sanding paper used to prepare the surface. What appears to be a small oxide on the stainless steel surface can be seen in Figure 41.

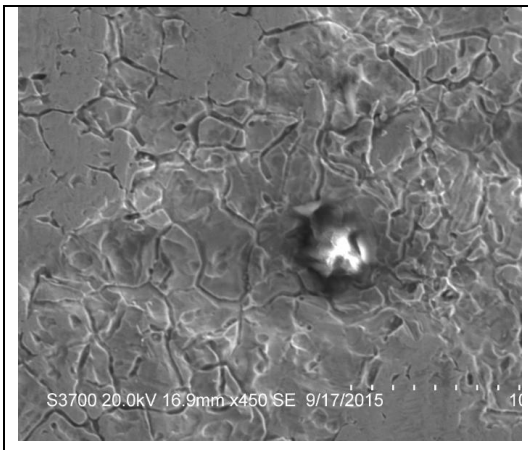

Figure 40 SEM Analysis - Stainless Steel 316L with Power Station A Solution

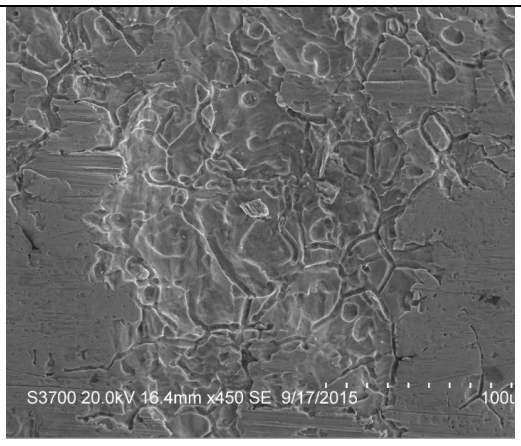

Figure 41 SEM Analysis - Stainless Steel 316L with 40% Peat Solution

6 Conclusion

The literature study has shown that there are countless different types of corrosion that are seen on a day to day basis across a variety of industries. The effects of corrosion can be very severe and in some cases it has been known to cause catastrophic failures in structures leading to the loss of lives. Unfortunately due to the time required to evaluate the level of corrosion it is often not fully considered in the design phase of structures and industrial equipments. It is difficult to consider corrosion on an individual basis as the occurrence of one kind may initiate the starting of further types.

Knowledge and firsthand experience of the problems of peat contamination have been gained from the industrial visit to several hydro power stations across Scotland. Each station presented different problems such as peat blocking cooling water pipework, that needed to be addressed by the hydro engineer on an ad hoc basis. However a common theme of galvanic corrosion being a problem was present throughout either through discussions, observations or past research. To identify and attempt to tackle this problems a collection of guidelines has been produced, ranging from selecting materials similar in the galvanic series to minimising the cathode-anode area ratio.

The laboratory testing has led to the following observations being made on the severity of corrosion in a variety of circumstance:

On review of the pH testing we have seen that the introduction of the peat compound into the neutral de-ionised water solution is effecting the acidity of the solution. By increasing the concentration of peat in the solution the more acidic it will be. Also observed was that the power station water sample in the North of Scotland is 100 times more acidic than the sample taken from the power station in the South-West of Scotland, it is concluded that this is due the higher depths and extent of peat soils in the North having more of an effect on the water solution pH value.

When comparing the polarisations curves of both stainless steels type 304L and 316L for the changing peat concentrations we have seen that at 20% peat solutions the 316L

material showed active/passive transitions whereas the 304L results were relatively uniform. A similar trend continued across the remaining three peat test solutions, which could be evidence of the very thin protective film of the 316L stainless steel breaking down and reforming very rapidly. The polarisation curves for the AISI 0-1 ground flat stock showed lower electrode potential and higher corrosion rates when compared to the two stainless steel samples. A particular example of this was seen in the 40% peat test where appears to be no protective film with the passive region broken almost straight away.

The conclusions drawn from the heat maps show that at lower chromium contents the resistance of the material to corrosion is significantly reduced. It was also evident that the pH of the solution is have a direct effect on the corrosion rates, at higher pH values (closer to pH value of 7) the severity of corrosion witnessed is low. Interestingly a severe rate of corrosion is seen between 19 - 20% composition of chromium and at a pH value of 4.7 to 5, whereas at this same point for a reduced 17-18% chromium content only a medium corrosion rate is observed. This is assumed to be due to molybdenum being present in the overall composition of the smaller chromium percentage samples which is improving the corrosion resistance far more than that of the higher chromium content only.

Appendix

6.1 Appendix 1 - Polarisation Curves

6.1.1 316L Individual Polarisation Curve Results

6.1.1.1 Polarisation Curve for Stainless Steel 316L with De-Ionised Water Solution

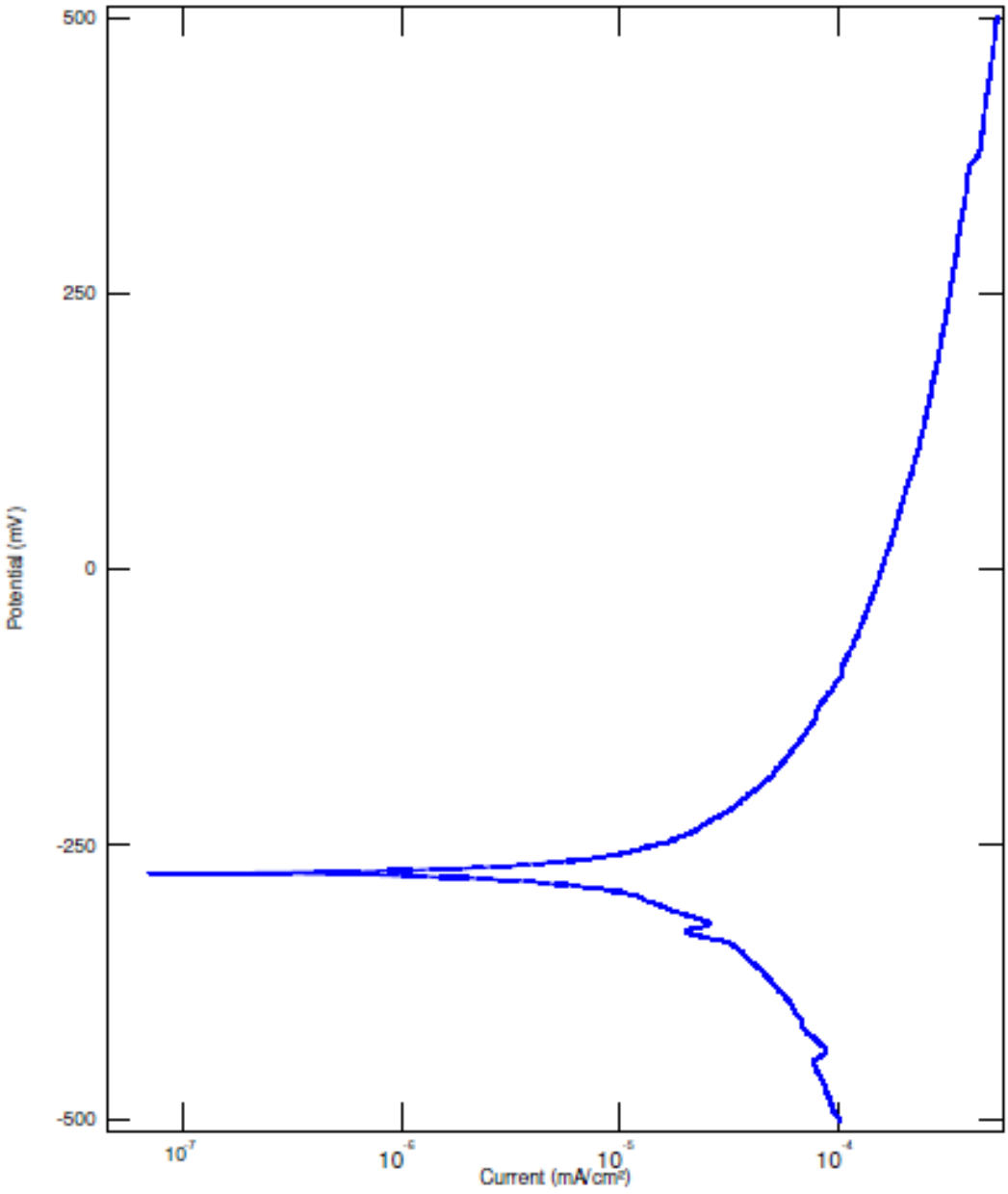

Graph 16 Stainless Steel 316L - Test 1 with De-Ionised Water

6.1.1.2 Polarisation Curve for Stainless Steel 316L with Power Station A Solution

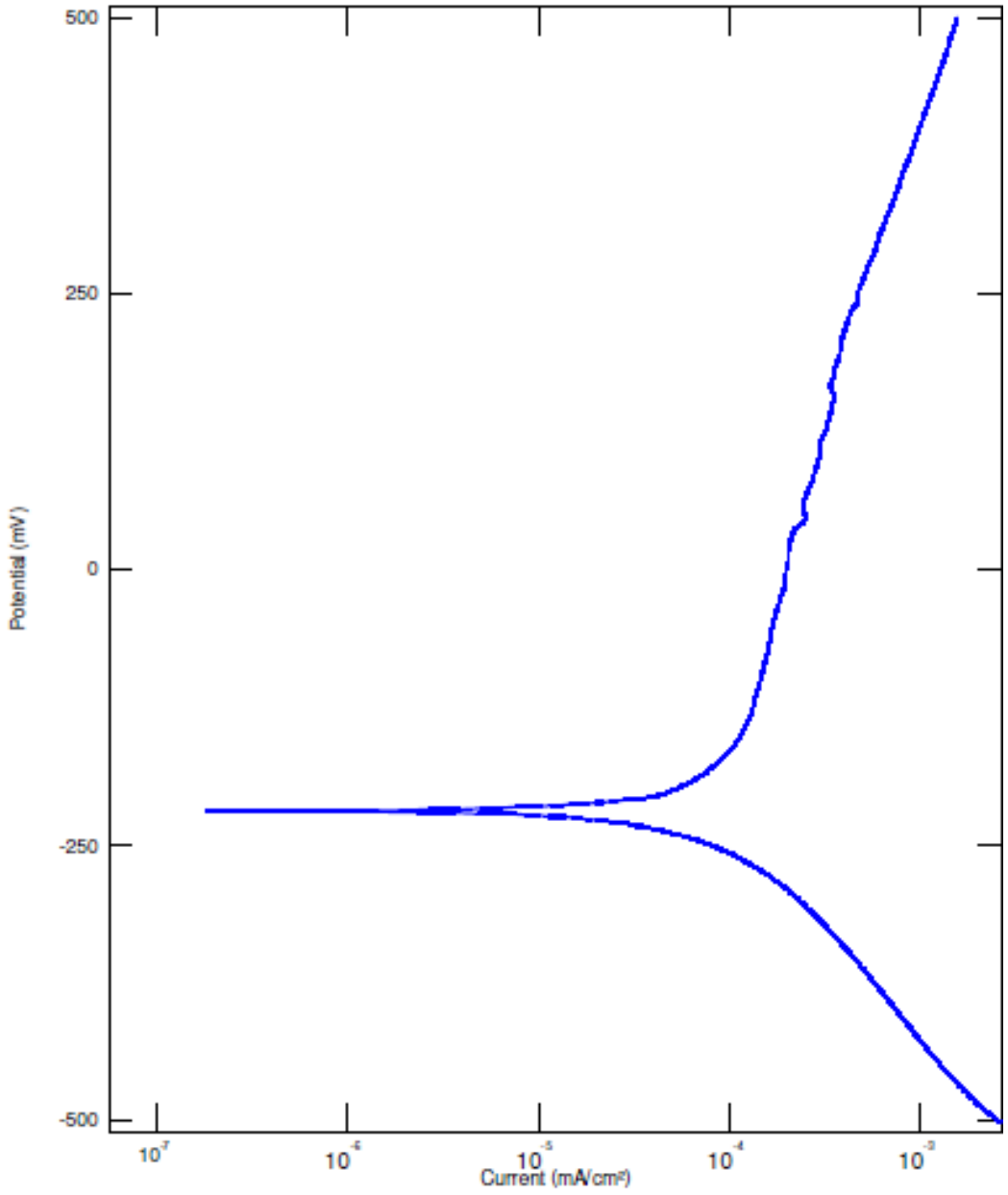

Graph 17 Stainless Steel 316L - Test 2 Power Station A Sample 1

6.1.1.3 Polarisation Curve for Stainless Steel 316L with Power Station B Solution - Sample 1

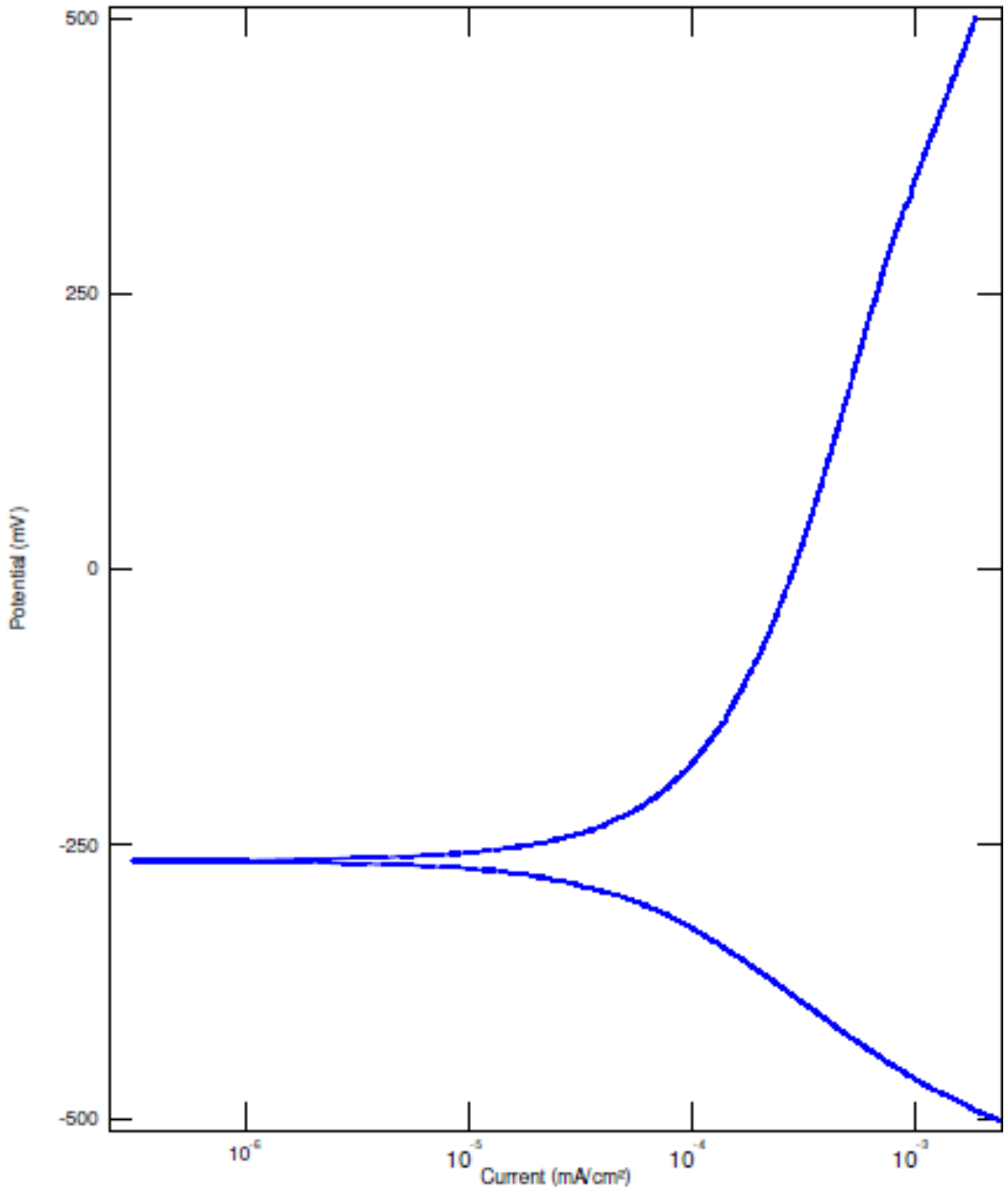

Graph 18 Stainless Steel 316L - Test 3 Power Station B Sample 1

6.1.1.4 Polarisation Curve for Stainless Steel 316L with Power Station B Solution - Sample 2

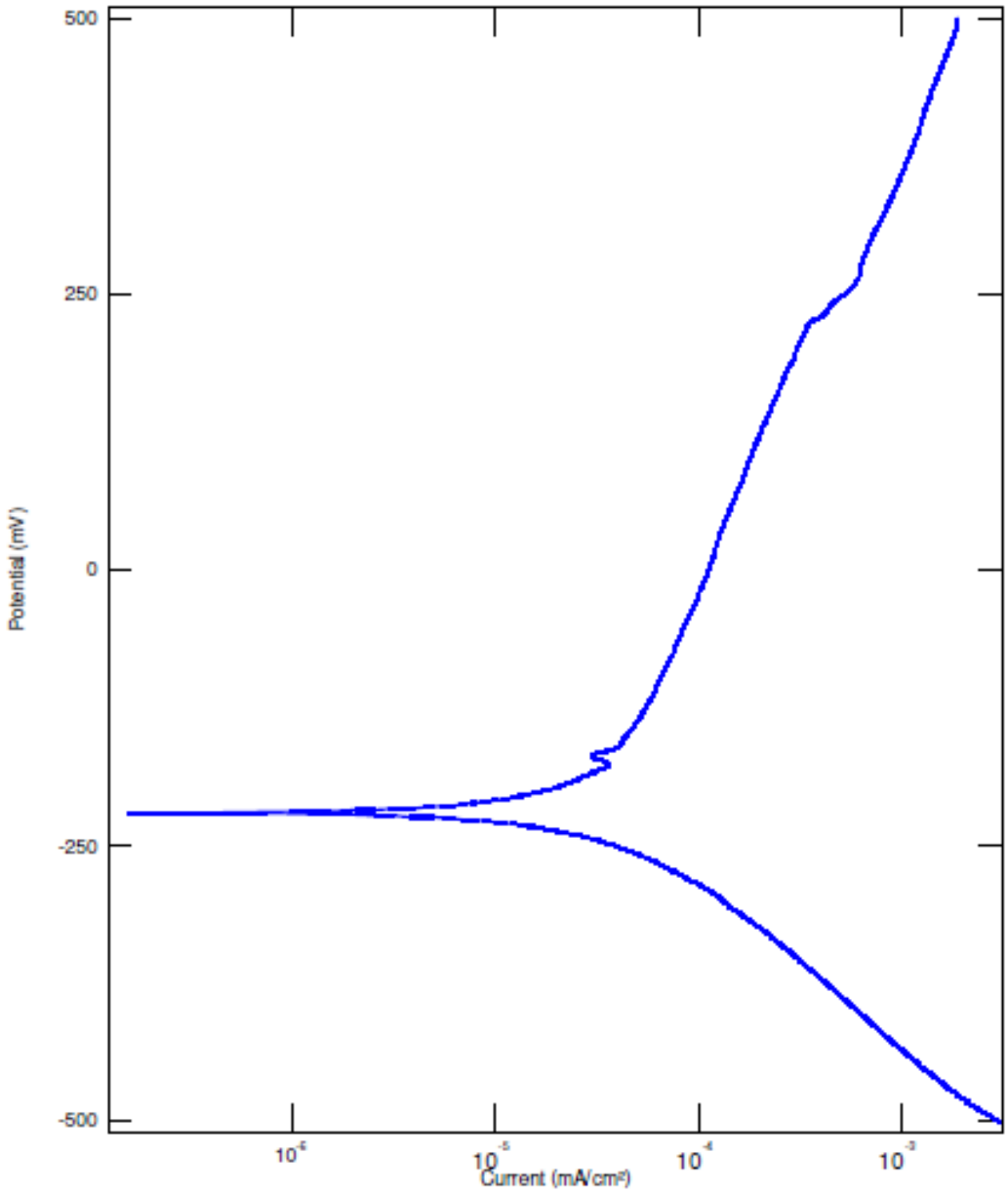

Graph 19 Stainless Steel 316L - Test 4 Power Station B Sample 2

6.1.1.5 Polarisation Curve for Stainless Steel 316L with a 20% Peat and 80% De-ionised Water Solution

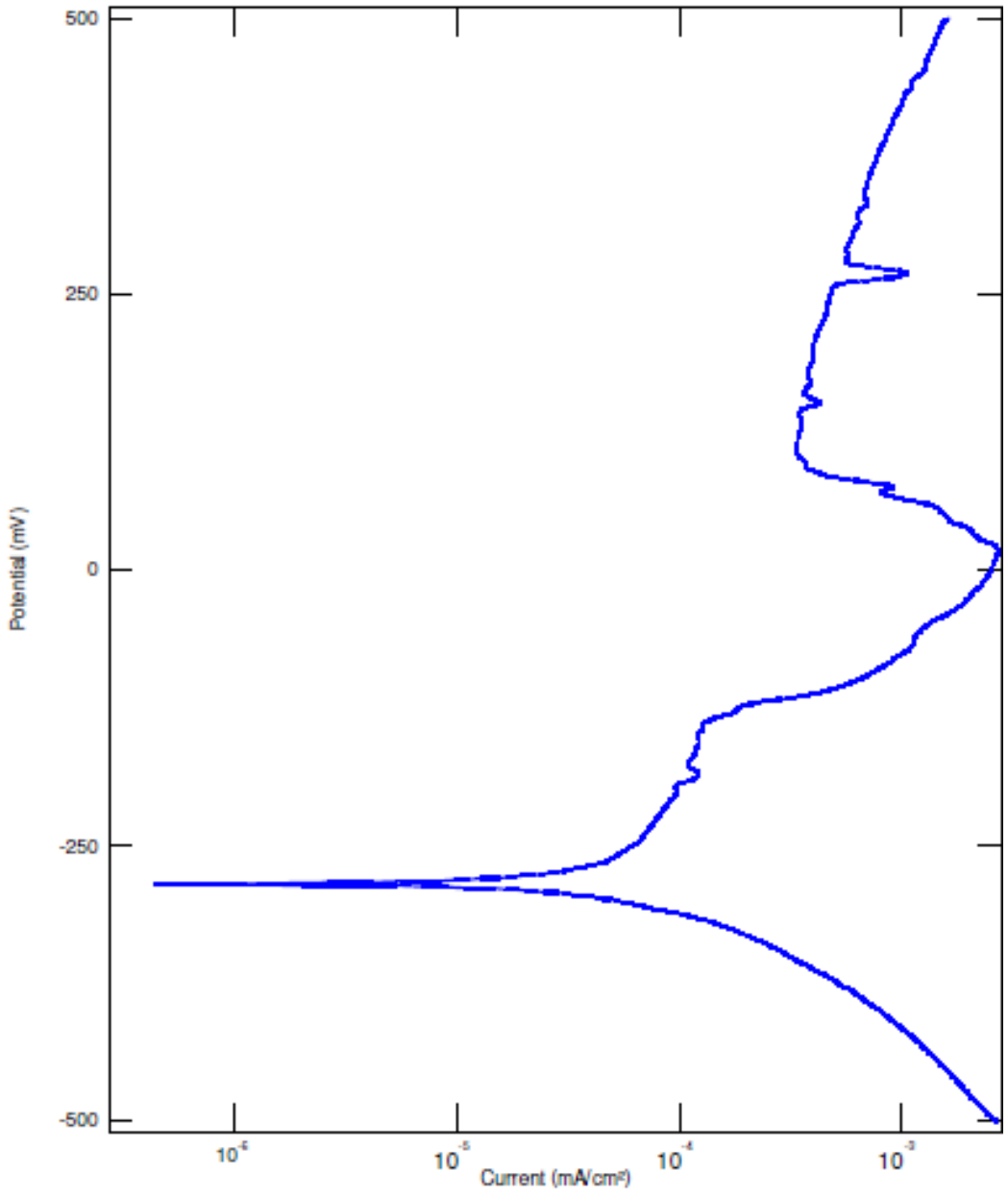

Graph 20 Stainless Steel 316L - Test 5 20% Peat Solution

6.1.1.6 Polarisation Curve for Stainless Steel 316L with a 40% Peat and 60% De-ionised Water Solution

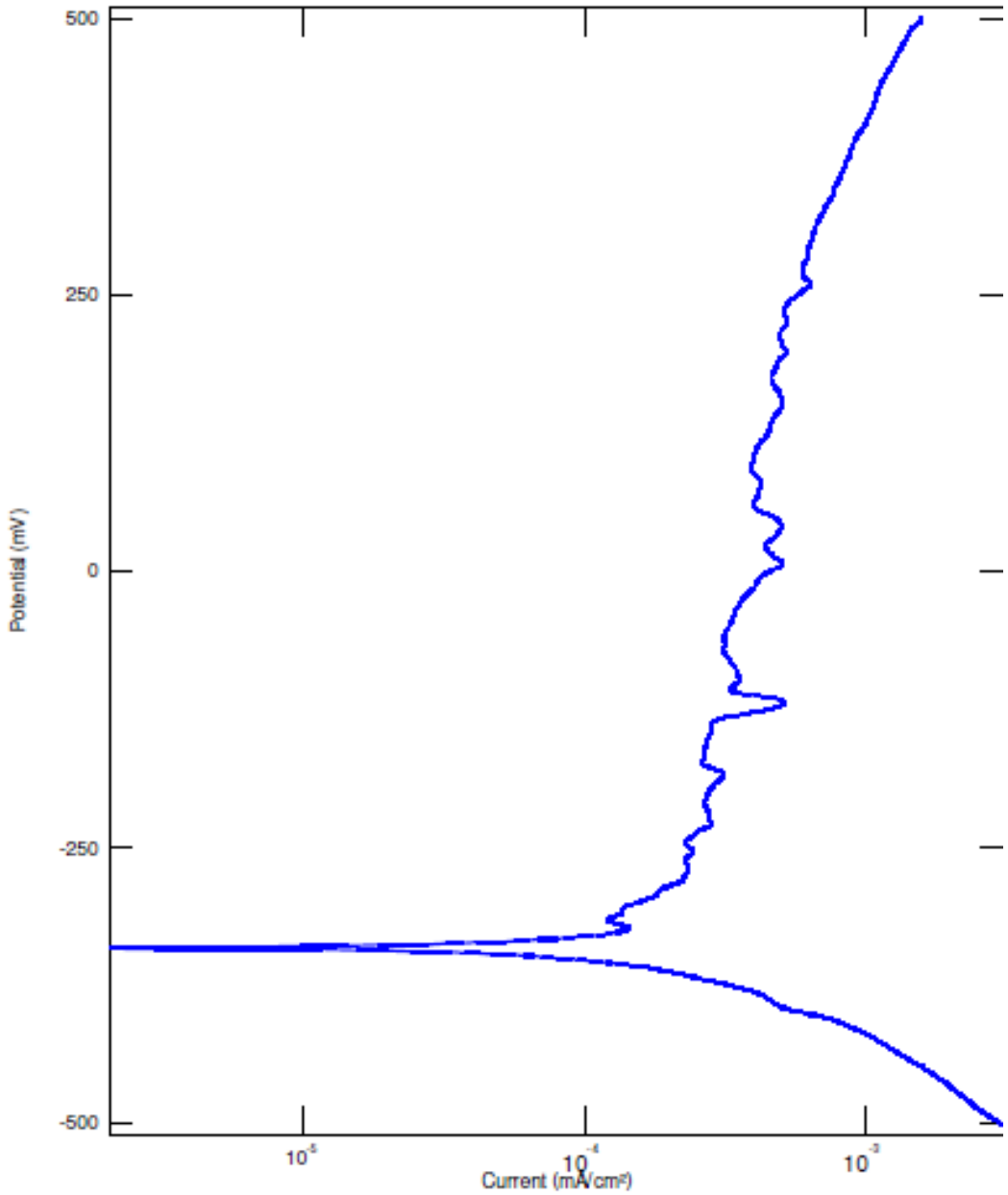

Graph 21 Stainless Steel 316L - Test 6 40% Peat Solution

6.1.1.7 Polarisation Curve for Stainless Steel 316L with a 5% Peat and 95% De-ionised Water Solution

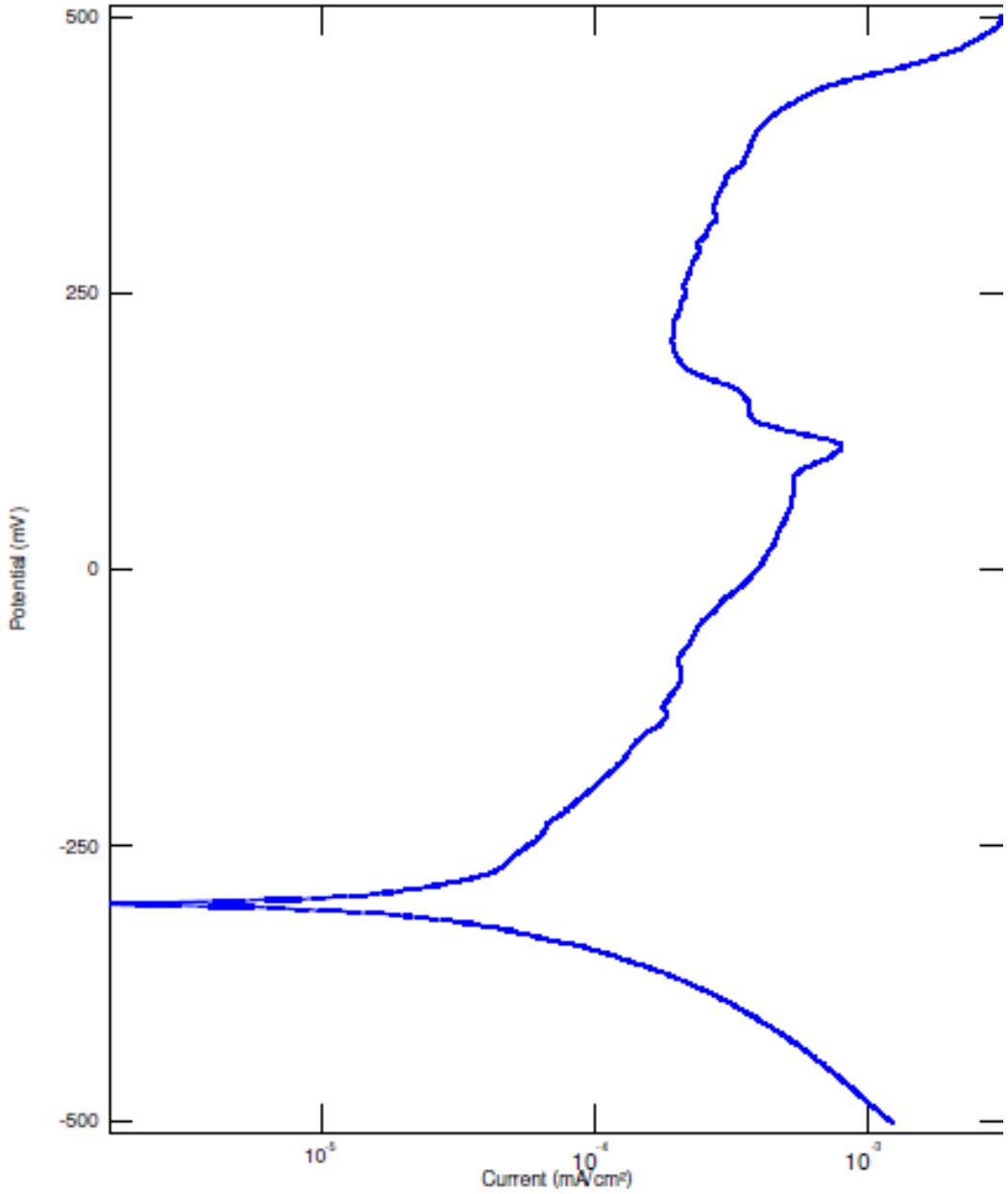

Graph 22 Stainless Steel 316L - Test 7 5% Peat Solution

6.1.1.8 Polarisation Curve for Stainless Steel 316L with a 10% Peat and 90% De-ionised Water Solution

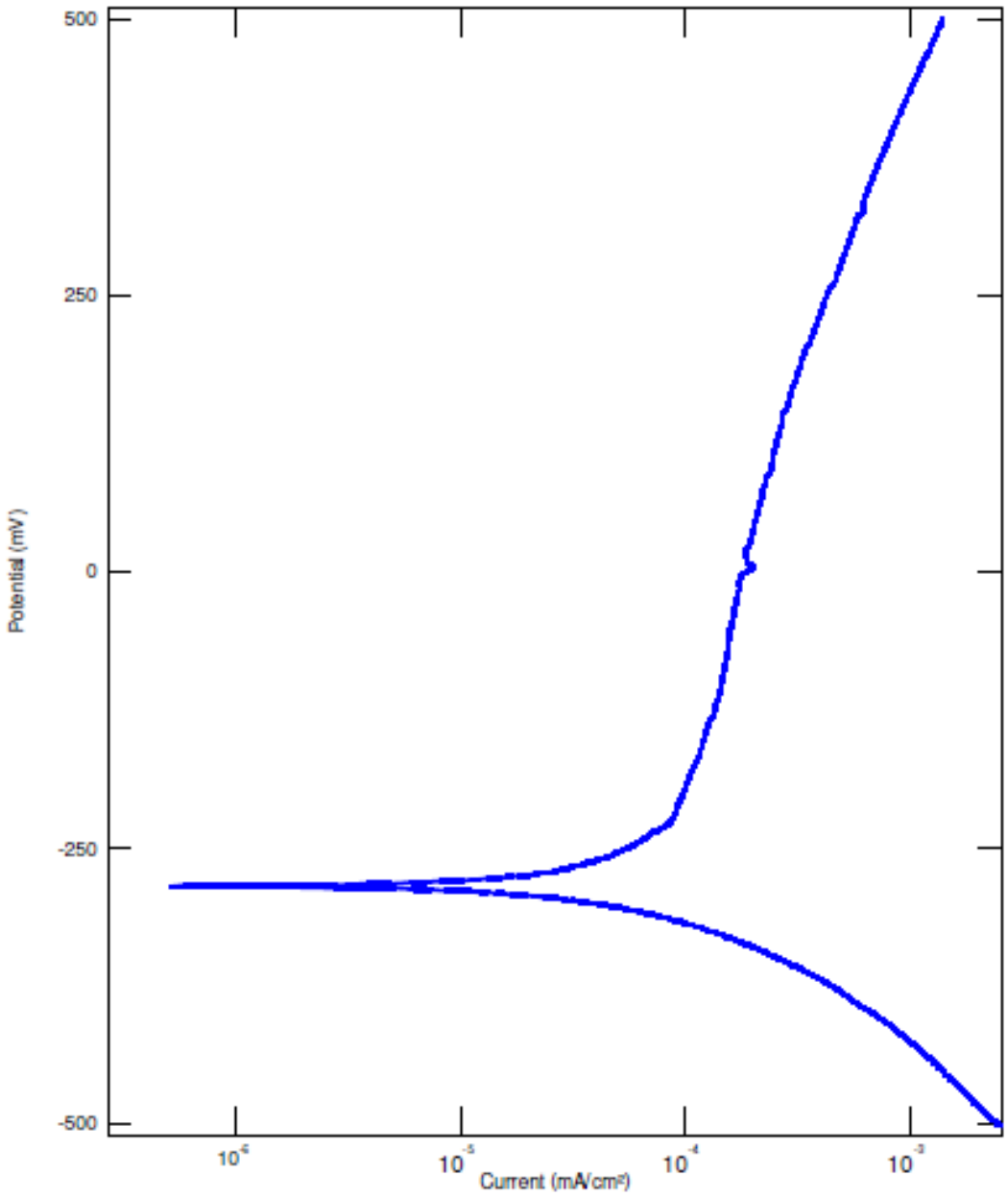

Graph 23 Stainless Steel 316L - Test 8 10% Peat Solution

6.1.2 304L Individual Polarisation Curve Results

6.1.2.1 Polarisation Curve for Stainless Steel 304L with De-Ionised Water Solution

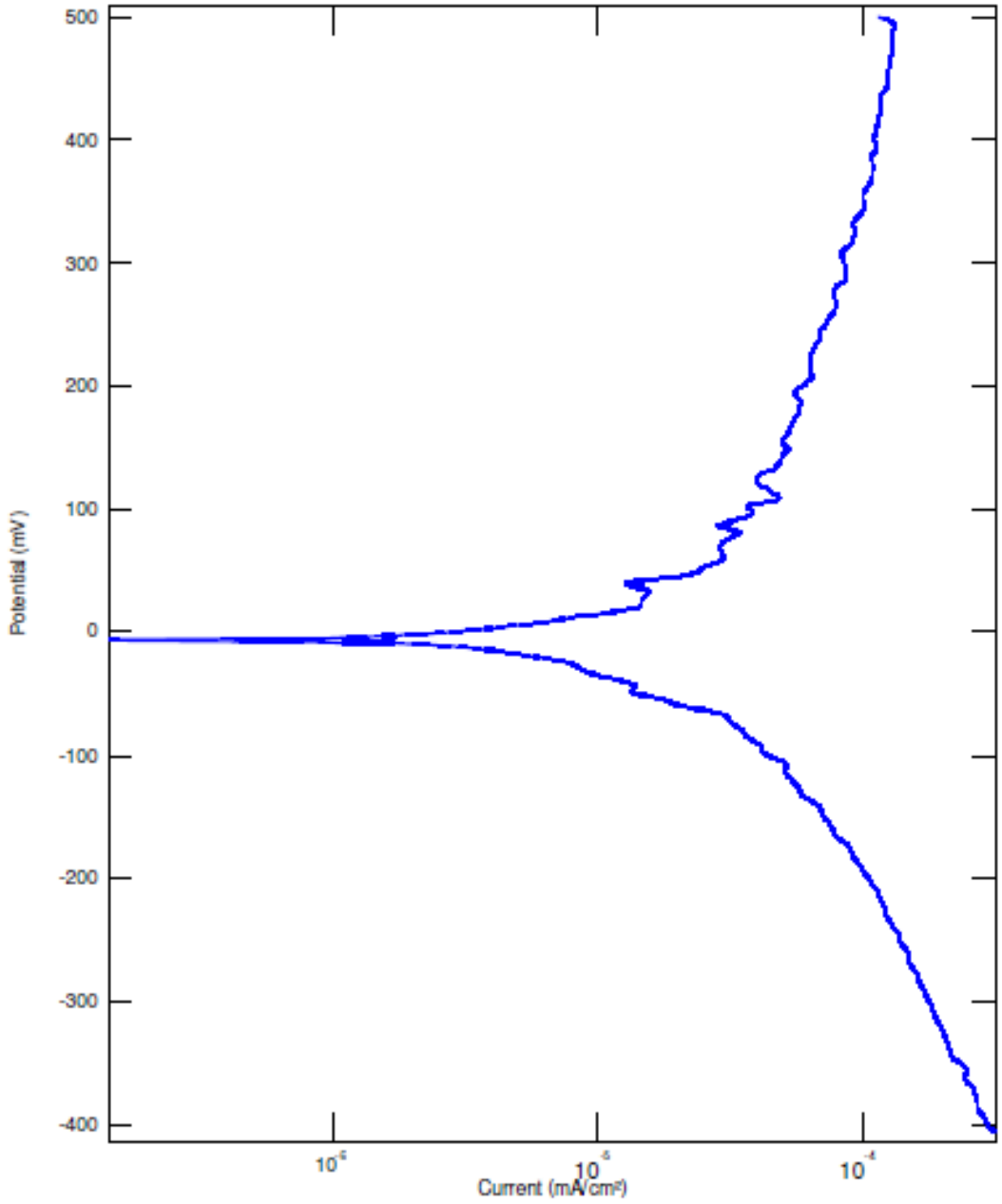

Graph 24 Stainless Steel 304L - Test 1 with De-Ionised Water

6.1.2.2 Polarisation Curve for Stainless Steel 304L with Power Station A Solution

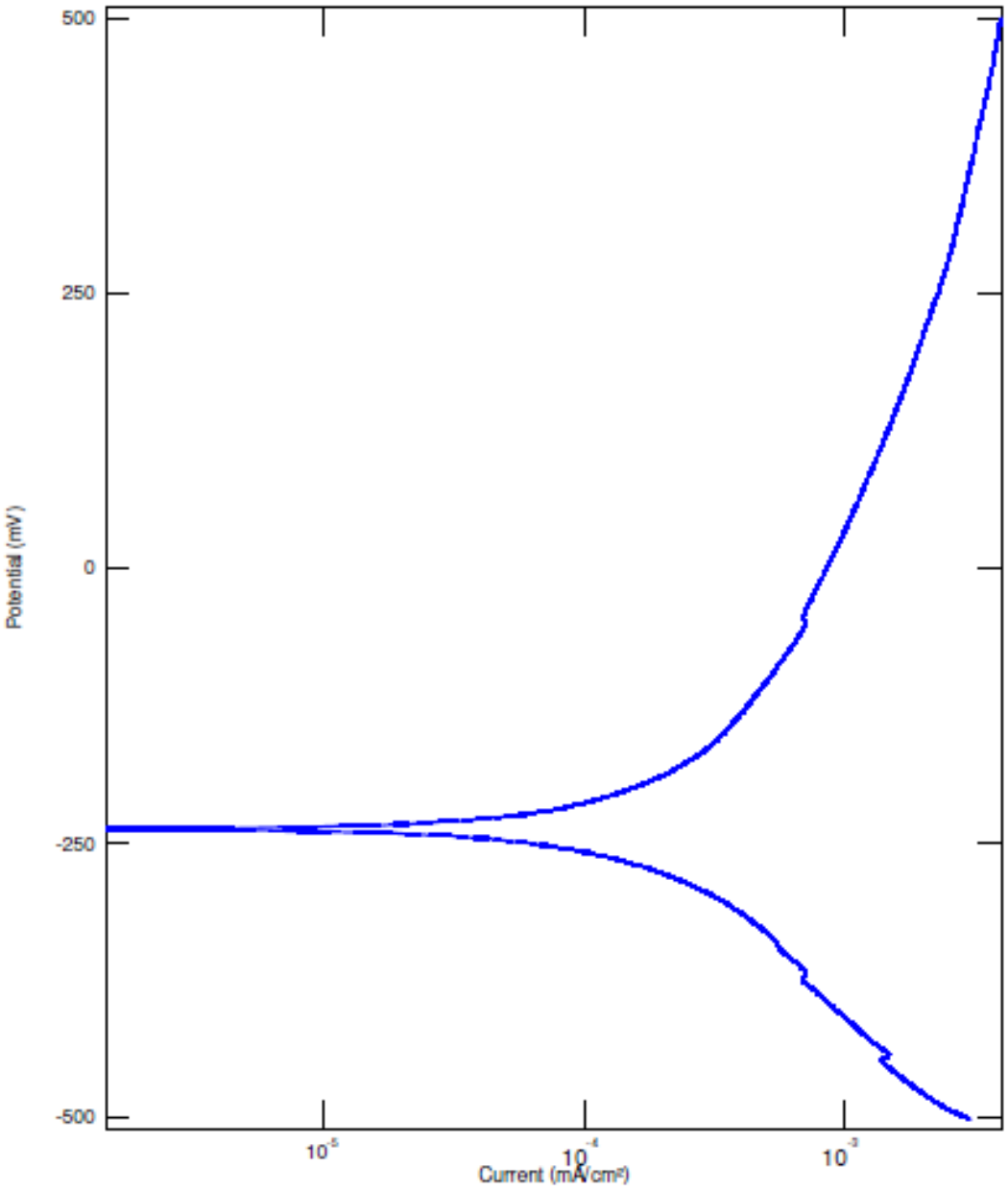

Graph 25 Stainless Steel 304L - Test 2 Power Station A Sample 1

6.1.2.3 Polarisation Curve for Stainless Steel 304L with Power Station B Solution - Sample 1

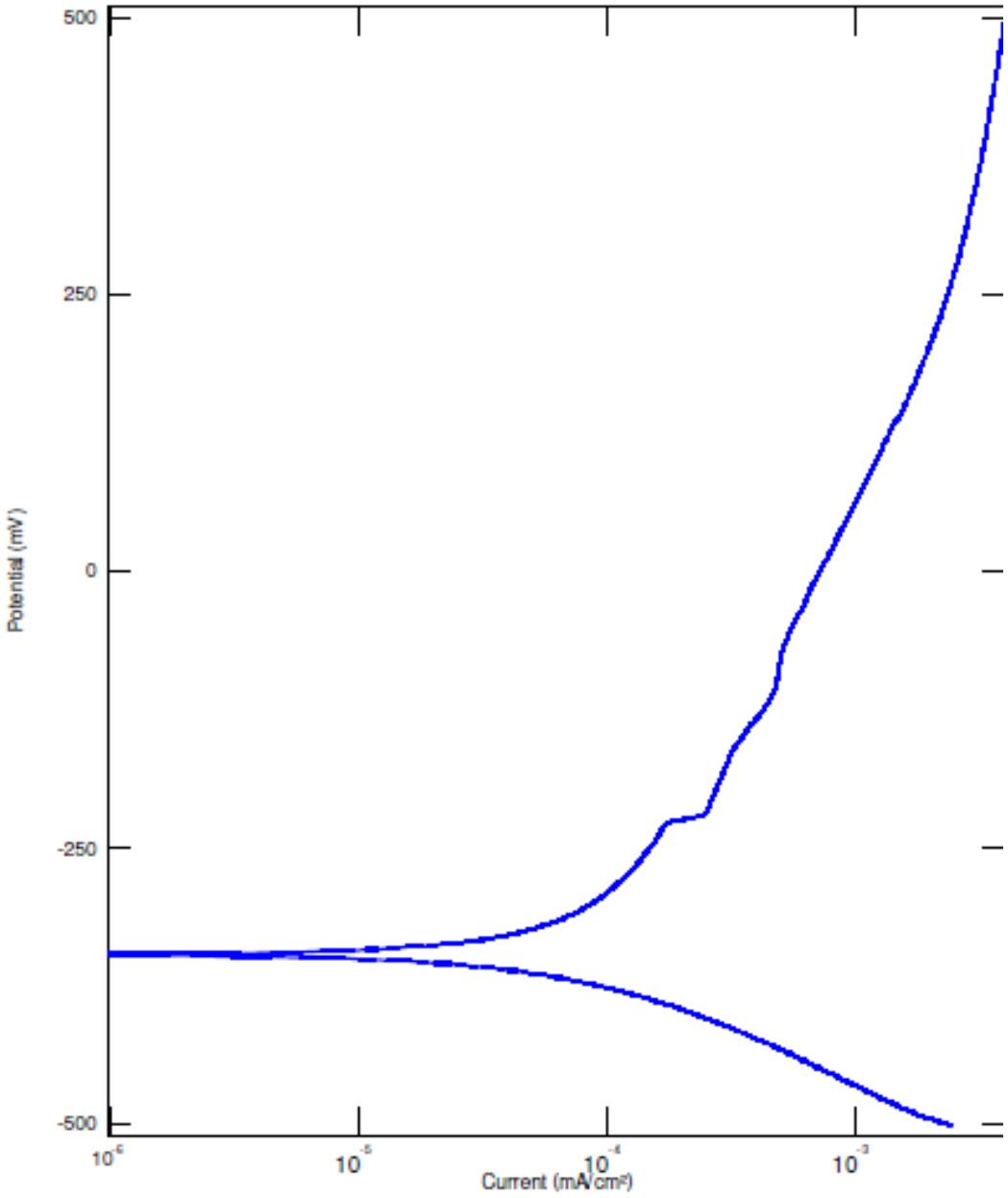

Graph 26 Stainless Steel 304L - Test 3 Power Station B Sample 1

6.1.2.4 Polarisation Curve for Stainless Steel 304L with Power Station B Solution - Sample 2

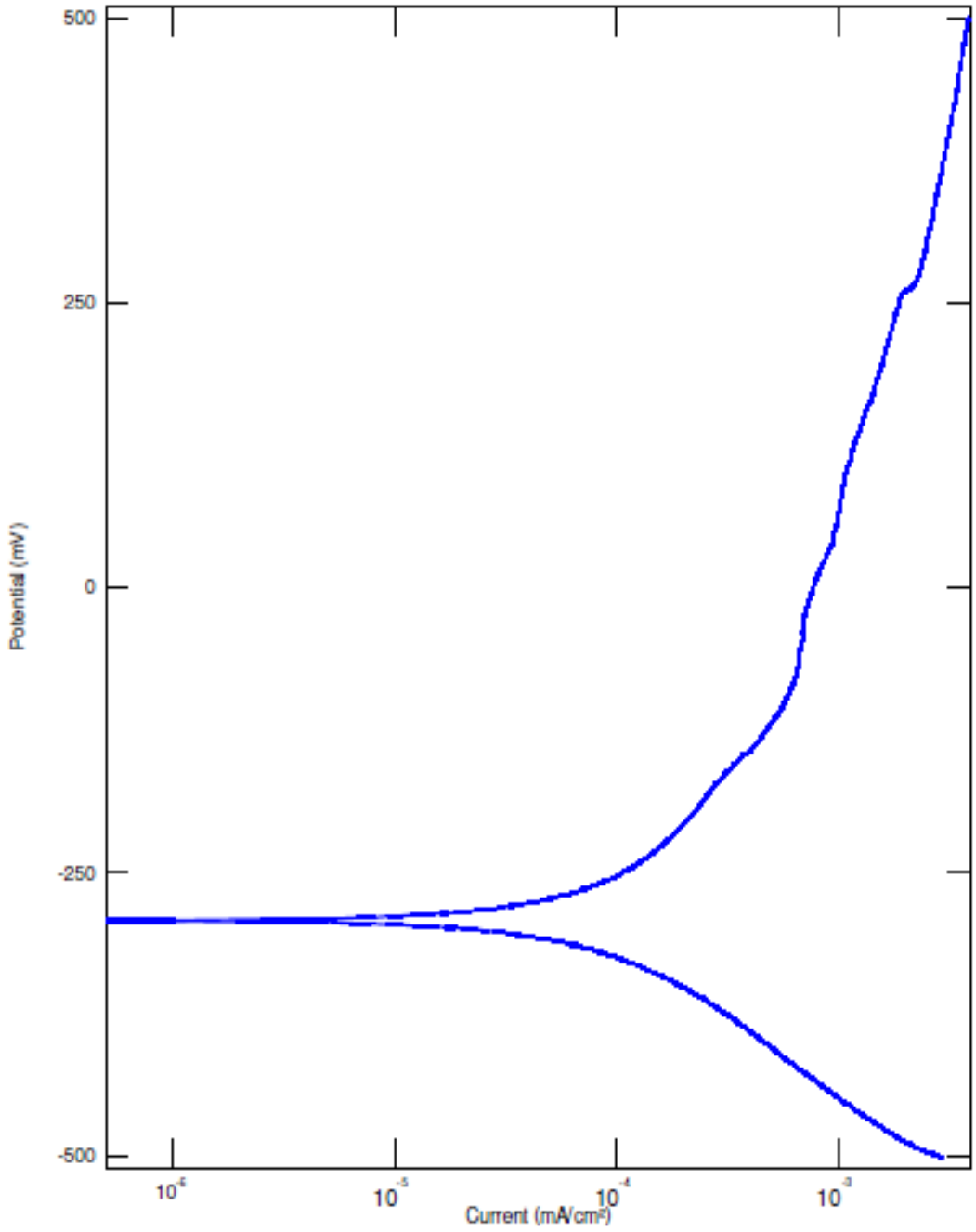

Graph 27 Stainless Steel 304L - Test 4 Power Station B Sample 2

6.1.2.5 Polarisation Curve for Stainless Steel 304L with a 20% Peat and 80% De-ionised Water Solution

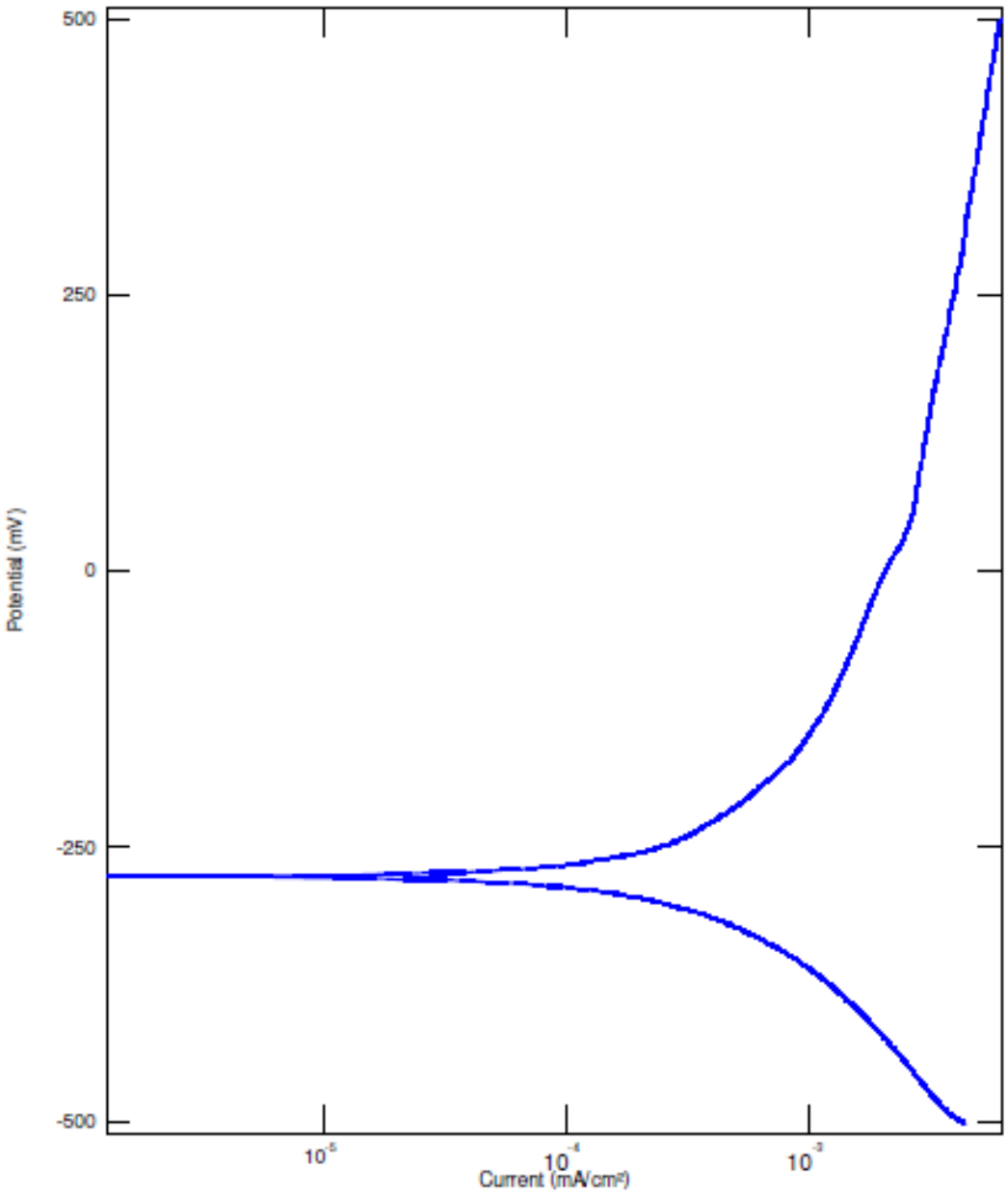

Graph 28 Stainless Steel 304L - Test 5 20% Peat Solution

6.1.2.6 Polarisation Curve for Stainless Steel 304L with a 40% Peat and 60% De-ionised Water Solution

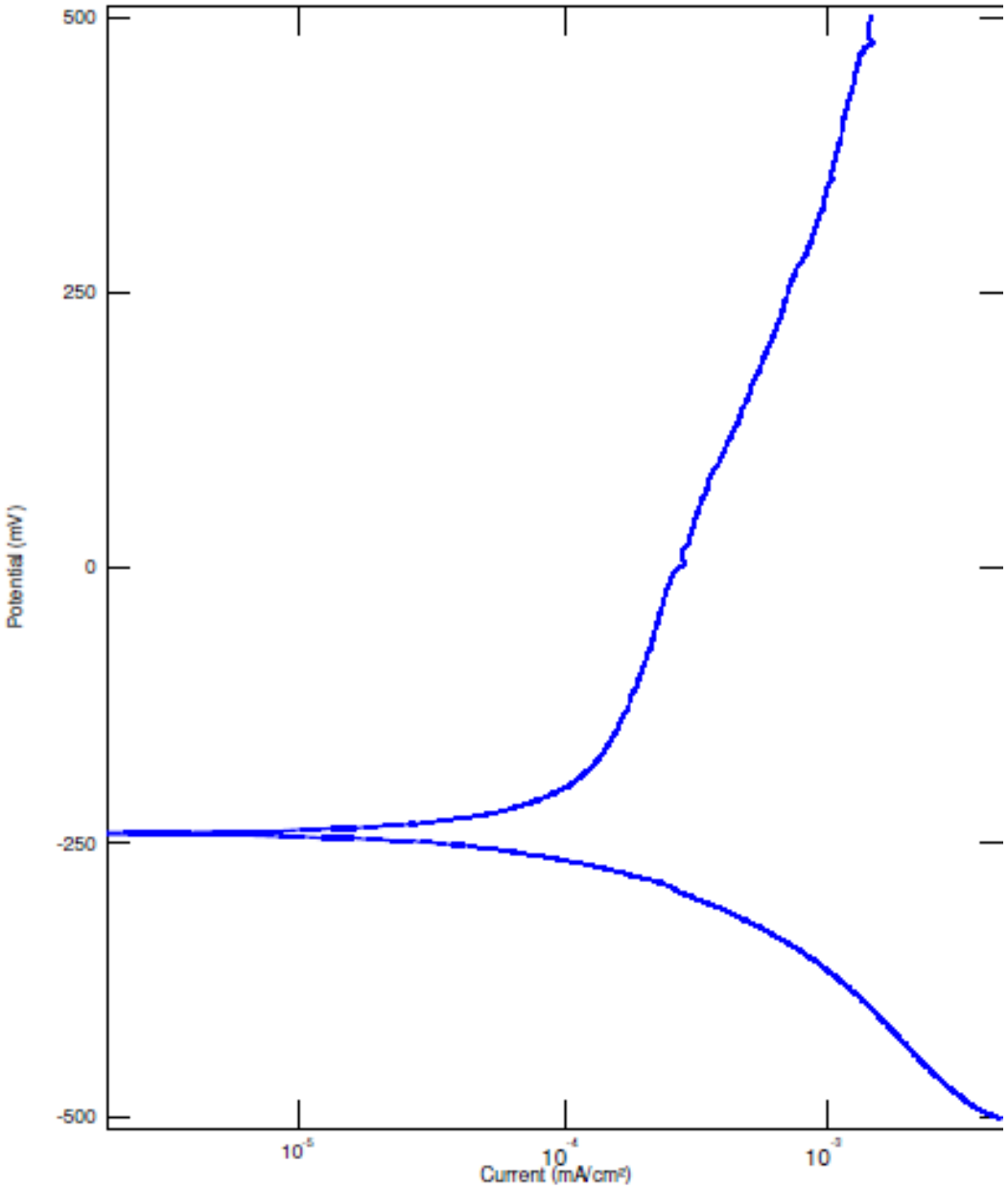

Graph 29 Stainless Steel 304L - Test 6 40% Peat Solution

6.1.2.7 Polarisation Curve for Stainless Steel 304L with a 5% Peat and 95% De-ionised Water Solution

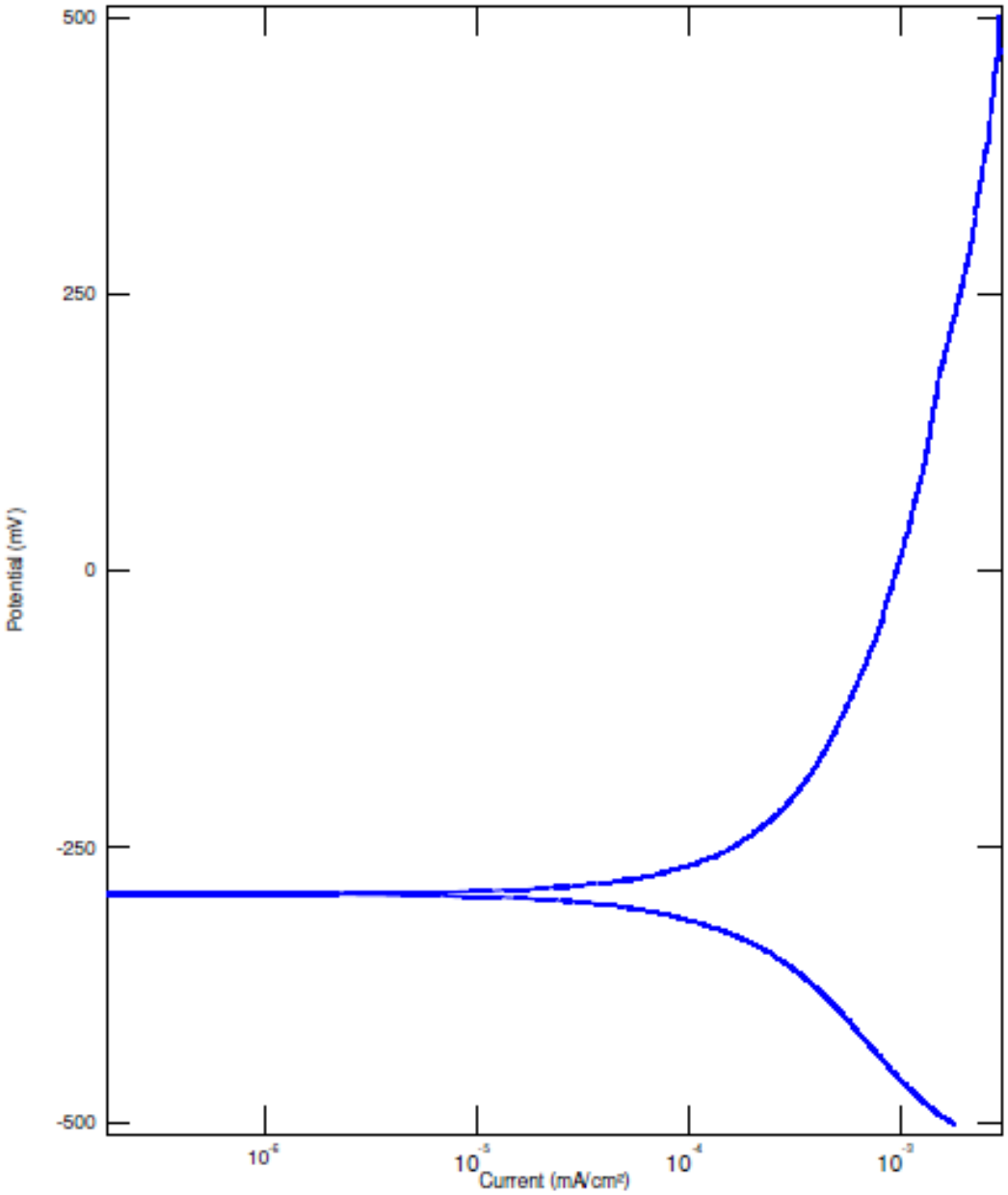

Graph 30 Stainless Steel 304L - Test 7 5% Peat Solution

6.1.2.8 Polarisation Curve for Stainless Steel 304L with a 10% Peat and 90% De-ionised Water Solution

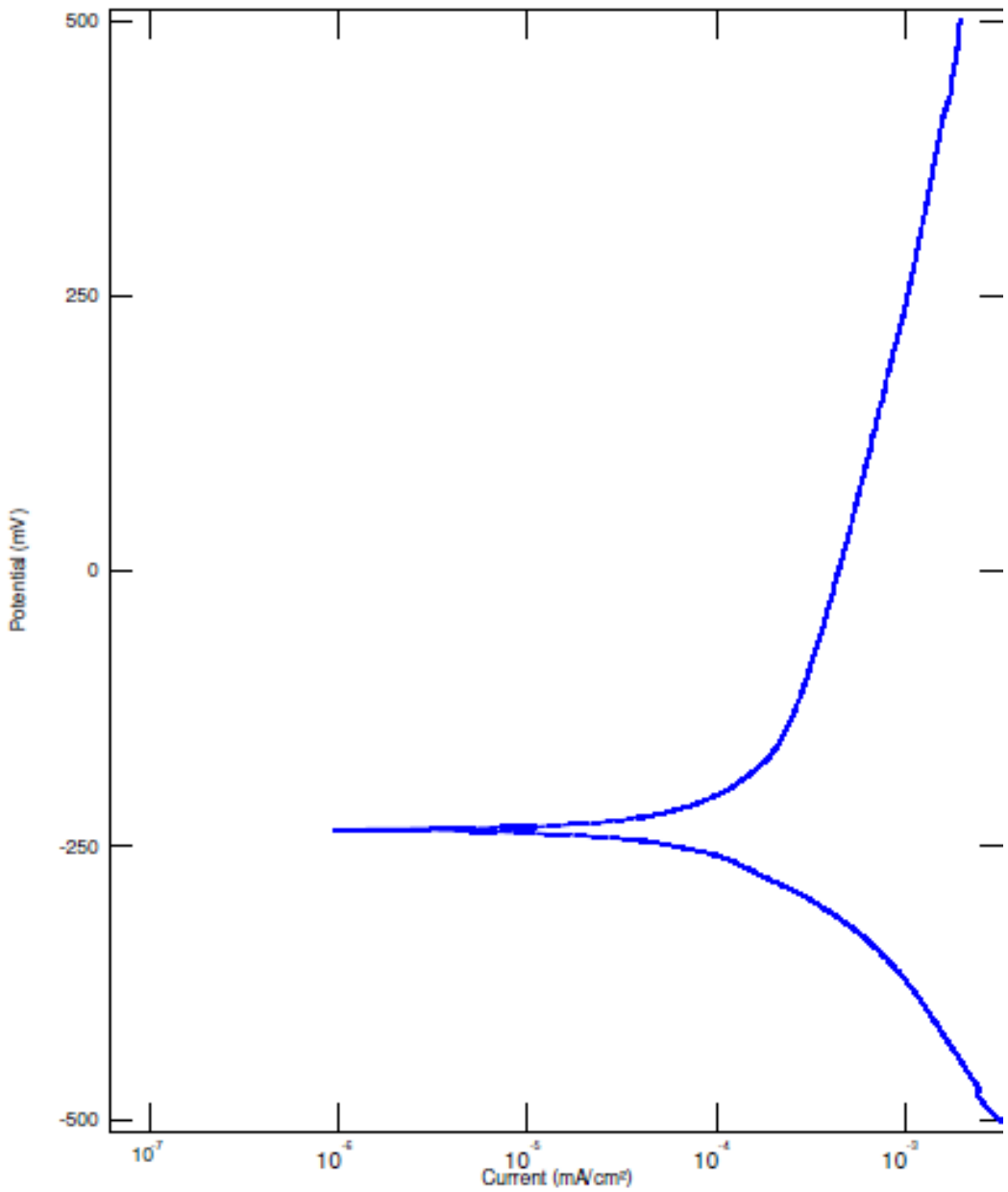

Graph 31 Stainless Steel 304L - Test 8 10% Peat Solution

6.1.3 AISI 0.1 Ground Flat Stock Results

6.1.3.1 Polarisation Curve for AISI 0.1 Ground Flat Stock with De-Ionised Water Solution

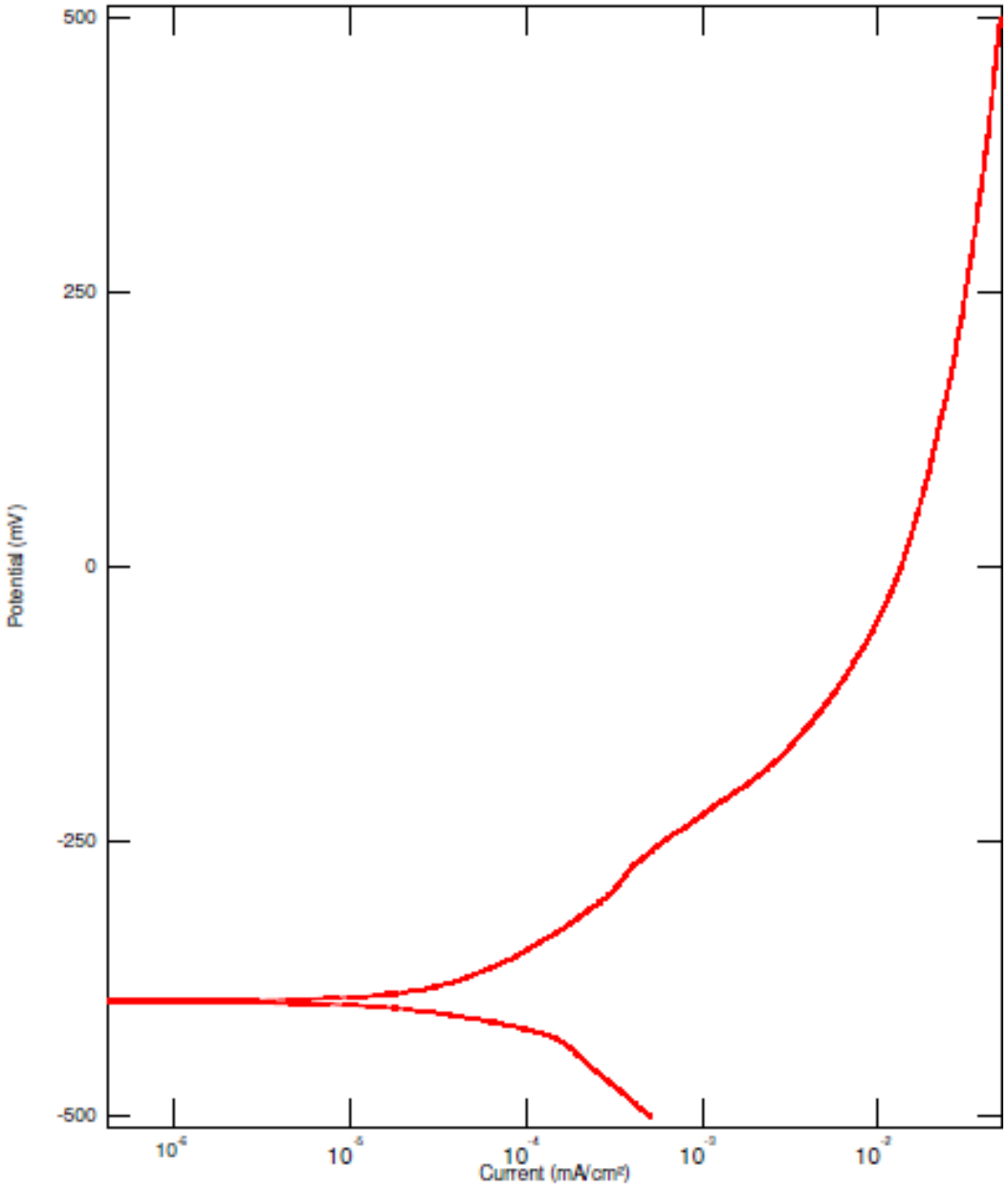

Graph 32 AISI 0.1 Ground Flat Stock - Test 1 De-Ionised Water

6.1.3.2 Polarisation Curve for AISI 0.1 Ground Flat Stock with Power Station A Solution

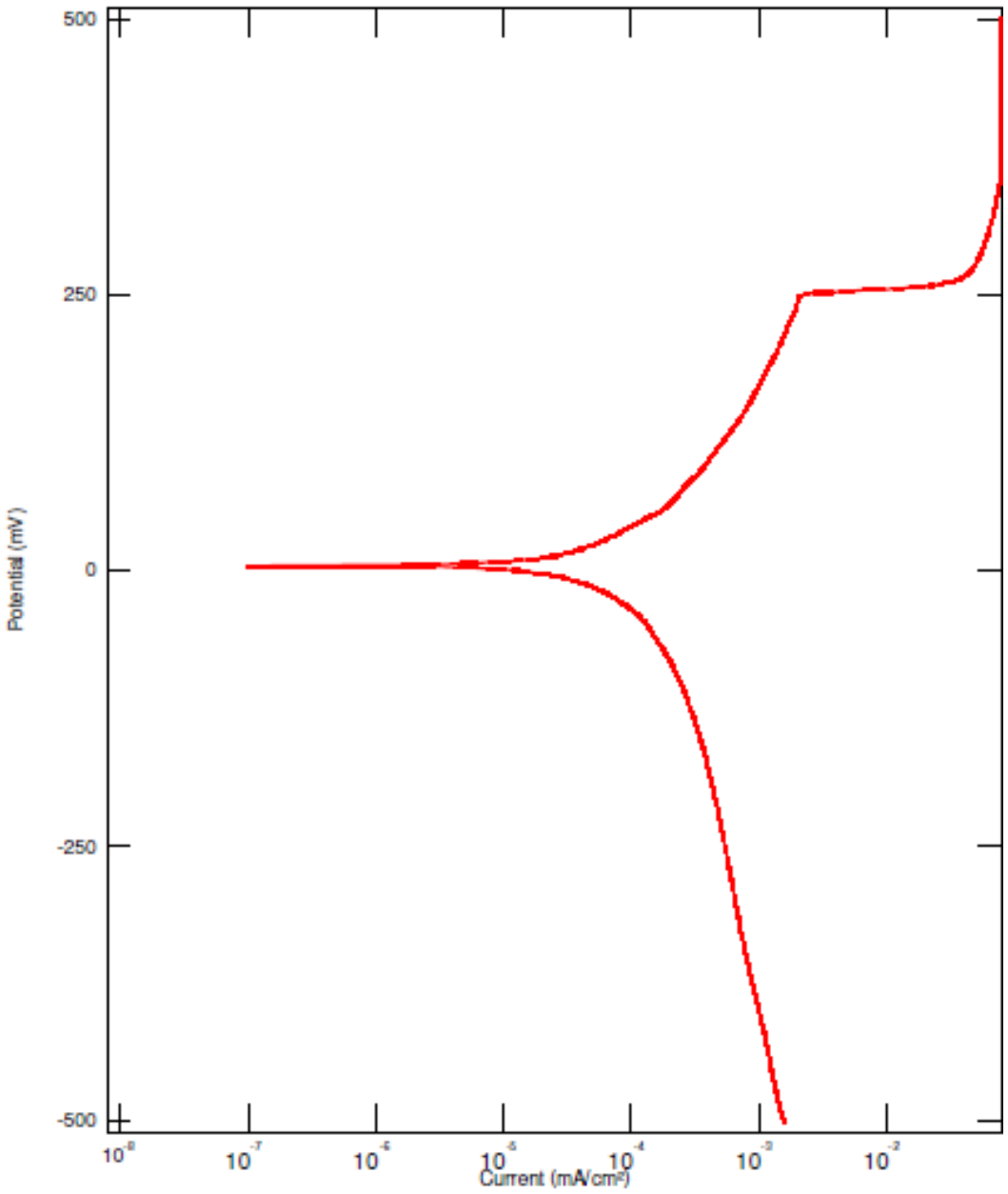

Graph 33 AISI 0.1 Ground Flat Stock - Test 2 Power Station A

6.1.3.3 Polarisation Curve for AISI 0.1 Ground Flat Stock with Power Station B Solution - Sample 1

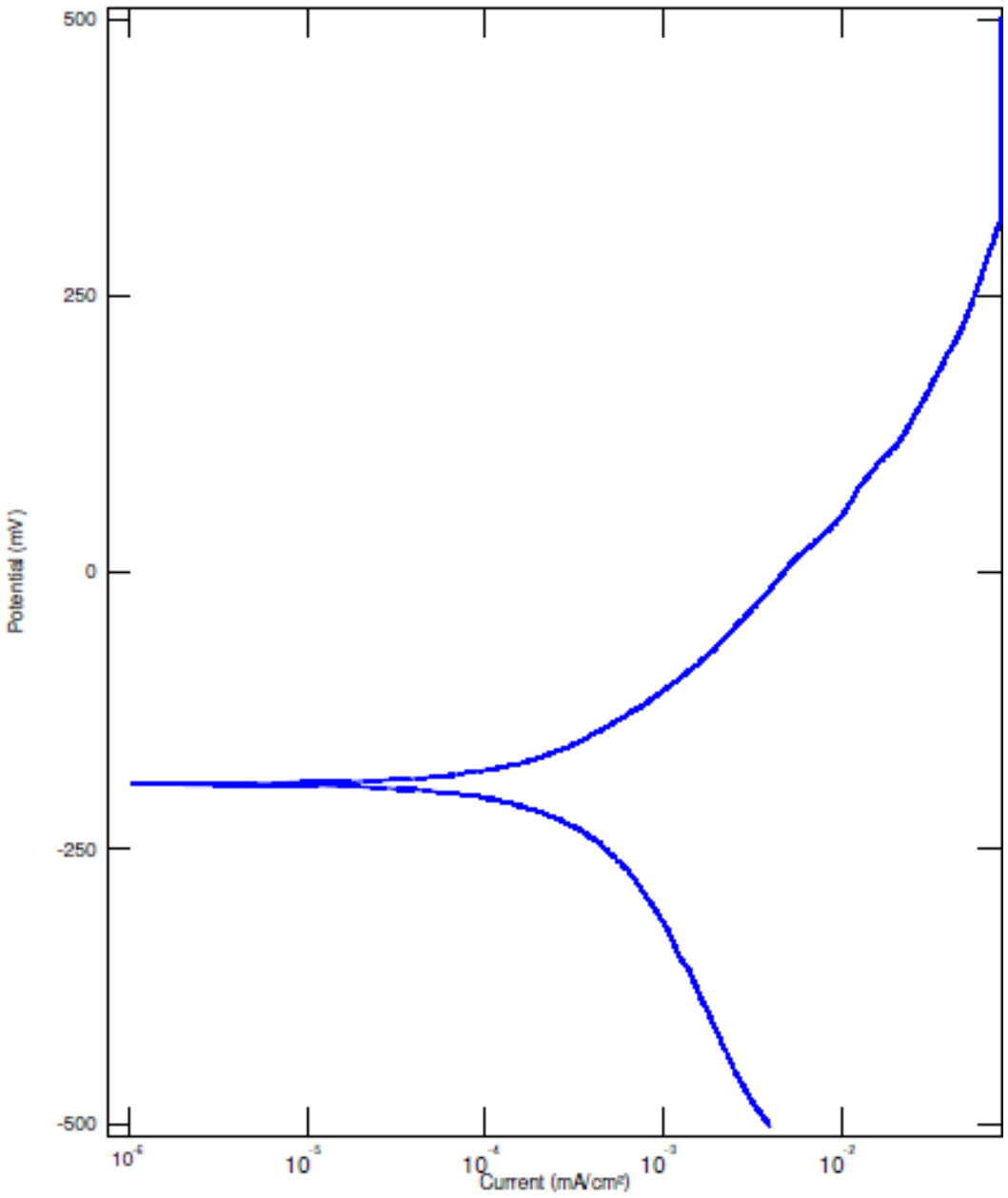

Graph 34 AISI 0.1 Ground Flat Stock - Test 3 Power Station B Sample 1

6.1.3.4 Polarisation Curve for AISI 0.1 Ground Flat Stock with Power Station B Solution - Sample 2

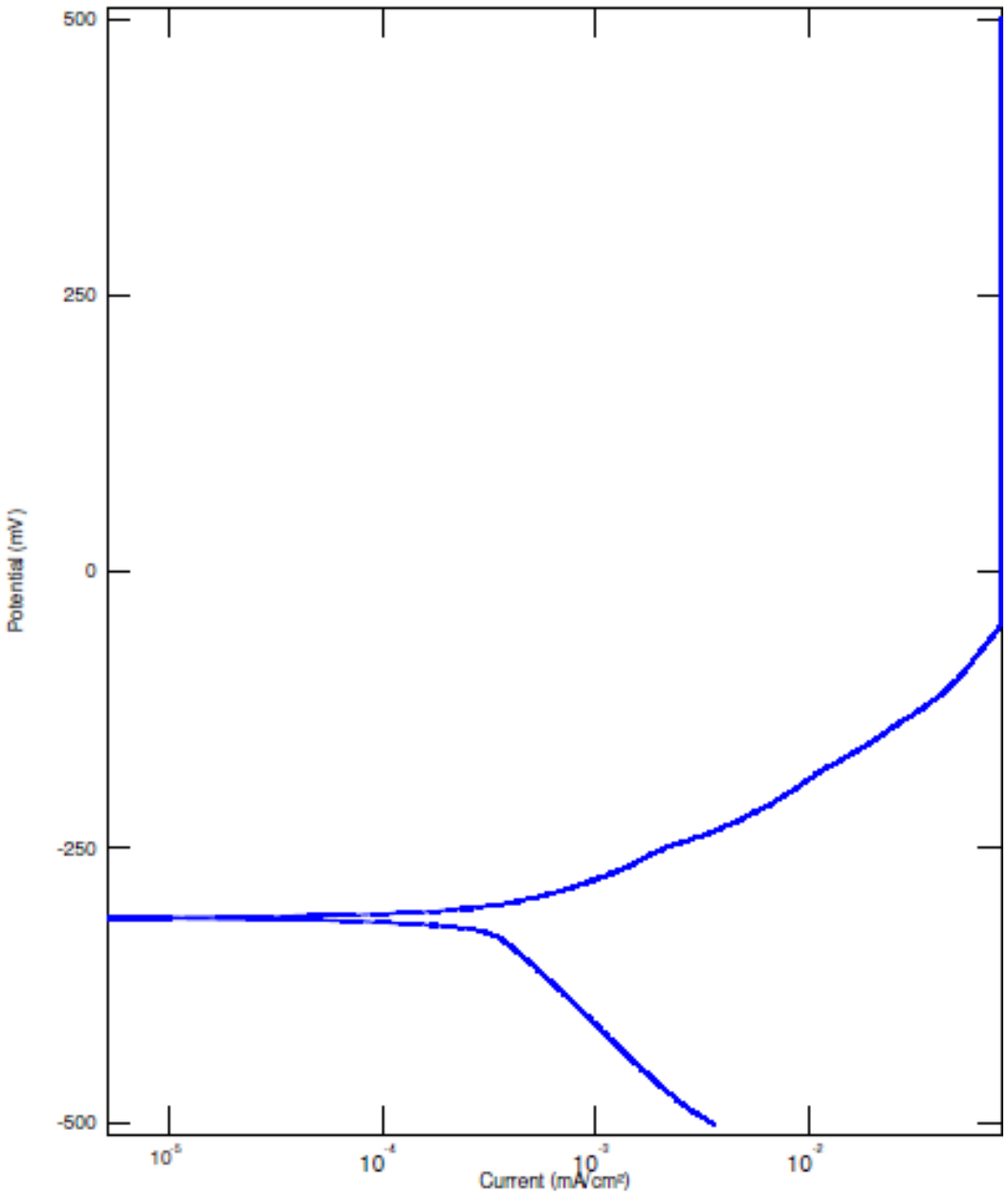

Graph 35 AISI 0.1 Ground Flat Stock - Test 4 Power Station B Sample 2

6.1.3.5 Polarisation Curve for AISI 0.1 Ground Flat Stock with a 20% Peat and 80% De-ionised Water Solution

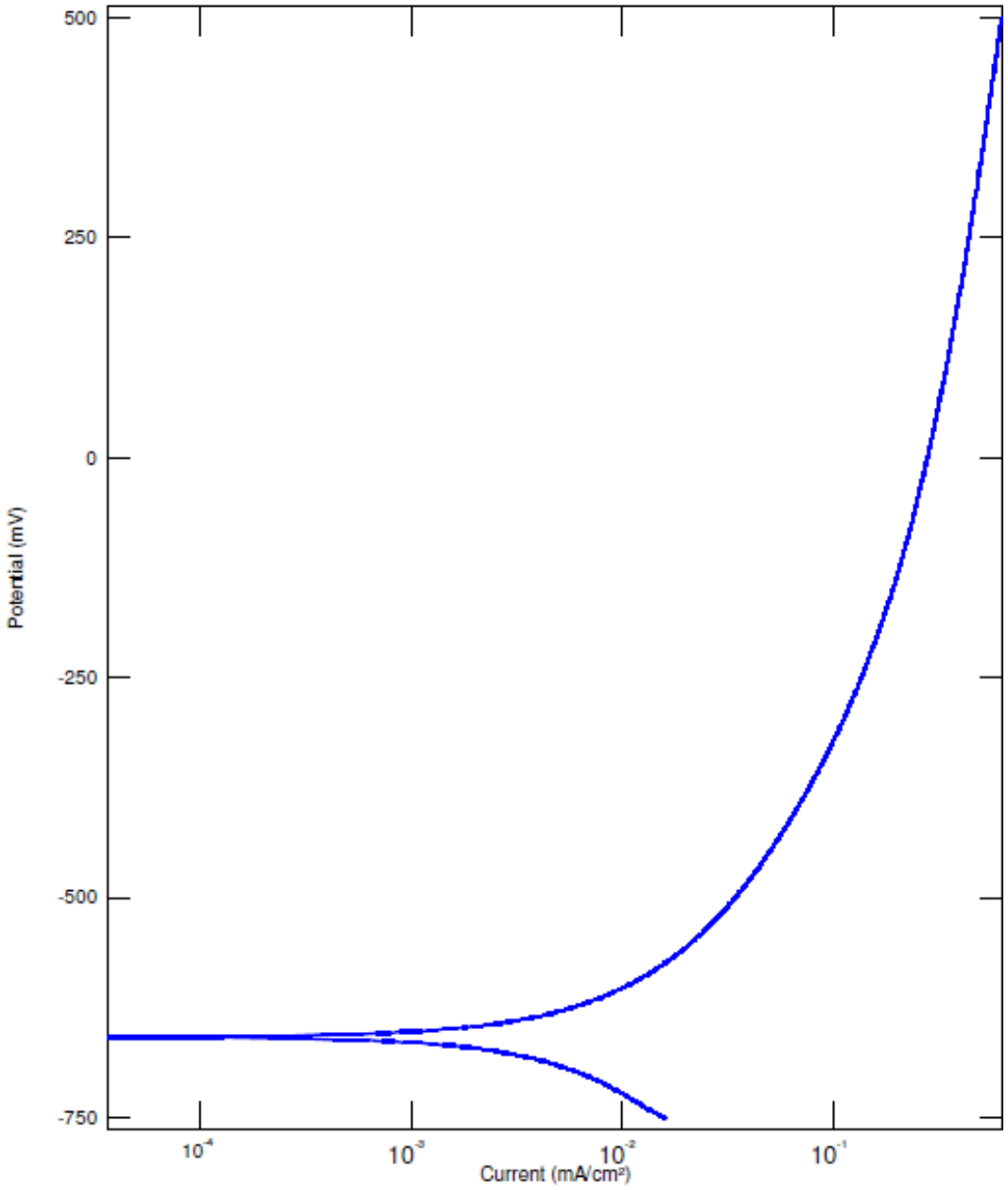

Graph 36 AISI 0.1 Ground Flat Stock - Test 5 20% Peat

6.1.3.6 Polarisation Curve for AISI 0.1 Ground Flat Stock with a 40% Peat and 60% De-ionised Water Solution

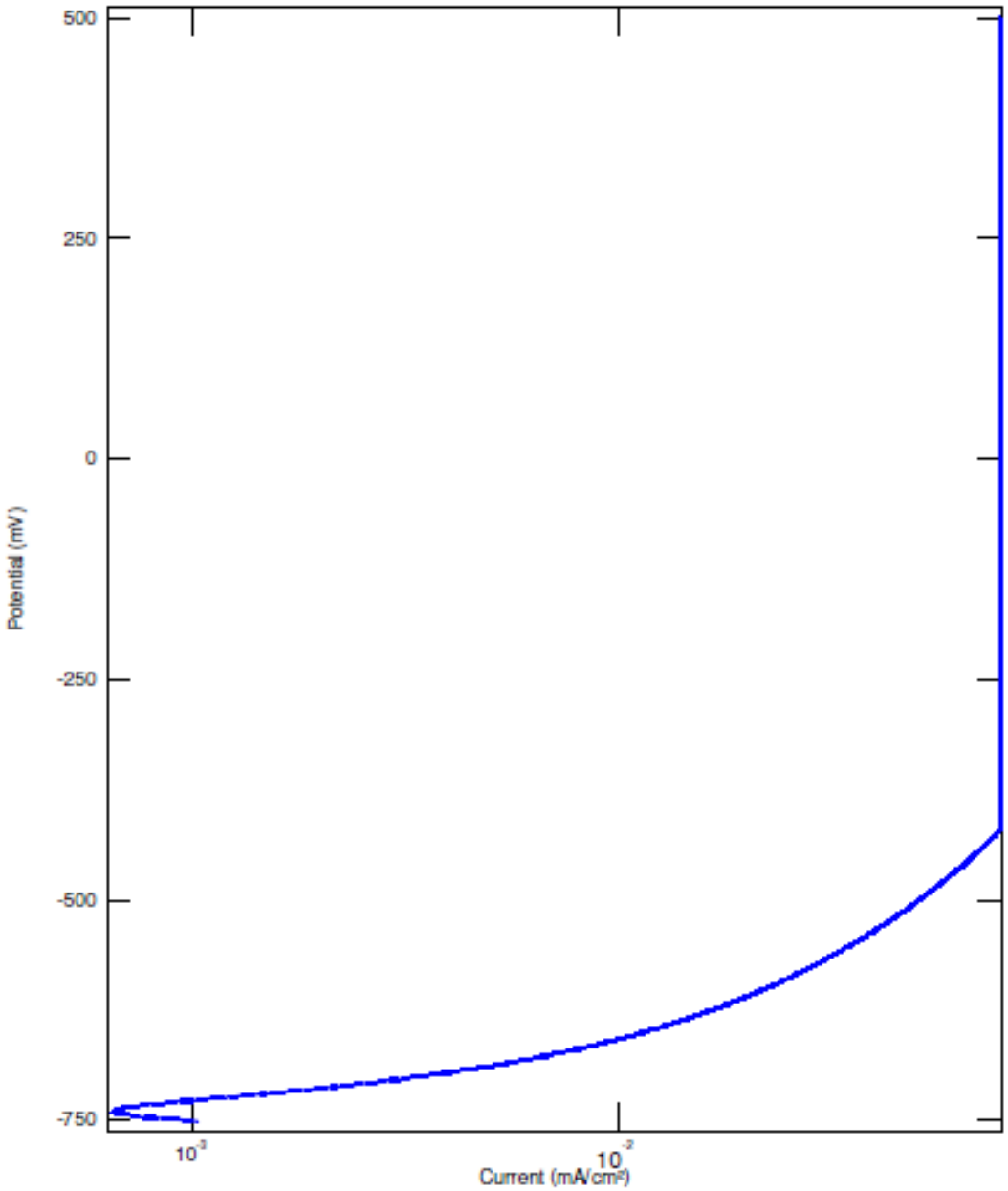

Graph 37 AISI 0.1 Ground Flat Stock - Test 6 40% Peat

6.1.3.7 Polarisation Curve for AISI 0.1 Ground Flat Stock with a 5% Peat and 95% De-ionised Water Solution

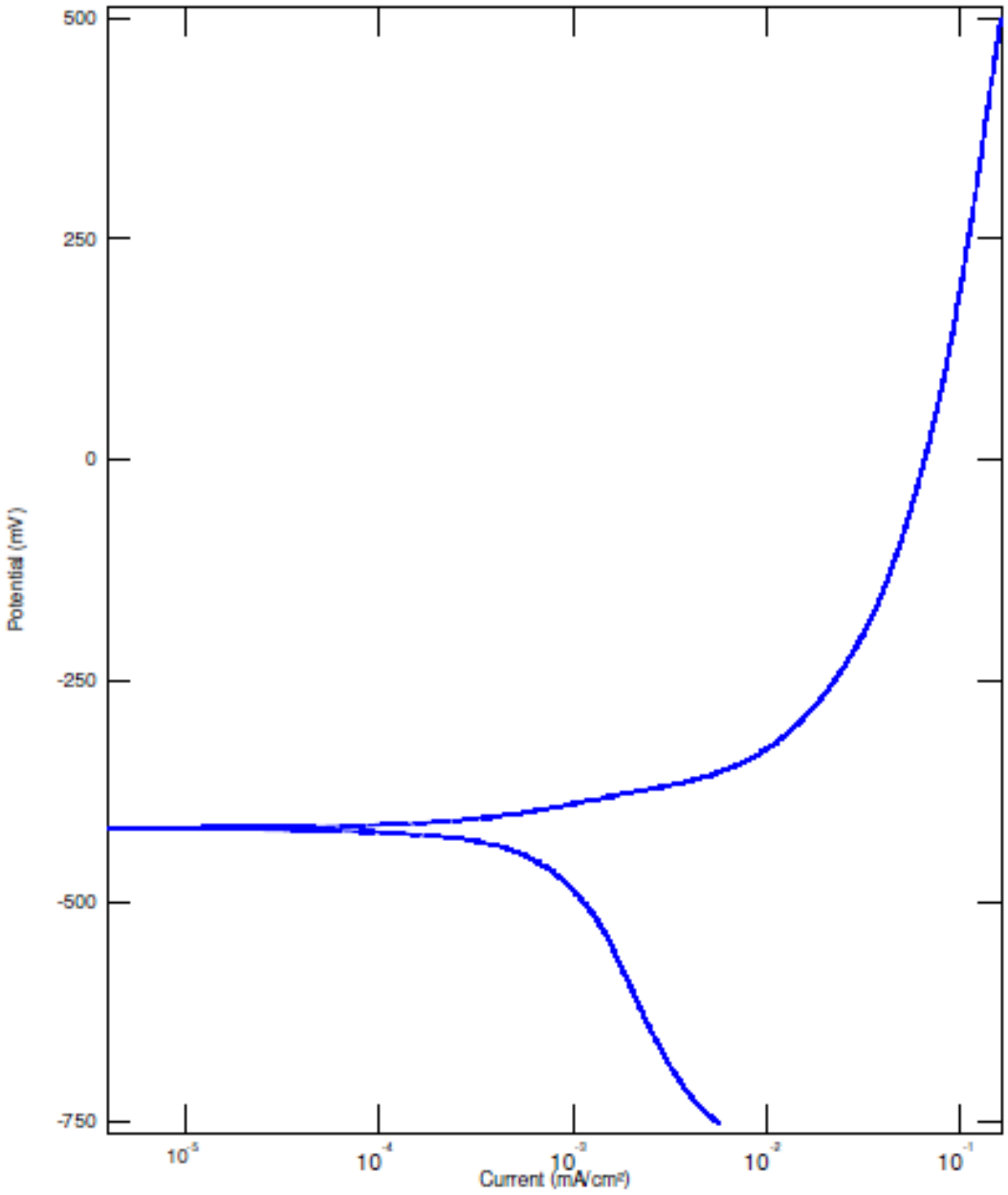

Graph 38 AISI 0.1 Ground Flat Stock - Test 7 5% Peat

6.1.3.8 Polarisation Curve for AISI 0.1 Ground Flat Stock with a 10% Peat and 90% De-ionised Water Solution

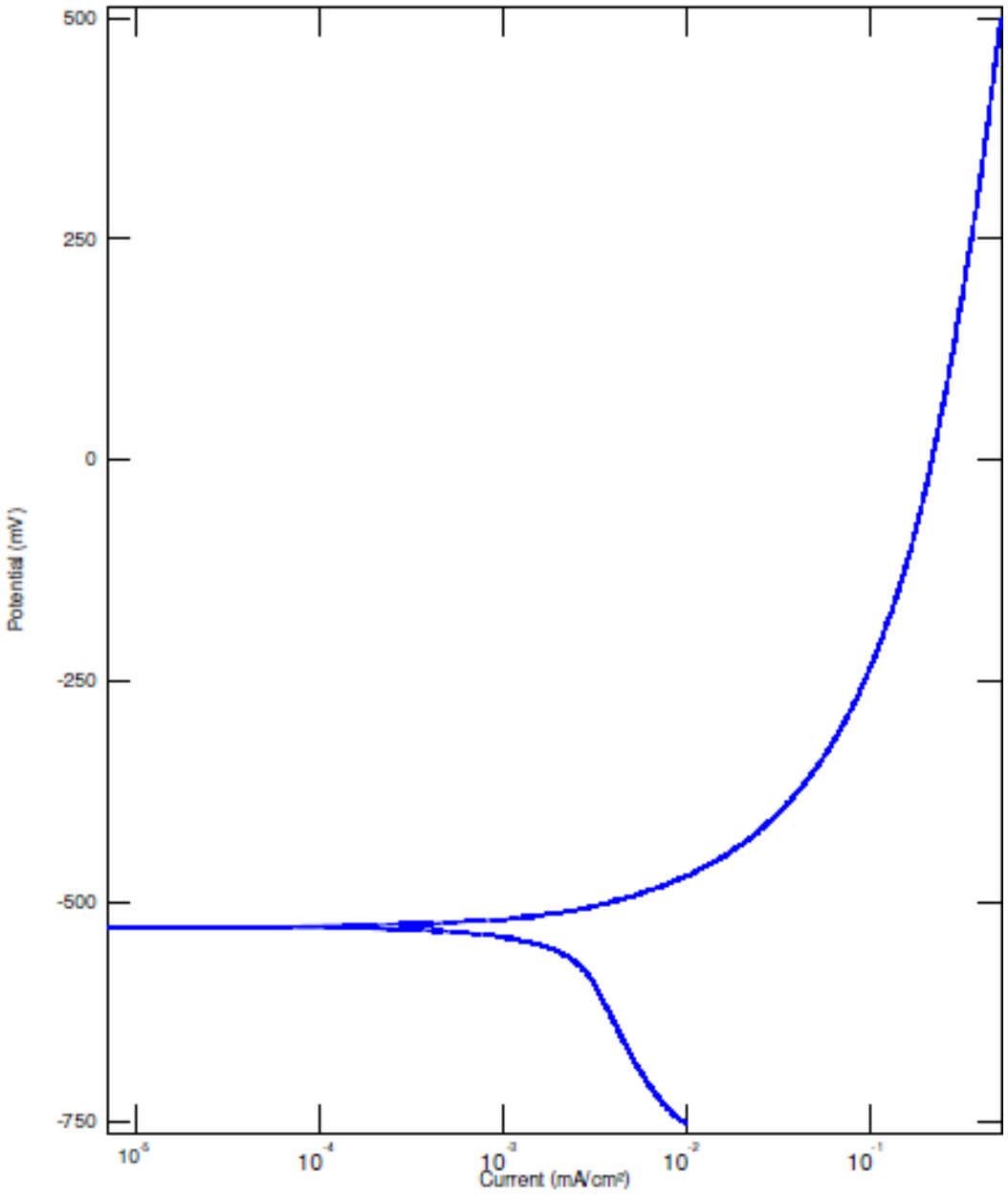

Graph 39 AISI 0.1 Ground Flat Stock - Test 8 10% Peat

6.1.4 Combined 304L and 316L Polarisation Curve Results

6.1.4.1 Polarisation Curve for Stainless Steel 304L and 316L with de-ionised water solution

The blue and red trends are the results for the Stainless Steel 316L and 304L samples respectively.

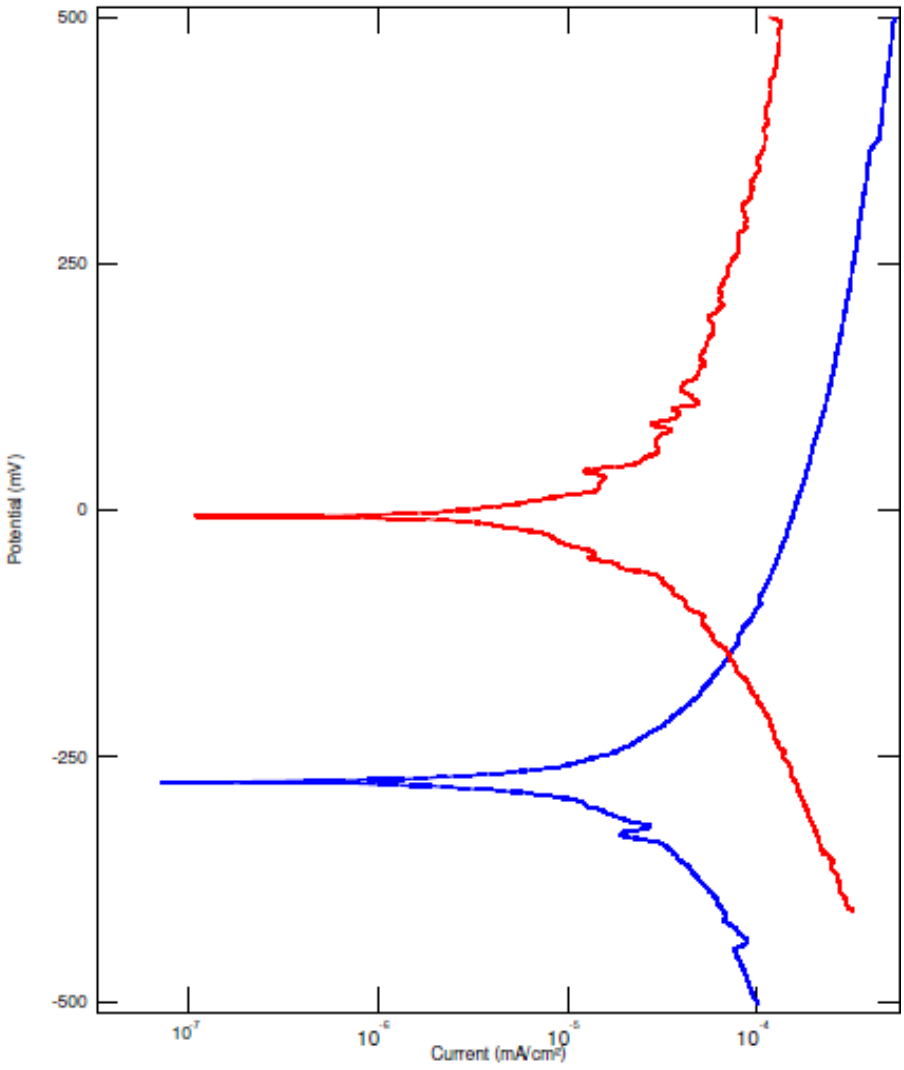

Graph 40 Stainless Steel 304L and 316L - Test 1 De Ionised Water

6.1.4.2 Polarisation Curve for Stainless Steel 304L and 316L with a Power Station B Water Solution - Sample 2

The blue and red trends are the results for the Stainless Steel 316L and 304L samples respectively.

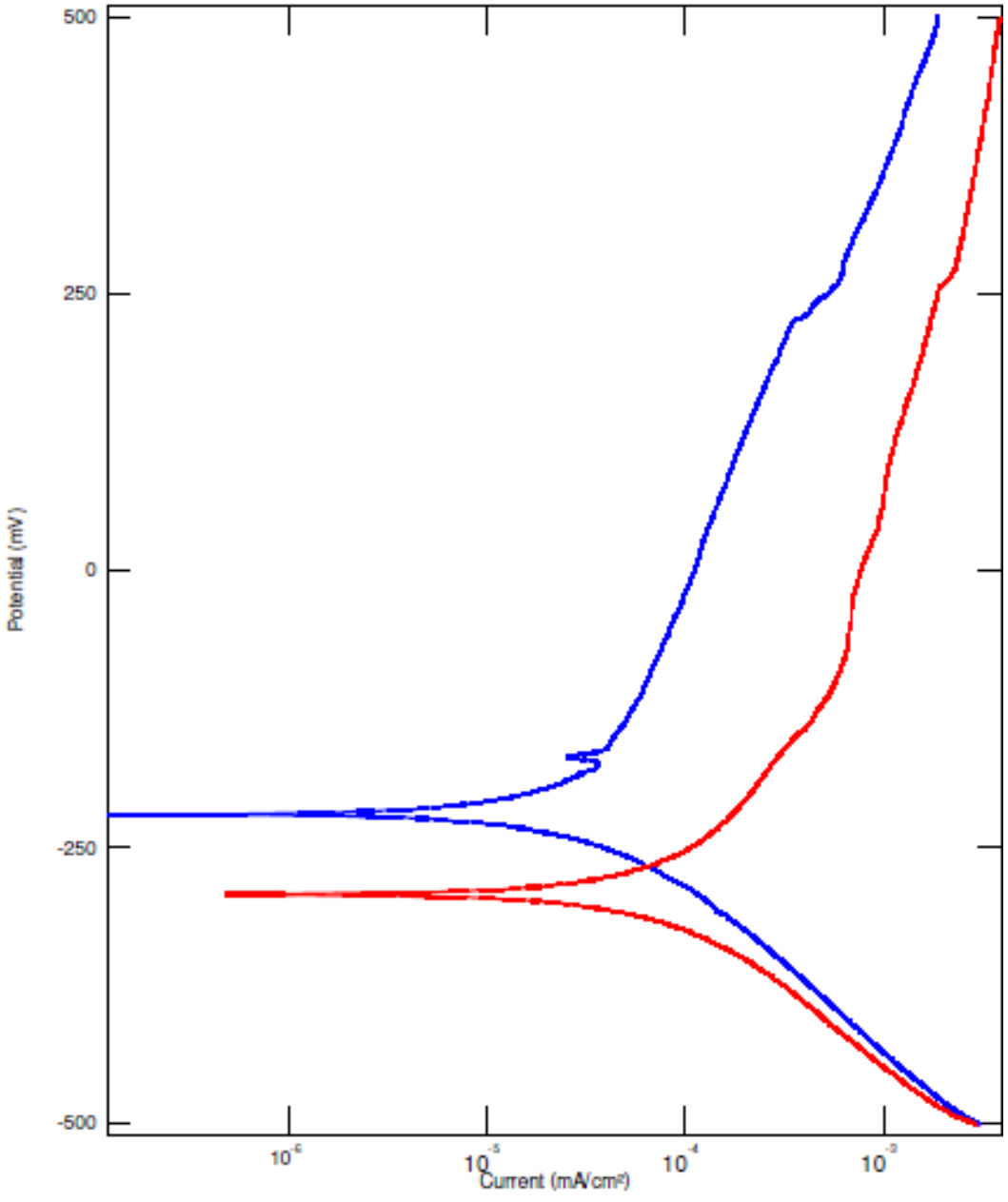

Graph 41 Stainless Steel 304L and 316L - Test 4 Power Station B Sample 2

6.1.4.3 Polarisation Curve for Stainless Steel 304L and 316L with a 10% Peat and 90% De-ionised Water Solution

The blue and red trends are the results for the Stainless Steel 316L and 304L samples respectively.

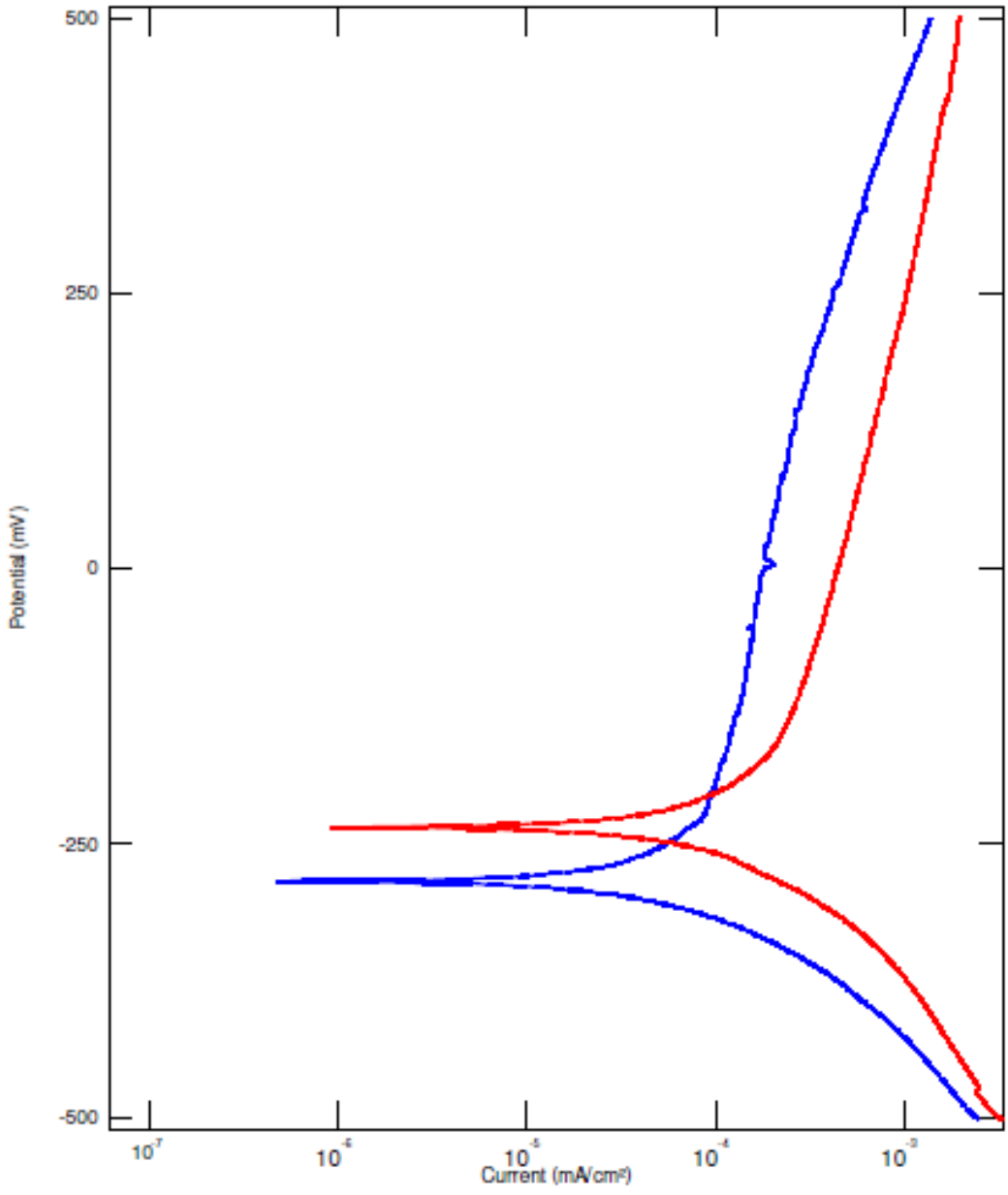

Graph 42 Stainless Steel 304L and 316L - Test 8 10% Peat

6.1.5 304L, 316L and AISI 0.1 Ground Flat Stock Polarisation Curves

6.1.5.1 Polarisation Curve for Stainless Steel 304L, 316L and AISI 0.1 Ground Flat Stock with a De-ionised Water Solution

The blue, red and green graph trends are the results for the Stainless Steel 316L, 304L and AISI 0.1 Ground Flat Stock material samples respectively.

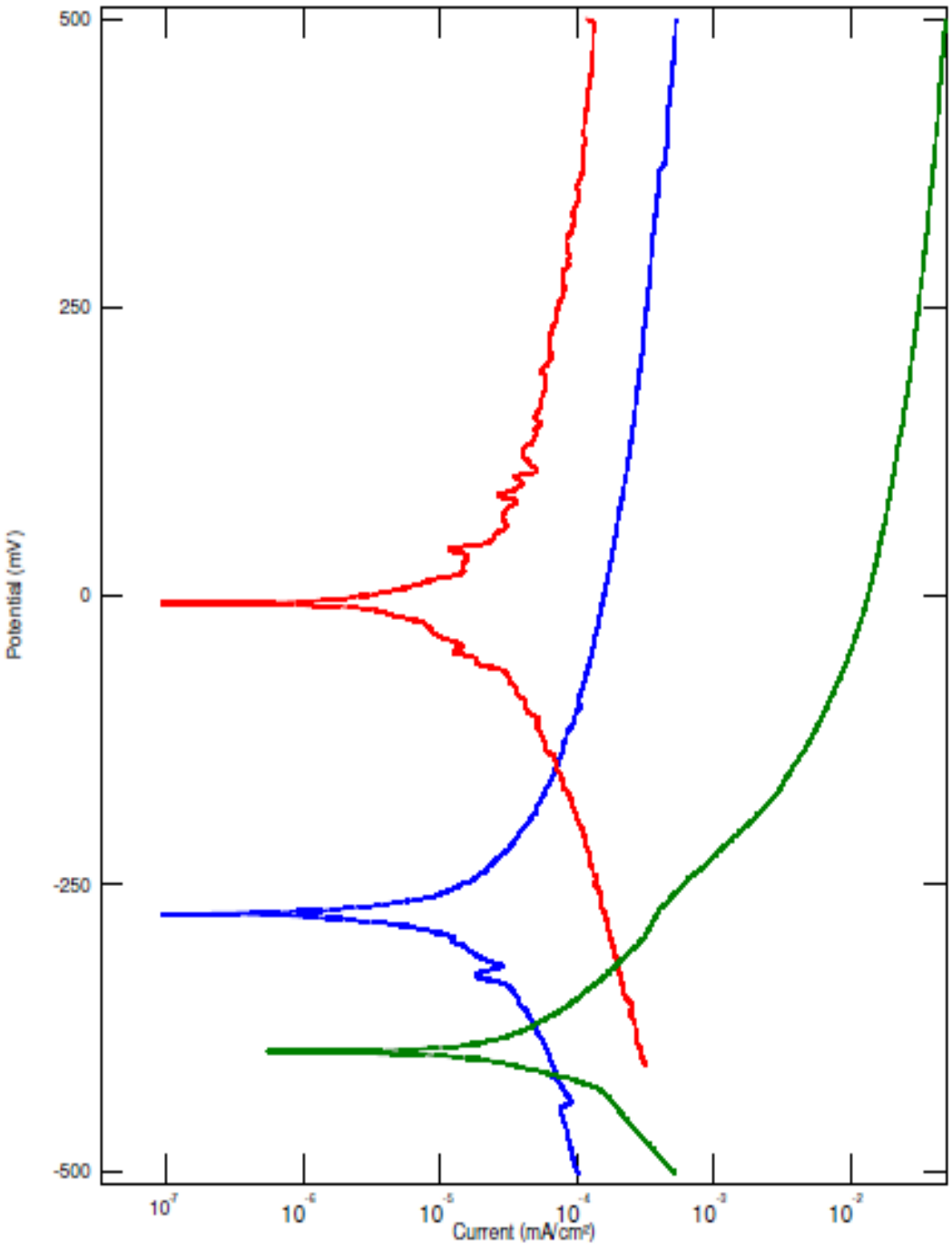

Graph 43 Combined 304L, 316L and AISI 0.1 Ground Flat Stock - De-Ionised Water

6.1.5.2 Polarisation Curve for Stainless Steel 304L, 316L and AISI 0.1 Ground Flat Stock with a Power A Water Solution

The blue, red and green graph trends are the results for the Stainless Steel 316L, 304L and AISI 0.1 Ground Flat Stock material samples respectively.

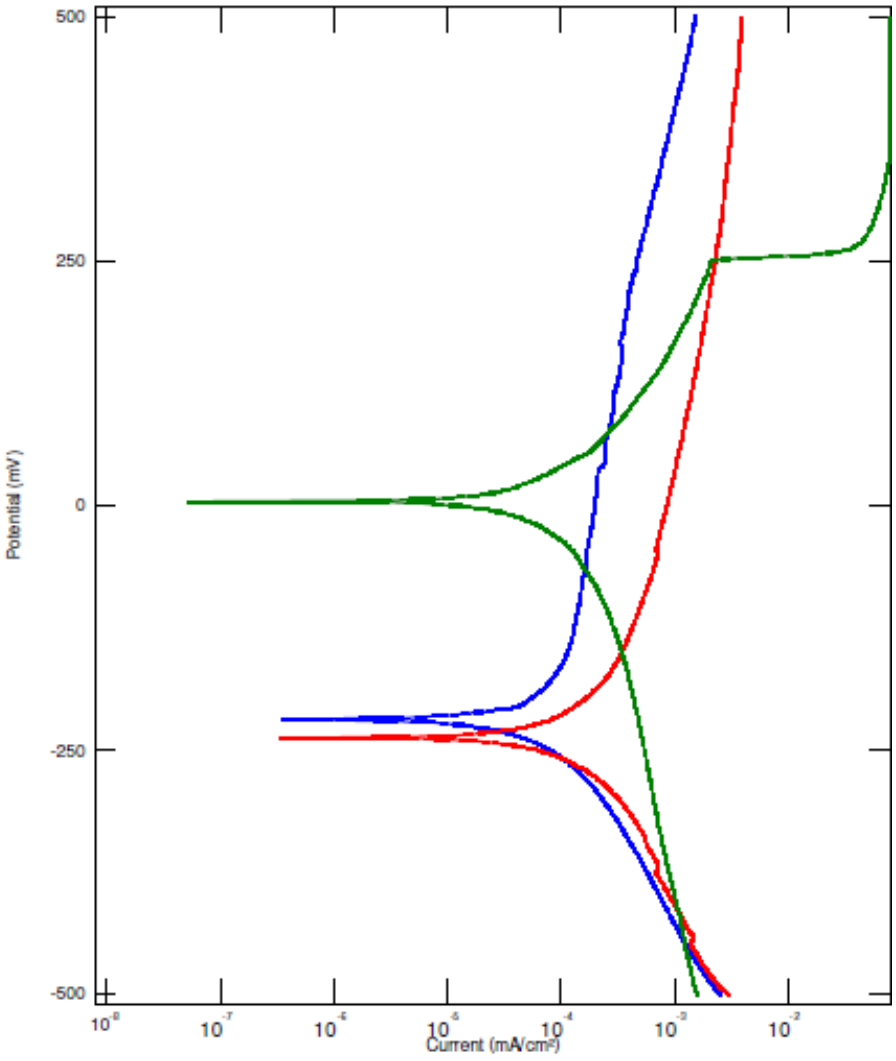

Graph 44 Combined 304L, 316L and AISI 0.1 Ground Flat Stock - Power Station A

6.1.5.3 Polarisation Curve for Stainless Steel 304L, 316L and AISI 0.1 Ground Flat Stock with a Power B - Sample 1 Water Solution

The blue, red and green graph trends are the results for the Stainless Steel 316L, 304L and AISI 0.1 Ground Flat Stock material samples respectively.

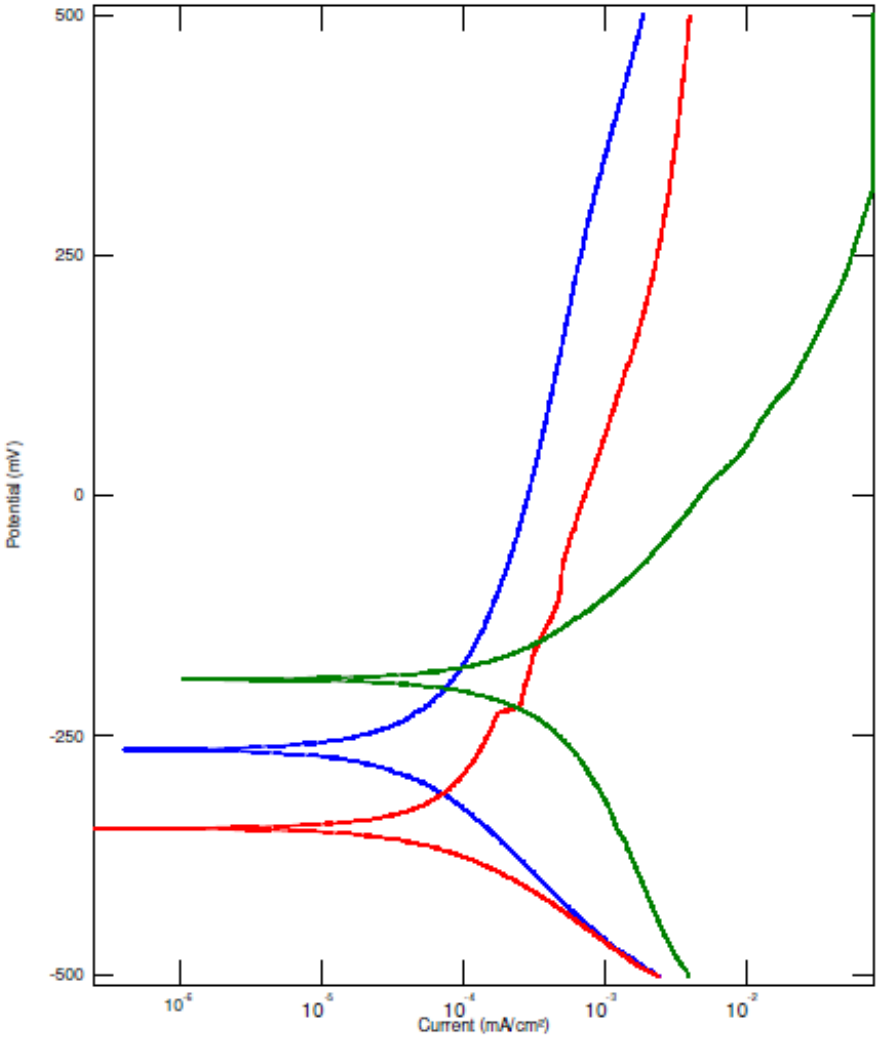

Graph 45 Combined 304L, 316L and AISI 0.1 Ground Flat Stock - Power Station B Sample 1

6.2 Appendix 2 - Corrosion Rate Map Calculation

6.2.1 Calculation Data

The following corrosion rates were calculated based on the data below.

Corrosion Rate Kc:

Solution	Material		
	316L	*304L*	*Steel Gauge Plate (AISI 0-1)*
0% Peat	6.46469E-08	1.7453E-07	5.15171E-05
5% Peat	1.43479E-07	1.46231E-06	0.000130876
10% Peat	1.34221E-07	1.13381E-06	0.000406339
20% Peat	8.29244E-07	3.05992E-06	0.000462199
40% Peat	1.34499E-07	9.86432E-07	7.20202E-05

Stainless Steel 316L										
Element	Carbon (C)	Manganese (Mn)	Silicon (Si)	Phosphorus (P)	Sulphur (S)	Chromium (Cr)	Molybdenum (Mo)	Nickel (Ni)	Nitrogen (N)	Iron (Fe)
% composition	0.03 max	2.00 max	0.75 max	0.03 max	0.03 max	17 - 20	2-4	12-14	0.1	Bal

Atomic Number	6	25	14	15	16	24	42	28	7	26
Atomic Mass (amu)	12.0107	54.93805	28.0855	30.97376	32.066	51.9961	95.94	58.6934	14.00674	55.845
Number of Valence Electrons	4	2	4	5	6	2	2	2	5	2

Stainless Steel 304L										
Element	Carbon (C)	Manganese (Mn)	Silicon (Si)	Phosphorus (P)	Sulphur (S)	Chromium (Cr)	Molybdenum (Mo)	Nickel (Ni)	Nitrogen (N)	Iron (Fe)
% composition	0.03 max	2.00 max	0.75 max	0.045 max	0.03 max	18 - 20		08-12	0.1	Bal
Atomic Number	6	25	14	15	16	24		28	7	26
Atomic Mass (amu)	12.0107	54.93805	28.0855	30.97376	32.066	51.9961		58.6934	14.00674	55.845
Number of Valence Electrons	4	2	4	5	6	2	2	2	5	2

Steel Gauge Plate (A.I.S.I 0-1- Ground Flat Stock)									
Element	Carbon (C)	Manganese (Mn)	Silicon (Si)	Phosphorus (P)	Sulphur (S)	Chromium (Cr)	Tungsten (W)	Vanadium (V)	Iron (Fe)
% composition	0.95	1.2	0.25	0.035	0.035	0.5	0.5	0.2	96.37
Atomic Number	6	25	14	15	16	24	74	23	26
Atomic Mass (amu)	12.0107	54.93805	28.0855	30.97376	32.066	51.9961	183.84	50.9415	55.845
Number of Valence Electrons	4	2	4	5	6	2	2	2	2

I = measured corrosion current

	316L	304L	Steel Gauge Plate (AISI 0-1)
0% Peat (De-ionised water)	0.00001627	0.00005637	0.0076784
5% Peat	0.00003611	0.0004723	0.0195065
10% Peat	0.00003378	0.0003662	0.0605631
20% Peat	0.0002087	0.0009883	0.0688887
40% Peat	0.00003385	0.0003186	0.0107343

M = atomic mass of material

316L =	434.55525
304L =	338.61525
Steel Gauge Plate =	500.69661

Z = valence electrons involved in the corrosion of the steel**

316L	34
304L	34
Steel Gauge Plate	29

Exposure Time

Sweep Rate = 33.333mV/min

304L and 316L:

Start Potential =	-500mV
Reverse Potential =	500mV
Exposure time (mins)=	30

Steel Gauge Plate

Start Potential =	-750mV
Reverse Potential =	500mV
Exposure time (mins)=	37.5

F = Faradays constant

(96,500 C mol -1)	96500

**Note: Transition metals in groups 3-12 have all been given 2 valence electrons, even though they don't always act that way

7 References

Abreu C M, Cristobal M J, Montemor M F, Novoa X R, Pena G, Perez M C, 2002; Galvanic coupling between carbon steel and austenitic stainless steel in alkaline media.

Electrochimica Acta 47 (2002) 2271-2279

Journal homepage: www.elsevier.com/locate/electacta

Ahmed W.H, 2010; Evaluation of the proximity effect on flow-accelerated corrosion.

Annals of Nuclear Energy 37 (2010) 598-605

Journal homepage: www.elsevier.com/locate/anucene

Andrew N, Giourntas L, Galloway A M, Pearson A, 2014; Effect of impact angle on the slurry erosion-corrosion of Stellite 6 and SS316.

Wear 320 (2014) 143-151

Journal homepage: www.elsevier.com/locate/wear

Baddoo N R, 2008; Stainless steel in construction: A review of research, applications, challenges and opportunities.

Journal of Construction Steel Research

Journal homepage: www.elsevier.com/locate/jcsr

British Standard PD6484:1979; Commentary on corrosion at bimetallic contacts and its alleviation.

Callister W D, Seventh Edition; Materials Science and Engineering - An Introduction.

Publishers John Wiley & Sons, Inc.

ISBN-13: 978-0-471-73696-7

ISBN-10: 0-471-73696-1

Chang H Y, Park Y S, Hwang W S, 1998; Initiation modelling of crevice corrosion in 316L stainless steel.

Journal of Material Processing Technology 103 (2000) 206 - 217

Journal Homepage: www.elsevier.com/locate/jmatprotec

Covert R A, Turthill A H, 2000; Stainless Steels: An Introduction to Their Metallurgy and Corrosion Resistance.

Dairy, Food and Environment Sanitation, Vol. 20, No.7, Pages 506-517

Copyright International Association for Food Protect

Dooley R.B, Chexal V.K, 2000; Flow-accelerated corrosion of pressure vessels in fossil plants.
International Journal of Pressure Vessels and Piping 77 (2000) 85-90
Journal Homepage: www.elsevier.com/locate/ijpvp
European Directive 2009; Directive 2009/28/EC OF THE EUROPEAN PARLIAMENT AND OF THE COUNCIL., 23 April 2009. Official Journal of the European Union
Fattah-alhosseini A, Vafaeian S, 2014; Effect of solution pH on the electrochemical behaviour of AISI 304 austenitic and AISI 430 ferritic stainless steels in concentrated acidic media
Egyptian Journal of Petroleum 2015
Journal homepage: www.elsevier.com/locate/egyjp
Ferritic Stainless Steel Article; From the British Stainless Steel Association - http://www.bssa.org.uk/topics.php?article=20
Finsgar M, 2013; Galvanic series of different stainless steels and copper - and aluminium based materials in acid solutions
Corrosion Science 68 (2013) 51-56
Journal homepage: www.elsevier.com/locate/corsci
Gammal M, Mazhar H, Cotton J.S, Shefski C, Pietralik J, Ching C.Y, 2010; The hydrodynamic effects of single-phase flow on flow accelerated corrosion in a 90-degree elbow.
Nuclear Engineering and Design 240 (2010) 1589-1598
Journal Homepage: www.elsevier.com/locate/nucengdes
Geringer J, Forest B, Combrade P, 2005; Fretting-corrosion of materials used as orthopaedic implants.
Wear 259 (2005) 943-951
Journal Homepage: www.elsevier.com/locate/wear
Geringer J, Macdonald D.D, 2012; Modelling fretting-corrosion wear of 316L SS against poly(methyl methacrylate) with the Point Defect Model: Fundamental theory, assessment and outlook.
Electrochimica Acta 79 (2012) 17-30
Journal Homepage: www.elsevier.com/locate/electacta
Hinds G; The Electrochemistry of Corrosion. Edited from the original work of J G N Thomas

Holmes D, Sharifi S, Stack M M, 2014; Tribo-corrosion of steel in artificial saliva.
Tribology International 75 (2014) 80-86
Journal Homepage: www.elsevier.com/locate/triboint
Islam Md A, Farhat Z N, Ahmed E M, Alfantazi A M, 2013; Erosion enhanced corrosion and corrosion enhanced erosion of API X -70 pipeline steel.
Wear 302 (2013) 1592-1601
Journal Homepage: www.elsevier.com/locate/wear
Kain V, 2011; Stress Corrosion Cracking, Theory and practice.
Edited by V.S. Raja and Tetsuo Shoji.
A volume in Woodhead Publishing Series in Metals and Surface Engineering
Loto C A, Popoola A P, Fayomi O S, Loto R T. 2012; Corrosion Polarization Behaviour of Type 316 Stainless Steel in Strong Acids and Acid Chlorides. International Journal of Electrochemical Science 7 (2012) 3787-3797
Journal Homepage: www.electrochemsci.org
Martensitic Stainless Steel Article; From the British Stainless Steel Association - http://www.bssa.org.uk/topics.php?article=253
Oldfield J W, 1988; Electrochemical Theory of Galvanic Corrosion.
Galvanic Corrosion, ASTM STP 978
Editor Havey P.Hack
ASTM publication code number (PCN) 04-978000-27
Olsson C O A, Landolt D, 2003; Passive films on stainless steels - chemistry, structure and growth.
Electrochimica Acta 48 (2003) 1093 - 1104
Journal homepage: www.elsevier/locate/electacta
Popov B N, First Edition; Corrosion Engineering - Principles and Solved Problems.
Elsevier Science Ltd (2 March 2015)
ISBN-10: 0444627227
ISBN-13: 9780444627223
Ren W, Wang P, Fu Y, Pan C, Song J, 2015; Effects of temperature on fretting corrosion behaviours of gold-plated copper alloy electrical contacts.
Tribology International 83 (2015) 1 - 11
Journal Homepage: www.elsevier.com/locate/triboint
Scottish National Heritage Commissioned Report No.701; Scotland's peatland - definitions & information resources.

Link: http://www.snh.org.uk/pdfs/publications/commissioned_reports/701.pdf

Shoji T, Lu Z, Peng Q, 2011; Factors affecting stress corrosion cracking (SCC) and fundamental mechanistic understanding of stainless steels.

Found in: Stress Corrosion Cracking, Theory and practice. Edited by V.S. Raja and Tetsuo Shoji.

A volume in Woodhead Publishing Series in Metals and Surface Engineering

Singh R, First Edition; Corrosion Control for Offshore Structures - Cathodic Protection and High Efficiency Coating.

Gulf Professional Publishing (August 2014)

ISBN: 978-0-12-404615-3

Speight J, **First Edition;** Oil and Gas Corrosion Prevention: From Surface Facilities to Refineries.

Gulf Professional Publishing (17 March 2014)

ISBN-10: 0128003464

ISBN-13: 9780128003466

Stack M M, Mathew M T, Hodge C, 2011; Micro-abrasion-corrosion interactions of Ni-Cr/WC based coatings: Approaches to construction of tribo-corrosion maps for the abrasion-corrosion synergism.

Electrochimica Acta 56 (2011) 8249-8259

Journal Homepage: www.elsevier.com/locate/electacta

Tian W, Du N, Li S, Chen S, Wu Q, 2014; Metastable pitting corrosion of 304 stainless steel in 3.5% NaCl Solution.

Corrosion science 85 (2014) 372-379

Journal Homepage: www.elsevier.com/locate/corsci

Vingsbo O, Soderberg S, 1998; On fretting maps.

Wear, 126 (1998), pp. 131 - 147

Wang Y, Xing, Z Z, Luo Q, Rahman A, Jiao J, Qu S J, Zhen Y G, Shen J, 2015; Corrosion and erosion - corrosion behaviour of activated combustion high-velocity air fuel sprayed Fe-based amorphous coatings in chloride-containing solutions.

Corrosion Science 98 (2015) 339-353

Journal Homepage: www.elsevier.com/locate/corsci

Yang Y Z, Jiang Y M, Li J, 2013; In situ investigation of crevice corrosion on UNS S32101 duplex stainless steel in sodium chloride solution.

Corrosion Science 76 (2013) 163-169

Journal Homepage: www.elsevier.com/locate/corsci

Zarras P, Stenger-Smith J.D; Corrosion processes and strategies for prevention: an introduction.

Found in: Handbook of Smart Coatings for Materials Protection. Edited by: A.S.H Makhlouf

Copyright at 2014 Woodhead Publishing Limited

Zeng L, Zhang G A, Guo X P, 2014; Erosion-corrosion at different locations of X65 carbon steel elbow.

Corrosion Science 85 (2014) 318-330

Journal Homepage: www.elsevier.com/locate/corsci

Zhang G X, 2011; Galvanic Corrosion,

Copyright 2011 John Wiley & Sons.

Retrieved from www.knovel.com

Zhang Z, Zhao H, Zhang H, Yu Z, Hu J, He L, Li J, 2015; Effect of isothermal aging on the pitting corrosion resistance of UNS S82441 duplex stainless steel based on electrochemical detections.

Corrosion science 93 (2015) 120-125

Journal Homepage: www.elsevier.com/locate/corsci

The images used in this thesis have been sourced from the following location:

Galvanic Corrosion Example 1 - From the Authors Personal Photo Collection

Galvanic Corrosion Example 2 - From the Authors Personal Photo Collection

Crevice Corrosion Example 1 - Courtesy of:

http://www.corrosionclinic.com/types_of_corrosion/crevice_corrosion.htm

Crevice Corrosion Example 2 - Courtesy of:

http://corrosion-doctors.org/Forms-crevice/Crevice.htm

Pitting Corrosion Example 1 - Courtesy of:

http://www.surescreen.com/scientifics/services-failure.php

Pitting Corrosion Example 2 - Courtesy of:

http://www.lambdatechs.com/pitting.html

Pitting Corrosion Example 3 - Courtesy of:

http://octane.nmt.edu/waterquality/corrosion/Crevice.aspx

Pitting Corrosion Example 4 - Courtesy of:

http://octane.nmt.edu/waterquality/corrosion/Crevice.aspx

Erosion-Corrosion Example 1 - Courtesy of:
http://sirius.mtm.kuleuven.be/Research/corr-o-scope/hcindex1/tutorial3.htm
Erosion-Corrosion Example 2 - Courtesy of:
http://www.exponent.com/Erosion-and-Corrosion-of-Rubber-Lined-Steel-Pipeline/
Erosion-Corrosion Example 3 - Courtesy of:
http://www.cdcorrosion.com/mode_corrosion/corrosion_erosion_gb.htm
Fretting Corrosion Example 1 - Courtesy of:
http://mdm.shawwebspace.ca/pages/view/trouble_shooting_and_failure_ana/
Fretting Corrosion Example 2 - Courtesy of:
Image from: http://arab-training.net/vb/t8193.html
MIV Control Water Rotary Filter - From the Authors Personal Photo Collection
Cooling Water Isolating Valve - From the Authors Personal Photo Collection
Cooling Water Flow Control Relay - From the Authors Personal Photo Collection
Cooling Water Isolating Valve - From the Authors Personal Photo Collection
Cooling Water Isolating Valve Close Up - From the Authors Personal Photo Collection
Flange from Power Station Visit - From the Authors Personal Photo Collection